Catalytic Studies of Metal Substituted Aluminophosphates and other Related Systems

Thesis submitted for the degree of Doctor of Philosophy

By

Ilona Louise Franklin

2005

Davy-Faraday Research Laboratory,
The Royal Institution of Great Britain

Department of Chemistry, University College London,
University of London

ProQuest LLC
789 East Eisenhower Parkway
P.O. Box 1346
Ann Arbor, MI 48106-1346

Abstract

The research within this thesis has concentrated around the identification and catalytic understanding of the acid and redox properties of a series of metal substituted aluminophosphates, silicoaluminophosphates and polyoxometalates. The aim being to understand how the active metal sites were co-ordinated, to what degree of substitution had been successfully achieved and finally the direct relation this information had in understanding the degree of reaction for the various catalytic processes. In most part hydrothermal synthesis was employed, the exception being in the case of the polyoxometalate and polyoxometalate layered double hydroxide synthesis. Characterisation was achieved through the use of many analytical techniques predominantly X-ray diffraction (XRD) and extended X-ray spectroscopy (XAS). In total, four commercially important reactions were studied.

Firstly, the shape selective and redox properties associated with (a) the substitution of different metal ions within the same aluminophosphate framework and (b) the substitution of the same metal ion within different aluminophosphate frameworks were characterised and investigated for the methanol to olefin (MTO) reaction to demonstrate the activity and selectivity of different frameworks in the production of a range of olefins. Secondly, several transition metal ion-exchanged zeolites and aluminophosphates were synthesised, characterised and subsequently analysed for the hydroxylation of phenol. Here temperature effects were also investigated to see what, if any effect it had upon the final conversion of phenol. Thirdly, a series of bifunctional platinum impregnated silicoaluminophosphate (Pt/SAPO) and metal substituted aluminophosphate (Pt/MeAlPO) catalysts were synthesised, characterised then investigated to understand how their acidic nature effected the catalytic activity and selectivity for the hydroisomerisation of n-heptane. Finally, the properties of several cobalt-substituted polyoxometalates (POM's) and polyoxometalate pillared layered double hydroxides (POM-LDH's) were studied and investigated for their catalytic activity for the oxidation of cyclohexane with molecular oxygen in the presence of TBHP.

Table of Contents

List of Figures

Chapter 1 Introduction

Chapter 2 Experimental Methods

Chapter 3 Study of the shape selective and redox properties of several framework metal substituted aluminophosphates for the Methanol to Olefin (MTO) reaction

Chapter 4 Investigation into the influence of transition metal ion exchange in zeolites and aluminophosphates for the hydroxylation of phenol

Appendix

List of Tables

Chapter 1 Introduction

Chapter 2 Experimental Methods

Chapter 3 Study of the shape selective and redox properties of several framework metal substituted aluminophosphates for the Methanol to Olefin (MTO) reaction

List of Equations

Chapter 1 Introduction

Chapter 2 Experimental Methods

2.1	$n\lambda = 2d \sin\theta$	39
2.2	$dI = -\mu(E)Idt$	42
2.3	$I = I_0 e^{-\mu(E)t}$	42
2.4	$k = \sqrt{(2m/\hbar^2)}.(E-E_o)$	45
2.5	$\mu_{total} = \mu_o[1+\chi ex]$	46
2.6	$\chi(k) = \Sigma A_j(k) \sin \Phi_j(k)$	46
2.7	$\sin \Phi_j(k) = \sin [2kR_j - \Phi_j(k)]$	46
2.8	$A_j(k) = (N_j/kR_j^2)\ S_o^2 F_j(k) e^{-2k\sigma j2} e^{-2Rj/\lambda j(k)}$	47
2.9	$\text{Area \% (x)} = \frac{\text{area (x)}}{\text{area (x)} + \text{area (y)}} \times 100$	56
2.10	Response Factor (x) = Area (x) / True %	56
2.11	$\frac{\text{RT (analyte)}}{\text{RT (methane)}} = \text{RRT}$	56

Chapter 3 Study of the shape selective and redox properties of several framework metal substituted aluminophosphates for the Methanol to Olefin (MTO) reaction

3.1	$\text{\% MeOH conversion} = \frac{\text{MeOH}_{\text{(prior to reac)}} - \text{MeOH}_{\text{(after reac)}}}{\text{Total Area}} \times 100$	75

Chapter 4 Investigation into the influence of transition metal ion exchange in zeolites and aluminophosphates for the hydroxylation of phenol

Chapter 5 Study into the acidic and shape-selective nature of platinum impregnated silicoaluminophosphates and metal substituted aluminophosphates, and their catalytic activity for the hydroisomerisation of n-heptane

Acknowledgements

Since starting my PhD at the DFRL/ Ri, I have had the opportunity to work with and alongside some really great people. I have thoroughly enjoyed my time in London and wish to thank everyone for making it such an enjoyable experience.

In particular I wish to thank my supervisor Dr. Sankar for his wisdom, advice, guidance and several G&T's throughout the completion of both the practical work and subsequent writing of this thesis. Furthermore, I would also like to thank Professor Avelino Corma and Dr. Fernando Rey at the university of Valencia and Professor Cesar Jimenez, Dr. Francisco J.Romero Salguero, Rafa Roldan Mesa and Aurora Cruz at the university of Cordoba for their hospitality and guidance during my trips to Spain whilst complete parts of my research.

In addition, I am extremely grateful to Dr. Andrew Beale for his many formative discussions and continuous assistance in the building of the catalysis lab. I would also like to say a big thankyou to other members of my group for their help and support, namely Dr. Manuel Sanchez Sanchez, Dr. Christianna Zennonos, Dr. Matt Johnson, Amber Welch and Matt O'Brien, to Mike Sheehy and Ian Watts for their technical support and to many other members of the DFRL and Ri including Dinah, Manisha, Donna, Nicola, Nikki, Rachel and Jo for many inspirational glasses of bubbly along the way.

Finally, I wish to thank my friends and family for their continued love and support and in particular my mum for her encouragement over the last twenty-seven years and without whom none of this would have been possible. Thankyou.

Chapter 1

Introduction

1.1 Present day Catalysis

Today's society relies upon many different catalysts for the preservation and improvement of day to day life. From medicinal advances through to fabrics, fertilisers, fuels and fine chemicals, catalysts are used in over 80% of industrial processes and therefore research into the development and understanding of these materials is of paramount importance [1,2].

Berzelius formulated the definition of 'catalysis' (meaning 'loosening down' in Greek) in 1836, however the phenomena had already been commercially exploited by Döbereiners' Tinderbox in the 1820's, this worked on the principle that metals glow when in contact with air and combustible gas [3]. By 1830 over 20,000 were in homes and offices in England and Germany.

Catalysis is a cyclic event (figure 1.1). Reactants adsorb onto the catalyst surface where they react, then desorb leaving free the active sites ready for the next reactant molecule.

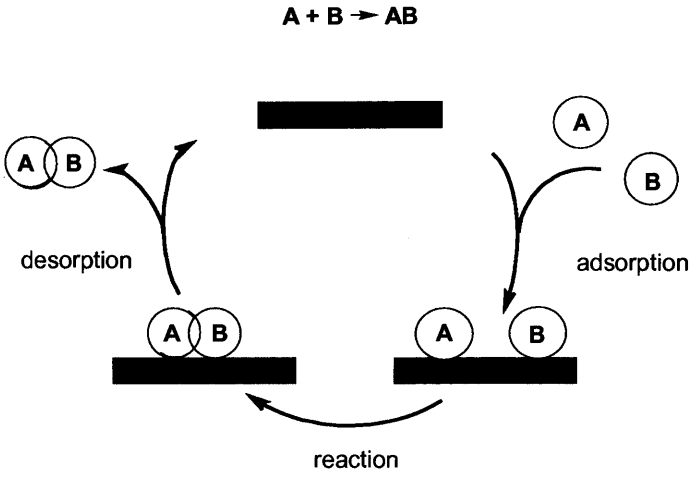

Figure 1.1 *Catalytic cycle*

The effect of a catalyst is purely kinetic therefore it is impossible to make a thermodynamically forbidden reaction work. The introduction of a catalyst to a system simply increases the rate at which a chemical reaction approaches equilibrium, without itself being consumed in the process. This is achieved by providing an alternative route for which the reaction can follow – one where the activation energy is lower, as shown below in figure 1.2. Activation energy is high in non-catalysed reactions due to the energy being expended to break bonds, before new bonds start to be made. Generally, catalysts reduce the activation energy by forming bonds, which eases the subsequent bond breaking and thus the time needed for the reaction to come to equilibrium is shortened. For example, a transition metal ion can catalyse a reaction by providing an alternative route between reactants and products, one that has a lower activation enthalpy. This is possible since transition metals are able to form stable compounds in many different oxidation states. During the reaction the transition metal ion is firstly oxidised by one reactant to a higher oxidation state before being reduced back to the original form by reaction with another reactant. The reactants are therefore converted to the same products as are formed without the catalyst except that the reactants are converted into the products more quickly.

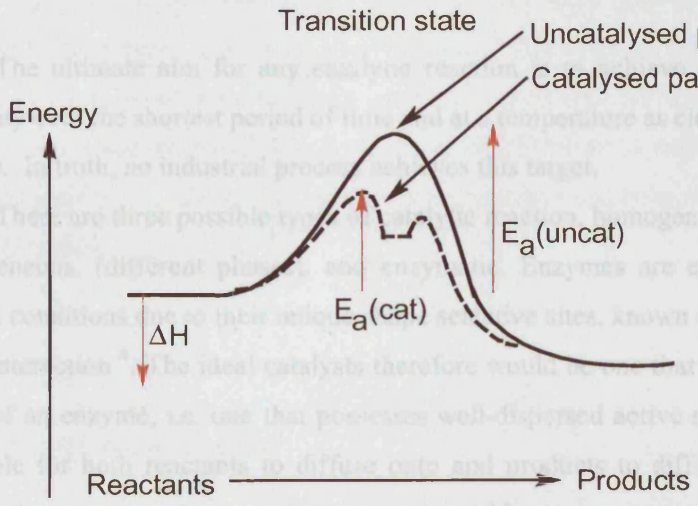

Figure 1.2 *Activation energy diagram*

The key characteristics of a good catalyst are its activity, long term stability and most importantly its selectivity. In the 1940's acid-treated clays used in catalytic cracking were found to have short lifetimes and gradually the more stable amorphous synthetic silica-alumina catalysts became the favoured choice. In 1960, Rabo et al. first reported synthetic zeolites to be exceptionally active and selective for the isomerisation of hydrocarbons. Their unique intracrystalline space available to reactant and product molecules lends them excellent shape-selective materials. Since this date, a large range of zeolites and materials with similar structures and properties have been synthesised and characterised and are presently used to catalyse a wide variety of industrially important reactions.

In today's society however the main challenge is concentrated around environmental issues, to reduce the amount of toxic and corrosive chemicals used and produced in present day processes by increasing their efficiency. Government laws are now starting to hit hard on chemical industries forcing them into either redesigning existing processes or developing entirely new processes whilst still ensuring economic viability. In general, catalytic research in today's society is directed around maximising yields and selectivities to ensure minimal waste and by-product formation.

1.2 Catalytic properties

The ultimate aim for any catalytic reaction is to achieve 100% activity and selectivity over the shortest period of time and at a temperature as close to ambient as is possible. In truth, no industrial process achieves this target.

There are three possible types of catalytic reaction, homogeneous (same phase), heterogeneous, (different phases), and enzymatic. Enzymes are extremely active at ambient conditions due to their unique shape selective sites, known as the lock and key model interaction [4]. The ideal catalysts therefore would be one that mimics the unique ability of an enzyme, i.e. one that possesses well-dispersed active sites that are easily accessible for both reactants to diffuse onto and products to diffuse away from the catalyst. A comparison between homogeneous and heterogeneous catalysis is shown in table 1.1.

	HOMOGENEOUS	HETEROGENEOUS
Form	Soluble metal complexes, usually mononuclear	Metals, usually supported, or metal oxides
Phase	Liquid	Gas/solid
Temperature	Low (<250^{0}C)	High (250-550^{0}C)
Activity	Moderate	High
Selectivity	High	Low
Diffusion	No problem	Can be very important
Heat Transfer	Facile	Can be problematic
Product Separation	Problematic	Facile
Catalytic Recycle	Expensive	Simple
Reaction Mechanisms	Reasonably well understood	Poorly understood
Example	Acetic acid synthesis (Monsanto process)	Methanol to Gasoline (MTG)

Table 1.1 *Homogeneous versus Heterogeneous catalysis*

1.2.1 Homogeneous Catalysis

Homogeneous catalysis' main importance is its high selectivity, the ability to produce very pure products in high yields. This is due to having more control over the rates of mixing, temperatures and gas feed of the reactants, than in heterogeneous catalysis since the reactant and catalyst are both in the same physical state [5].

In homogeneous catalysis it has been found that by selecting the ligands around the active centre, better reproducibility can be obtained together with greater control of catalyst poisons and increased selectivity. It should therefore be easier to design a more active homogeneous catalyst rather than a heterogeneous one because of the positioning of its active sites.

1.2.2 Heterogeneous Catalysis

Whatever the apparent advantages maybe in using homogeneous catalysts, industries prefer to use heterogeneous catalysts because of their higher activity,

robustness and ease of product separation. Examples of important heterogeneous catalysts include the use of zeolite H-ZSM-5 for the conversion of methanol to gasoline, Bi_2MoO_6 for the oxidation of hydrocarbons and TS-1 (titanosilicate–1) in the epoxidation of alkenes.

There are two types of solid heterogeneous catalysis namely bulk and supported catalytic materials. Bulk materials are uniform, whereas the supported materials have the active phase finely dispersed over the surface of another material that possesses a large surface area.

1.2.3 Shape selectivity

Weisz first proposed the concept of shape selectivity in molecular sieves in 1960 [6]. In today's society, this concept is of intense research. Zeolites and layered systems are both excellent shape selective catalysts. Layered materials, for example layered double hydroxides, are good since it is possible to vary their interlayer spaces by the intercalation of different ions, for example Keggin ions. In contrast, zeolites are rigid materials. They are made up of one-, two- or three-dimensional pores and channels lending them very efficient shape selective catalysts. Shape selectivity works by the catalyst sieving out unwanted reactants and/ or products (figure 1.3). For this reason, microporous catalysts are being used significantly more for clean technologies in many applications such as fuels, foodstuffs and pharmaceuticals [7].

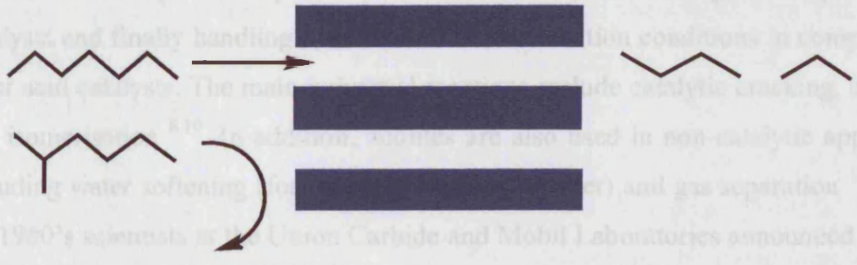

Figure 1.3 *Schematic of reactant shape selectivity*

1.3 Catalytic materials

1.3.1 Introduction to zeolites

The definition of Zeolite is 'the stone that's boils'. It was back in 1756 that a Swede named Crønsted used the term zeolite to describe the property of the mineral stilbite, which upon heating acts as if it is boiling. This name can be given to any microporous material composed of silicon and aluminium, that possesses cages and/ or channels of 3 – 10Å in diameter and is capable of accommodating water or other polar molecules within these voids [8]. Zeolites, also known as aluminosilicates, consist of an intricate framework structure of tetrahedral $Si(IV)O_4$ and $Al(III)O_4$, linked through oxygen atoms and arranged so as to avoid Al-O-Al linkages [9]. Substitution of Al(III) for Si(IV) imparts a negative charge on the neutral framework within a silica matrix which is compensated by charge balancing and exchangeable extra framework cations. When the cation is a proton, a Brønsted acid site is formed; this is the principle origin of solid acid properties in zeolites.

Zeolites occur naturally in the earth's crust, however, since they possess very useful properties a great deal of research has been carried out into the preparation of synthetic analogues, improving and expanding their capabilities and qualities.

Zeolites have been used extensively in the petrochemical, fine chemical and oil refining industries for several decades for a variety of different reactions due to their unique properties. Namely, their high surface area, large number of available structures ranging in pore size and diameter which can act as hosts for other ions such as transition metals, their unique microporous structures which lend them good shape selective catalysts and finally handling benefits and milder reaction conditions in comparison to other acid catalysts. The main industrial reactions include catalytic cracking, alkylation and isomerisation [8,10]. In addition, zeolites are also used in non-catalytic applications including water softening (for example washing powder) and gas separation [10]. During the 1960's scientists at the Union Carbide and Mobil Laboratories announced dramatic improvements in the use of zeolites as solid acid catalysts [11,12]. Since then, huge interest in this area has led to the development and discovery of a wide range of new materials and zeolites are now classed as catalysts of growing commercial importance and are having a huge impact in industrial processes [2,10].

1.3.1.1 Introduction to aluminophosphates

In the 1980's a new group of microporous materials, closely related to the aluminosilicates were synthesised. It was discovered that when small amounts of silicon in the aluminosilicate framework were replaced with phosphorous, a new material, silicoaluminophosphate (SAPO) was produced. On replacement of phosphorous for all the silicon, another new material, aluminophosphate (AlPO) was produced. These materials, also known as zeotypes, were soon followed by further synthetic analogues created by the substitution of other elements, including transition metals, from the periodic table for either aluminium or phosphorus. These materials are best known as metal substituted aluminophosphates, or MeAlPOs. However, certain limitations have been observed with these materials. For example regarding the amount of metal loading possible before the material becomes thermally unstable and the structure collapses on removal of the structure-directing agent (SDA) [13,14].

1.3.2 Introduction to polyoxometalates

Due to their unique catalytic properties allowing them to be synthesised either as a potential acid, redox or bifunctional catalyst [15,16], polyoxometalates possess a large range of applications. The catalytic reactions can be either homogeneous, heterogeneous or biphasic.

For many decades people have been interested in polyoxometalates because of their magnetic, structural and catalytic properties, not only in the chemical industry (as homogeneous and heterogeneous catalysts) but also in the medical (as antiviral and antitumoral agents) [17,18] and electronic industries (in magnetic and conductance studies) [19,20]. Polyoxometalates have been used as catalysts since the start of the last century, although it wasn't until the early 1970's that investigation's into the properties and behavioural aspects of polyoxometalates recognised the great potential of these materials for catalytic applications [16,20-22]. The majority of the pioneering work was carried out in Japan and Russia, of which the outcome has been many successful industrial applications, as shown in Table 1.2 [23].

Presently, catalytic applications are by far the most important use of polyoxometalates. As much as 80-85% of recent publications and patent applications on POM's are related in one way or another to catalysis [24]. Today's research is mainly concentrated in two important areas, acid catalysis and selective oxidation, with around 70% of the catalytic applications involving polyoxometalates of the Keggin structure.

Reaction	Phase	Catalyst	Year
Propene + H_2O → 2-Propanol	liquid-phase hydration	$H_4SiW_{12}O_{40}$	1972
Methacrolein + O_2 → Methacrylic acid	vapour-phase oxidation	Mo-V-P-POM	1982
Isobutene +H_2O → Isobutanol	liquid-phase hydration	$H_3PMo_{12}O_{40}$	1984
THF + H_2O → polymeric diol	biphasic polymerisation	$H_3PW_{12}O_{40}$	1985
n-Butenes + H_2O → 2-Butanol	liquid-phase hydration	$H_3PMo_{12}O_{40}$	1989
Ethylene + O_2 → Acetic Acid	direct oxidation	Pd-$H_4SiW_{12}O_{40}$	1997
Ethylene + Acetic acid → Ethyl Acetate	direct reaction in the vapour phase	$H_4SiW_{12}O_{40}/SiO_2$	2001

Table 1.2 *Industrial processes catalysed by polyoxometalates*

In the late 1990's Misono et al [21,25] categorised catalytic reactions by polyoxometalates into three types, table 1.3 [26]. The surface type applies to Langmuir-Hinshelwood processes that occur on the surface of both bulk and supported polyoxometalates. The bulk type I category applies to acid catalysis by a bulk polyoxometalate for the conversion of a polar substrate which is able to absorb into the catalyst. Whilst the third category, bulk type II, applies to catalytic oxidation's that occur predominantly on the surface on the catalyst.

TYPE	COMMENT	EXAMPLE
Surface Type	Common type of surface reaction, e.g. Langmuir-Hinshelwood type *Rate α catalyst surface area*	Alkane Isomerisation Oxidation of aldehydes, CO
Bulk Type I	"Pseudoliquid Phase"; reactants absorb in the solid bulk and react pseudohomogeneously *Rate α catalyst volume (weight)*	Dehydration of *I*-PrOH
Bulk Type II	Reaction occurs on the surface, with the bulk diffusion of e^- and H^+ playing a key role *Rate α catalyst volume (weight)*	Oxidative dehydrogenation Oxidation of H_2

Table 1.3 *Different types of heterogeneous catalysis attainable using polyoxometalates*

1.4 Catalytic reactions

1.4.1 Oxidation catalysis

The oxidation of organic compounds with high selectivity is of extreme significance in today's chemical industries. Important reactions include the transformation of alcohols, the oxidation of sulphides to sulphoxides and alkenes to epoxides and diols [27,28]. This thesis has concentrated on one small area of this field, namely epoxidation.

Epoxides are of great importance and as a result much research is concentrated in this area. Epoxides can be easily transformed into a number of products including diols, allylic alcohols and ketones. The epoxidation reaction can be carried out using a number of different oxidants however many produce large amounts of waste. Several on the other hand are classed as 'green' since a high percentage of active O_2 is produced and the by-products are of no harm to the environment (table 1.4) [29,30].

Oxidant	% Active Oxygen	By-product
O_2	50/100	H_2O/none
H_2O_2	47	H_2O
O_3	33	O_2
N_2O	36	N_2
NaOCl	21	NaCl
CH_3COOOH (peracetic acid)	21	CH_3COOH (acetic acid)
t-C_4H_9OOH (TBHP)	18	*t*-C_4H_9OH (*t*-butanol)
CrO_3	16	Cr^{3+} salts
MnO_2	19	Mn^{2+} salts

Table 1.4 *Comparison of oxidants used within industry*

The incorporation of redox metals (transition metals) into acidic materials produces interesting heterogeneous redox oxidation catalysts. The absorption properties of a redox molecular sieve can be altered due to the hydrophobic – hydrophilic character of the material. This feature increases the activity and selectivity of the material in that it is able to choose which reactants are adsorbed into the pores. One example of a commercial oxidation catalyst is the use of TS-1 for the production of catechol and hydroquinone from phenol [31,32].

1.4.2 Acid catalysis

This is another very important area of research within today's chemical industries. One example of an acid catalyst is a polyoxometalate, these are strong solid acid catalysts and have the potential for use in reactions such as alkylation and skeletal isomerisation of hydrocarbons. Zeolites are another example of a strong solid acid catalyst. Their catalytic interests stem from the possibility to substitute different metal ions within their microporous frameworks altering the acidic strength of the material. Zeolites are commonly used in industrial applications as hydrocarbon cracking catalysts.

1.5 Preparation of catalytic materials

The route to synthesising a catalyst can have a large impact on its catalytic properties. When preparing catalysts, many different features must firstly be addressed. For example; nature of the surface required, structure of the active sites, porosity, surface area, stability, regenerability, cost, toxicity and application [29].

Synthesis of these materials can be achieved via several different methods including precipitation, where the catalytically active phase is generated as a new solid phase and impregnation where the active phase is deposited on a pre-existing support material. Precipitation is most commonly used in the production of solid acid catalysts and centres around the mixing of aqueous metal salts and alkali solutions. The formation of a new solid phase material is achieved through either physical (i.e. temperature (hydrothermal techniques), agitation) or chemical (pH and ionic strength) transformations and is a result of particle nucleation and subsequent amassing of the particles. Depending on the final application, the solid phase may require further processing in order to increase the catalyst's activity, in the form of ageing, washing, filtration, drying, grinding, impregnation and calcination.

Multi-component systems, for example zeolites, use a co-precipitation method (also known as the sol-gel method) in order to obtain homogeneity. This homogeneity however is also dependent on preparative techniques, including temperature, pH and even the order of addition of the reactants.

Impregnation is used when small amounts of the active phase are required to be deposited on the support material. This technique is effective in predetermining the catalytic properties of the final catalyst (e.g. particle size and dispersion) through the choice of support material and aqueous phase concentration, temperature, pH and ionic strength [33].

1.6 Characterisation of catalysts

The different physical properties of a catalyst can be measured using a variety of techniques. For example, the surface area can be measured using nitrogen physisorption, typically calculated using the BET method and the type of acid sites can be determined using temperature programmed desorption (TPD) typically with pyridine or ammonia. Other techniques can be carried out *in situ,* these studies are very important in understanding changes in the catalyst during a reaction. These techniques include the examination of phase purity and crystallinity by X-ray diffraction (XRD), co-ordination and oxidation states by X-ray absorption spectroscopy (XAS) and infrared (IR) analysis [34,35,36].

In conclusion, the application of such techniques can aid the understanding of how a catalyst functions during a reaction. This information can ultimately help optimise the synthesis of the catalyst and subsequently improve the efficiency of the catalytic reaction.

1.7 References

(1) Johnson Matthey website, http://www.synetix.com/technical/catalysts.htm, 2002.

(2) Thomas, J. M.; T., Thomas, W.J. *Principles and Practice of Heterogeneous Catalysis*; VCH Weinheim, 1997.

(3) Dobereiner, J. W. *Ann Chim Phys (Paris)* 1823, *24*, 91-95.

(4) Cooper, G. M., http://www.ncbi.nlm.nih.gov/books/bv.fcgi?tool=bookshelf&call=bv.View..ShowSection&searchterm=enzymes&rid=cooper.section.279, 2000.

(5) Whyman, R. (conference notes) *Catalysis Fundamentals and Practice*, 2001.

(6) Degnan, T. F. *Journal of Catalysis* 2002, *216*, 32-46.

(7) Sankar, G. L., Lewis, D.W. (private communication) 1998.

(8) Kang, M. *Journal of Molecular Catalysis a-Chemical* 2000, *160*, 437-444.

(9) Li, J.; Xiong, G.; Feng, Z.; Liu, Z.; Xin, Q.; Li, C. *Microporous and Mesoporous Materials* 2000, *39*, 275-280.

(10) Olah, G. A.; Molnar, A. *Hydrocarbon Chemistry*; Wiley, New York, 1995.

(11) Plank, C. J.; Rosinski, E. J.; Hawthorne, W. P. *Ind. Eng. Chem. Prod. Res Dev.* 1964, *3*, 165-168.

(12) Popova, M.; Minchev, C.; Kanazirev, V. *Applied Catalysis a-General* 1998, *169*, 227-235.

(13) Popova, M.; Minchev, C.; Kanazirev, V. *Reaction Kinetics and Catalysis Letters* 1998, *63*, 379-384.

(14) Rabo, J. A. *Catalysis Reviews-Science and Engineering* 1981, *23*, 293-313.

(15) Kozhevnikov, I. V. (conference notes), NATO ASI, Polyoxometalate Molecular Science, 2001.

(16) Kwon, T.; Doeuff, M.; Pinnavaia, T. J. *Abstracts of Papers of the American Chemical Society* 1989, *198*, 253-263.

(17) Kwon, T.; Tsigdinos, G. A.; Pinnavaia, T. J. *Journal of the American Chemical Society* 1988, *110*, 3653-3654.

(18) Maestre, J. M.; Lopez, X.; Bo, C.; Poblet, J. M.; Casan-Pastor, N. *Journal of the American Chemical Society* 2001, *123*, 3749-3758.

(19) Mair, J. A.; Waugh, J. L. T. 1950, 2372-2376.

(20) Manasse, E. *Atti Soc. Toscana Sci. Nat.* 1915, *24*, 92-94.

(21) Kozhevnikov, I. V. *Chemical Reviews* 1998, *98*, 171-198.

(22) Marignac, C. *Ann. Chem. Phys.* 1863, *69*, 41-48.

(23) Misra, C.; Perrotta, A. J. *Clays and Clay Minerals* 1992, *40*, 145-150.

(24) Mizuno, N.; Kiyoto, I.; Nozaki, C.; Misono, M. *Journal of Catalysis* 1999, *181*, 171-174.

(25) Mizuno, N.; Misono, M. *Chemical Reviews* 1998, *98*, 199-217.

(26) Mizuno, N.; Nozaki, C.; Hirose, T. O.; Tateishi, M.; Iwamoto, M. *Journal of Molecular Catalysis A - Chemical, 1997, 117, 159-168.*

(27) Mallat, T.; Baiker, A. *Catalysis Today* 2000, *57*, 1-2.

(28) Raja, R.; Thomas, J. M. *Jounal of Molecular Catalysis A - Chemical* 2001, 3-14

(29) Thomas, J. M.; Raja, R. *Chemical Communications* 2001, 675-687.

(30) Shilov, A. E.; Shul'pin, G. B. *Chemical Reviews* 1997, *97*, 2879-2932.

(31) Perego, C.; Carati, A.; Ingallina, P.; Mantegazza, M. A.; Bellussi, G. *Applied Catalysis A - General* 2001, 221, 63-72.

(32) Clerici, M. G.; Ingallina, P. *Catalysis Today* 1998, *41*, 351-355.

(33) Schwarz, J. A. *Chemical Review* 1995, *95*, 477-493.

(34) Niemantsverdriet, J. W. (conference notes) *Catalysis fundamentals and practice*, 2001.

(35) Thomas, J. M.; Catlow, C. R. A.; Sankar, G. *Chemical Communications* 2002, 2921-2925.

(36) Muncaster, G.; Davies, A. T.; Sankar, G.; Catlow, C. R. A.; Thomas, J. M. *Phys. Chem. Chem. Phys.* 2000, *2*, 3523-3527.

Chapter 2

Experimental Methods

2.1 Chapter Overview

Many different experimental techniques have been used to characterise the materials studied throughout this thesis. Similarly several pieces of analytical equipment have been used to analyse reactants and products from the subsequent catalytic reactions. This chapter focuses on discussing the basic theory behind the use of these techniques and the interpretation of the data obtained.

2.2 Synthesis of aluminophosphates (AlPOs), silicoaluminophosphates (SAPO's) and their metal substituted analogues

Synthesis of AlPOs and their metal substituted analogues is performed using hydrothermal conditions. An aluminium source (usually aluminium hydroxide ($Al(OH)_3$)), phosphorus source (typically phosphoric acid (H_3PO_4)), water and a structure-directing agent (SDA) (normally an amine, what kind depends on the framework required to be synthesised) were vigorously stirred to form a homogeneous gel. If a metal substituted aluminophosphate (MeAlPO) is required, then the metal (usually a soluble metal salt) is added in solution at this point. The resulting gel is placed into an autoclavable Teflon liner with lid and this placed into a metal autoclave. This is securely fastened then placed into an oven for anything from one hour to one week and at temperatures ranging from 140-240°C dependent once again upon the framework being synthesised and the amount of substituent being incorporated. Apart

from the SDA, time, temperature and species of metal ion required to form a phase pure material, the pH of the gel is also a critical parameter in the synthesis.

Synthesis of SAPO's and their metal substituted analogues is identical to the above method except that a silicon source (usually fumed silica (SiO_2)) is also used in the preparation.

Other synthesis techniques that have more recently been created for the preparation of SAPO's include the rapid crystallisation method [1,2]. This method aims to produce a homogeneous gel mix, which the authors demonstrate is essential in obtaining a satisfactory catalyst for the MTO reaction. The preparative method involves the addition of seed crystals, milling for a period of time, treatment with ultrasonic waves and the further treatment with a rapid crystallisation programme. Consequently they were able to produce small, uniform crystals with low internal and external surface acid densities.

2.3 X-ray diffraction

X-ray diffraction (XRD) is commonly used for the study of long-range ordering of materials. Throughout this thesis this technique has been used solely to study the purity and crystallinity of the materials since their crystallographic structures have been previously characterised and reported and can be checked against a database to clarify that they are indeed phase pure [3].

2.3.1 Theory of X-ray diffraction

M. Von Laue first discovered the diffraction of X-rays in 1912 and thanks to his work, the arrangement and spacing of atoms in crystalline materials have since been deduced leading to a clearer understanding of the physical properties of materials [4,5].

However it was W. L. Bragg whom in 1913 derived a simple mathematical equation (equation 2.1) to explain why it was that the faces of crystals reflected X-ray beams, as a function of incident angle (θ) and the distance (d) between the atomic layers in a crystal [6]. The variable lambda (λ) is the wavelength of the incident X-ray beam and n is an integer.

$$n\lambda = 2d\sin\theta \qquad (2.1)$$

Bragg's Law can be determined by considering the conditions required to make the phases of the beams coincide when the incident angle equals the reflecting angle. For example, when two incident beams hit the material in parallel at the same point but at different atomic planes, the top beam strikes the top layer at atom z but the second photon strikes at a lower plane, angle θ. This beam has to travel twice the distance (i.e. AB+BC = 2θ) so as to continue travelling parallel with the first photon (figure 2.1). Translating this difference into d-spacing produces a diffraction pattern.

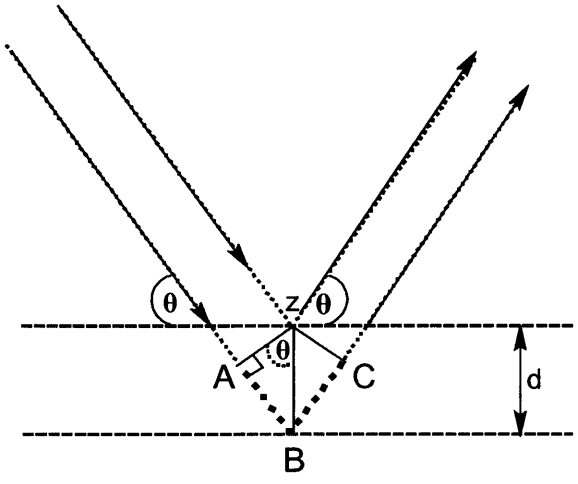

Figure 2.1 *Schematic showing the derivation of Bragg's Law using reflection geometry. The lower beam has to travel double the distance of the top beam in order to continue travelling in parallel*

Diffraction patterns were collected on fine homogeneous powder samples in angular-dispersive mode using Bragg-Brentano geometry. The diffractometer used was a Siemens D500 equipped with an X-ray tube and copper target. A schematic of the XRD is shown in figure 2.2.

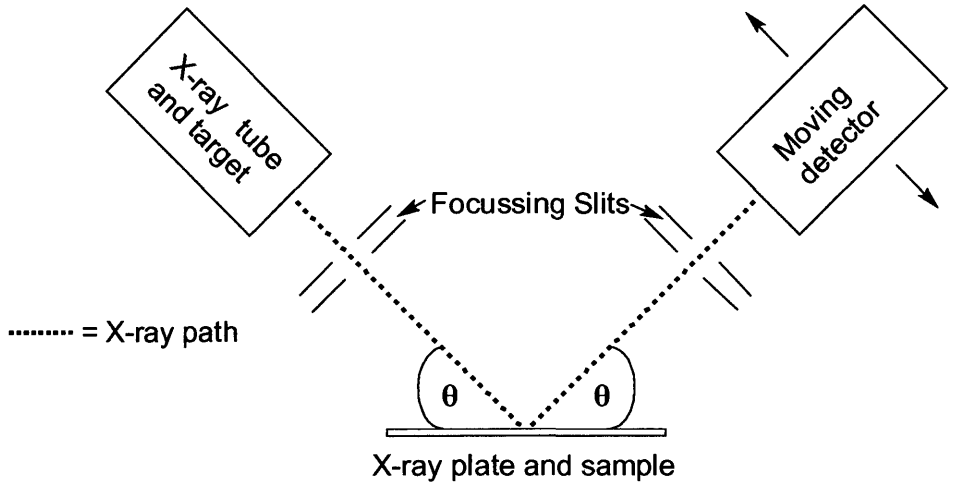

Figure 2.2. *Schematic of the laboratory based angular-dispersive X-ray Diffractometer using Bragg-Brentano geometry (the arrows show the stepwise movement the detector takes when collecting reflections at 2θ values)*

XRD data was converted into x_y mode and extracted as a diffraction pattern though powder cell and Origin 5.0 computer programs.

2.4 Synchrotron radiation for the characterisation of materials

Synchrotron radiation (SR), particularly in the form of X-ray absorption spectroscopy (XAS), has been used throughout this research to determine the local structure around the atoms under examination. From the information gathered, the bond lengths and co-ordination geometry of the material were obtained. The work undertaken during this research was carried out on a number of stations at the SRS Daresbury Laboratories, United Kingdom and at the European Synchrotron Radiation Facility (ESRF), France.

When electrons, accelerated in magnetic fields, are deflected from their course SR is emitted [7,8]. Scientific benefits were uncovered from the use of this technique, which led to the construction of storage rings solely for this purpose [7]. Figure 2.3 below depicts the basic fundamentals associated with a storage ring. The electrons are initially fired from a linear accelerator (LINAC) into the booster ring where they are further accelerated prior to being injected into the storage ring. The storage ring consists of numerous bending magnets, whose purpose is to constrain the electron orbit under vacuum. When they reach a bending magnet within the ring the SR that they emit is subsequently utilised for analysis purposes on numerous stations situated around the periphery of the storage ring at different intervals. The loss in energy has to be replenished at least once a day by the introduction of a new batch of electrons into the storage ring via the LINAC.

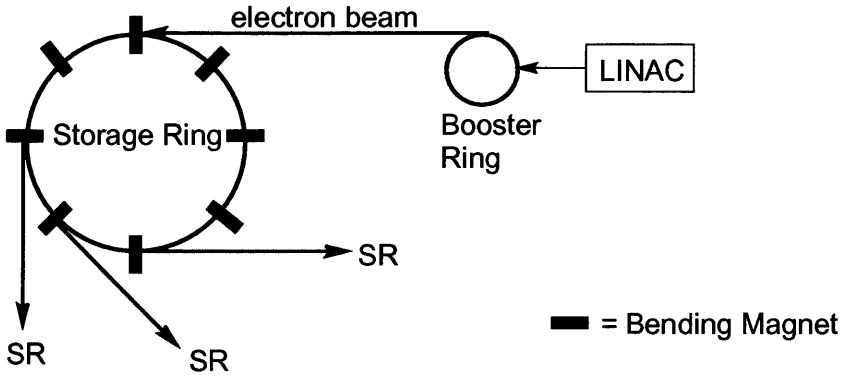

Figure 2.3 *Schematic of a second-generation storage ring, depicting the angular output of SR from the bending magnets*

2.4.1 X-ray Absorption Spectroscopy (XAS)

The benefit of this technique is that it provides structural and electronic information on the catalyst under analysis similar to X-ray Diffraction, except that information can be obtained here even when long-range order is absent. Structurally it can provide information on the interatomic distance between the metal in question and the first, second, third and fourth nearest neighbouring atoms. Additionally it can give information on the co-ordination number of the metal being studied. XAS also has the very important added benefit of obtaining information *in situ,* therefore ultimately being able to study a catalyst throughout a reaction.

When an X-ray beam is shone on a material, photons are absorbed by atoms and on passing through the sample the intensity I of the beam is decreased. The amount of reduction dI, is determined by the materials absorption characteristics and can be calculated using equation 2.2 below.

$$dI = -\mu(E)Idt \qquad (2.2)$$

Where: dt = Path length of the radiation through the material

$\mu(E)$ = Linear absorption coefficient.

Lambert's law (equation 2.3) attenuates the varied energy of the X-ray photons as they pass through a sample, achieved by integration of equation 2.2 over t, the total thickness of the material being analysed [9,10].

$$I = I_0 e^{-\mu(E)t} \qquad (2.3)$$

Where: I and I_o are the transmitted and incident radiation intensities, respectively.

An absorption spectrum (figure 2.4) comprises of three main regions, namely the pre-edge, edge and post-edge. The first part pre-edge and the edge regions are also called X-ray absorption near edge structure (XANES) and the post-edge is termed as Extended X-ray absorption fine structure (EXAFS). The absorption process is due to incoming photons exciting a bound or occupied electron from the core energy level to a vacant state.

XAS data is analysed by the use of several steps. Data collected on the SRS is obtained as a list of values from the several signal detectors collected at various points in the spectrum. These points are defined by the position of the monochromator in milli-degrees. In order for the EXAFS oscillations to be extracted from the spectrum, the x-axis must be turned into energy by converting the milli-degree scale into eV and the y-axis into absorption by dividing the signal reading by the reference reading for fluorescence data (EXCALIB). The absorption is then background subtracted by removing the smooth background curve of the pre-edge and post-edge regions (EXBROOK) to give the EXAFS. Finally the EXCURV98 program is used to refine the local structure around the atom under investigation.

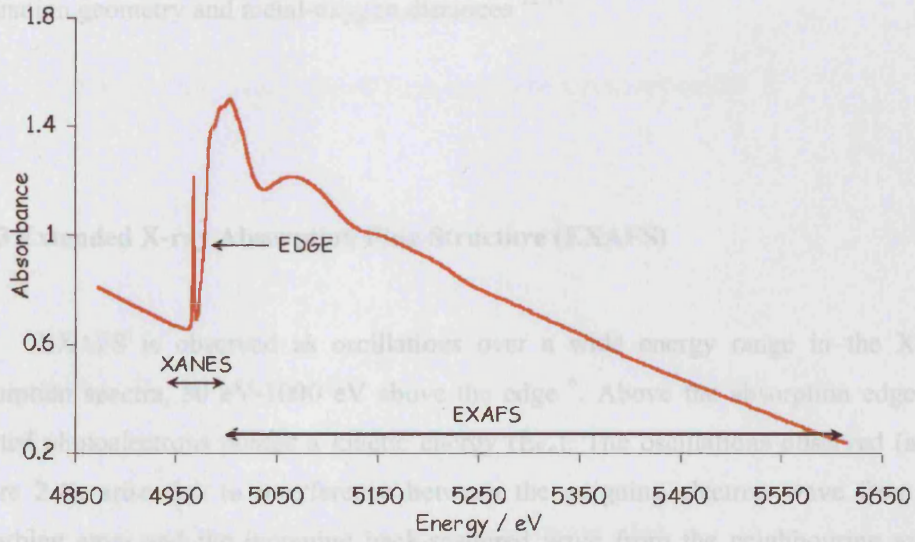

Figure 2.4 *Schematic of an XAS spectrum depicting the three main regions observed when characterising a material*

2.4.2 XANES

This region is associated with an initial decrease in intensity due to mass absorption followed by a sudden increase caused by electrons being excited to vacant or partially occupied states. Different classes of absorption are observed depending on whether the X-ray energy excites the electron from the 1s level, producing a K-edge, or 2s, $2p_{1/2}$, or $2p_{3/2}$, resulting in LI or LII or LIII absorption edges, respectively [10].

This region around 50 eV below and 100 eV above the absorption edge, as shown in figure 2.5, contains information regarding the oxidation state, co-ordination number and local structure of the absorbing species as it is associated with the excitation process of electrons to bound or quasi-bound states [10,11]. In the pre-edge region, a sudden increase may be observed due to transition from the core level to a partially occupied state, for example the 3d state of a first row transition metal. This transition is sensitive to the coordination geometry of the absorbing atom as well as the electronic state. The transition observed on the top of the edge also provides information about the coordination geometry. For example, a higher intensity is observed for octahedrally co-ordinated systems than for tetrahedral ones since there is less multiple scattering effects for tetrahedral geometry compared to octahedral. In addition, this intensity can be enhanced through other multiple scattering effects, co-ordination geometry and metal-oxygen distances [12-14].

2.4.3 Extended X-ray Absorption Fine Structure (EXAFS)

EXAFS is observed as oscillations over a wide energy range in the X-ray absorption spectra, 50 eV-1000 eV above the edge [6]. Above the absorption edge the ejected photoelectrons posses a kinetic energy (E_{Ke}). The oscillations observed (as in figure 2.4), arise due to interference between the outgoing electron wave from the absorbing atom and the incoming back-scattered wave from the neighbouring atoms (figure 2.5).

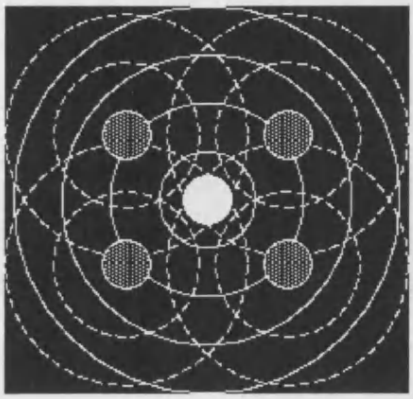

Figure 2.5 *Radial portion of the outgoing photoelectron wave (solid lines) being backscattered by the neighbouring atoms (dotted lines) (the white circle portrays the excited atom whilst the grey circles are its four nearest neighbours)*

The wave vector, represented by k, is outlined in equation 2.4 [10,11].

$$k = \sqrt{(2m/\hbar^2).(E-E_o)} \qquad (2.4)$$

Where: m = Electron mass

$\hbar = h/2\pi$ (where: h = Planck's constant)

E = Energy of the X-ray

E_o = Energy of the X-ray at the absorption edge

Experimentally the result of the interference, seen as oscillations in the XAS data, can be described as in equation 2.5 below.

$$\mu_{total} = \mu_o[1+\chi ex] \qquad (2.5)$$

Where: $\mu(E)$ = Linear absorption coefficient

χex = Sum of all the interference from neighbouring atoms

The sum of the total interference consists of the amplitude of the oscillations, $A_j(k)$, and the phase which is represented by a sine function, $(sin\ \Phi_j(k))$ and is given as,

$$\chi(k) = \Sigma A_j(k)\ sin\ \Phi_j(k) \qquad (2.6)$$

Where: χ = EXAFS function.

The amplitude and sine parts can both be further expanded as shown below in equations 2.7 and 2.8.

$$sin\ \Phi_j(k) = sin\ [2kR_j - \Phi_j(k)] \qquad (2.7)$$

Where: R_J = The interatomic distance between the adsorbing and scattering species

$\Phi_j(k)$ = Phase shift for both the central absorbing atom and the back scattering one

$$A_j(k) = (N_j/kR_j^2)\ S_o^2 F_j(k) e^{-2k\sigma j^2} e^{-2Rj/\lambda j(k)} \qquad (2.8)$$

Where: N_j = The number of atoms of type j at a distance or R_j (Coordination number)

R_j = Interatomic Distance

σ_j^2 = Mean square relative displacement which is due to both static and thermal disorder

$F_j(k)$ = Back-scattering amplitude factor, as a function of k

S_o^2 = Amplitude reduction factor

$\lambda_j(k)$ = Mean free path of the photoelectron

2.4.4 Fluorescence mode

Fluorescence mode is used when analysing low concentrations of absorbing species. Data is recorded over several individual fluorescence detectors giving a better sensitivity to the XAS measurements since the background absorption is reduced [10]. Figure 2.6, demonstrates the positioning of apparatus used to record XAS data. The sample itself was loaded into an *in situ* cell (figure 2.7) prior to analysis so that it could be analysed under any required environment.

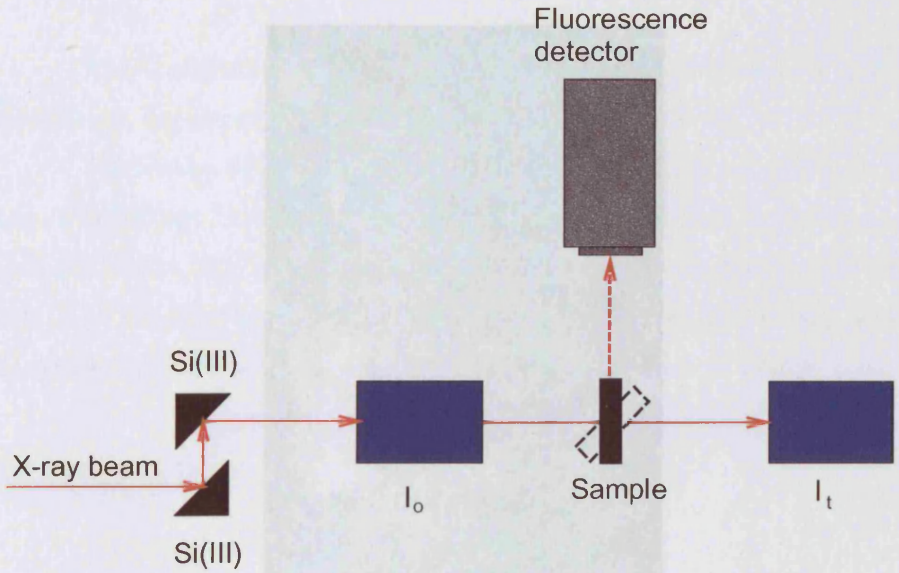

Figure 2.6 *Schematic of the positioning of a fluorescence detector when collecting XAS data. The sample is placed in the beam at 0-45° (dashed line) between the incident (I_o) and transmission (I_t) ion chambers*

All XAS data in this thesis were collected in the fluorescence mode since the concentration of absorbing species was very low.

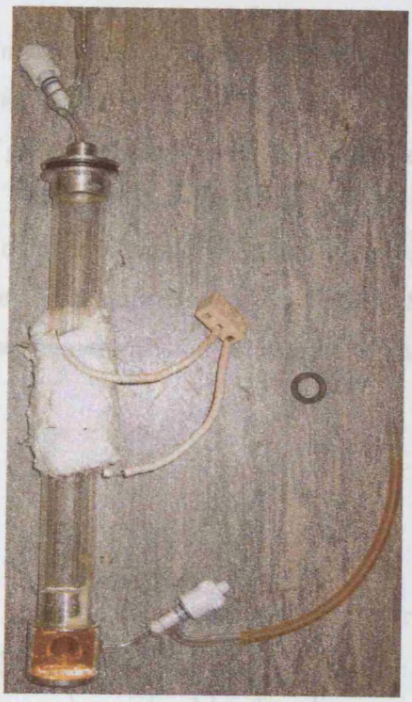

Figure 2.7 *In situ cell used for XAS experiments*

2.5 Gas-liquid Chromatography (GLC)

Two Gas chromatographs were used throughout this thesis, one for gaseous analysis and the other for liquid analysis.

The concept of gas-liquid chromatography was first discovered back in 1941 by Martin and Synge [5,15]. This technique involves a sample being vaporised and injected onto the head of the chromatographic column, where it is then carried through the column by a flow of inert, gaseous mobile phase (figure 2.8). The column itself contains a liquid stationary phase, immobilised on the surface of an inert solid.

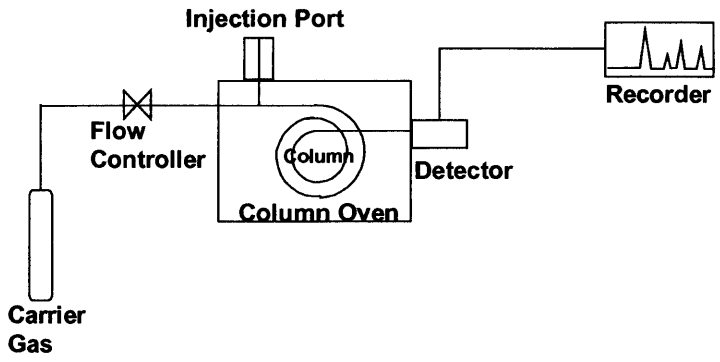

Figure 2.8. *Schematic representation of a gas-liquid chromatograph*

The inert carrier gas used is often dependent upon the type of detector used. During this research, helium (80 psi) was used. Nitrogen may also be used except occasionally it may interfere with the resolution of particular peaks. The carrier gas passes through a molecular sieve trap prior to entering the GC in order to remove water and other impurities.

Temperature ramping was used to control the elution of components from a sample, especially if the sample had a wide boiling point range. The column

temperature was increased stepwise as separation occurred, so as to achieve optimum separation over a minimum time span.

Sample volumes for each of the reactions varied, typical volumes were between 0.1 and 0.5μL. In order to achieve optimum column efficiency, the sample was introduced onto the column either using a rotary sample valve (for gaseous analysis) or a microsyringe (for liquid analysis). The temperature of the injection port was set at a constant high temperature, >250°C, so that all the material evaporated onto the column.

2.5.1 Rotary sample valve

Due to the GC being used for on-line analysis for the MTO reaction, a sample loop was used to inject material onto the column (figure 2.9). The rotary sample valve was set automatically via the GC so that at a specified time after the GC programme had started the sample loop ABC was filled with the sample. The valve then rotated by 45°C and a reproducible volume of sample (that originally was in the loop ABC) was introduced onto the column. The valve then rotated back to its original position where it vented to atmosphere.

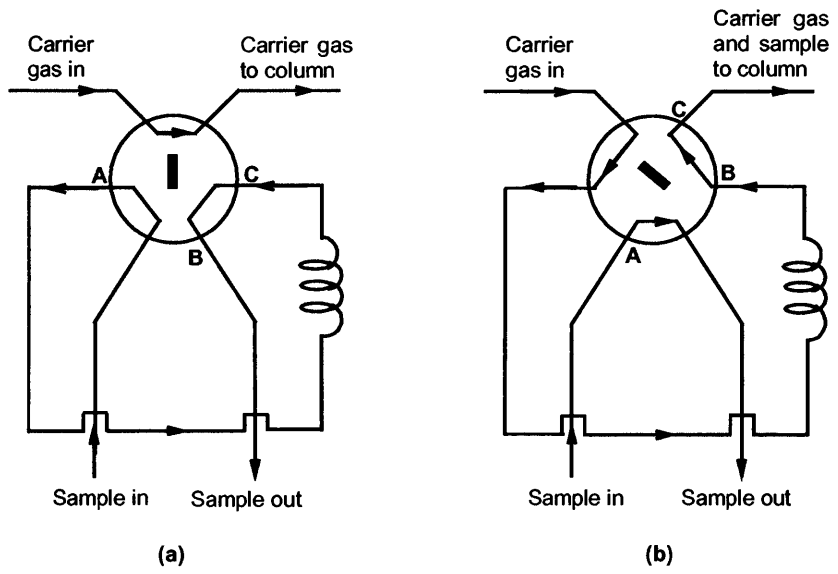

Figure 2.9 *Schematic of a rotary sample valve for (a) filling sample loop ABC and (b) introduction of sample onto the column*

2.5.2 Split/ splitless injection

Some reactions involved the use of splits to control the amount of sample injected onto the column. If the injector is in the split mode, then the carrier gas can enter the vaporisation chamber and exit by three different routes. When the sample is injected through the septum, it vaporises and forms a mixture of carrier-gas, vaporised solvent and vaporised solutes. This mixture then passes onto the column, the quantity depending on the split ratio chosen. The septum purge outlet is used in order to prevent any of the septum bleed components from entering the column. Figure 2.10 shows a split/splitless injector.

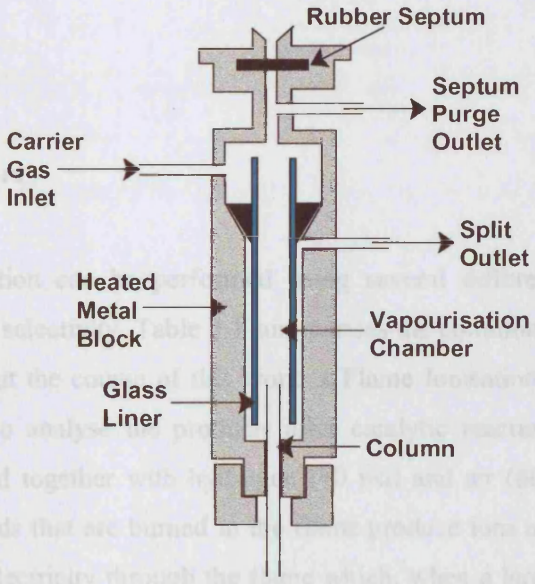

Figure 2.10 *Schematic of a split/ splitless injector*

2.5.3 GC columns

Two types of column were used throughout this thesis, capillary columns (for liquid analysis) and packed columns (for gaseous analysis). Capillary columns are more efficient than packed columns because the internal diameter of a capillary column is only a few tenths of a millimetre. There are two types available: wall-coated open tubular (WCOT) or support-coated open tubular (SCOT). WCOT columns, the more efficient of the two, are coated with a liquid stationary phase, whereas for the SCOT columns, the inner wall is lined with a thin layer of support material, onto which the stationary phase has been adsorbed. In comparison, packed columns are made from glass, metal or Teflon typically 2-3 metres long with an I.D. of 2-4mm. The tubes are tightly packed with solid support or packing material, coated in a thin layer of the stationary phase.

2.5.4 GC detectors

GC detection can be performed using several different methods, all giving different types of selectivity. Table 2.1 summarises the common GC detectors.

Throughout the course of this work, a Flame Ionisation Detector (FID) (figure 2.11) was used to analyse the products after catalytic reaction. The gases from the column are mixed together with hydrogen (40 psi) and air (60 psi) and ignited. Any organic compounds that are burned in the flame produce ions and electrons. These are able to conduct electricity through the flame which, when a large electrical potential is applied at the burner tip, a collector electrode located above the flame produces a current that is then measured. The advantages of using a FID detector are that it is very efficient in the detection of organic compounds, it is highly sensitive, has a large linear response range, and low background noise. The only main disadvantage with using a FID is that it destroys the sample.

Detector	Type	Support gases	Selectivity	Detectability	Dynamic range
Flame ionisation (FID)	Mass Flow	Hydrogen and Air	Most organic compounds	100 pg	10^7
Thermal Conductivity (TCD)	Concentration	Reference	Universal	1 ng	10^7
Electron capture (ECD)	Concentration	Make-up	Halides, nitrates, nitriles, peroxides, anhydrides, organometallics	50 fg	10^5
Nitrogen-phosphorus	Mass flow	Hydrogen and air	Hydrogen and air	10 pg	10^6
Flame photometric (FPD)	Mass flow	Hydrogen and air possibly oxygen	Oxygen Sulphur, phosphorus, tin, boron, arsenic, germanium, selenium, chromium	100 pg	10^3
Photo-ionisation (PID)	Concentration	Make-up	Aliphatics, aromatics, ketones, esters, aldehydes, amines, heterocyclics, organosulphurs, some organometallics	2 pg	10^7
Hall electrolytic conductivity	Mass flow	Hydrogen, oxygen	Halide, nitrogen, nitrosamine, sulphur		

Table 2.1 *Characterisation of the detectors commonly used in GC* [15]

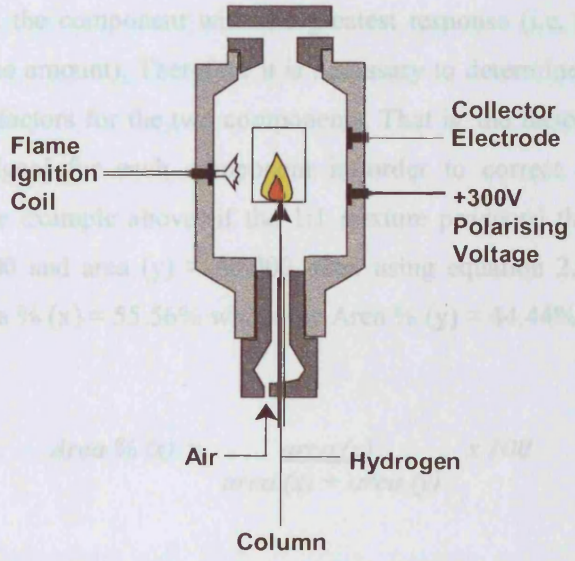

Figure 2.11 *Schematic of a Flame Ionisation Detector (FID)*

2.5.5 Quantitative and qualitative analysis

Quantitative analysis was based upon a comparison of the area beneath the analyte peak, i.e. peak area, with that of a known standard.

2.5.5.1 Peak area analysis

With almost any detector used on a chromatograph (GC or LC) the signal produced for a fixed amount of different substances can be very different. The degree to which a component produces a signal is called the response, with some compounds having a very good response (e.g. hydrocarbons on an FID) and other compounds having a very poor response (e.g. halocarbons on an FID). If you were to prepare a two

component mixture (x/y) of a known composition (50% each) containing compounds with different responses, then the area percent report produced would show the analysis weighted towards the component with the greatest response (i.e. it produces a better signal for the same amount). Therefore it is necessary to determine what are known as relative response factors for the two components. That is, the factor which needs to be applied to the signal for each component in order to correct it for the different responses. For the example above, if the 1:1 mixture produced the following results, area (x) = 100,000 and area (y) = 80,000, then using equation 2.9 the results would show that the Area % (x) = 55.56% whilst the Area % (y) = 44.44%.

$$Area\ \%\ (x) = \frac{area\ (x)}{area\ (x) + area\ (y)} \times 100 \qquad (2.9)$$

It is obvious that component (x) has a better response than component (y). Using their response factors (equation 2.10) the results can be corrected and hence the true percentages can be calculated. This type of calculation is called normalisation.

$$Response\ Factor\ (x) = Area\ (x) / True\ \% \qquad (2.10)$$

It is common to fix one of the response factors at unity and ratio all the others to it. In the above example, these would be, RRF (x) = 1 and RRF (y) = 0.8.

Retention time (RT) is measured with respect to a standard whose elution time is known. For example in the case of the MTO reaction methane was used. Relative retention times (RRT's) are then calculated accordingly (equation 2.11) for all other analytes.

$$\frac{RT\ (analyte)}{RT\ (methane)} = RRT \qquad (2.11)$$

2.5.5.2 Standardising a chromatographic method

There are two types of standards, internal and external. Internal standards are most frequently used because they achieve the highest precision for quantitative analysis since errors such as sample injection, flow rate and column conditions are excluded. With the use of an appropriate internal standard precision's of between 0.5% and 1% are achievable, whereas errors >5% are acquired when using an external standard.

2.5.5.2.1 Internal standardisation

Not all components will have a linear response and for this reason, it is important either to prepare a standard that closely represents the sample composition, or to prepare multiple standards (different compositions) and determine a calibration curve. Once the response factors have been obtained you can determine the composition of any mixture of x and y, but only when these are the only two components present. If a third component were present, then to calibrate the GC an Internal Standard method is used. The retention time of the standard should not coincide with any of the other components in the sample mixture. For example for the phenol hydroxylation reaction, mesitylene was used as the internal standard. Here the RRF for mesitylene is fixed at 1 and all the others proportioned accordingly.

2.6 Infrared (IR) absorption spectroscopy

Infrared analysis has been applied within this thesis as a qualitative tool to characterise specific co-ordination of substituents within the framework materials and moreover to ascertain as to whether further materials had been successfully formed (chapter 6, section 6.4.2.3).

The mid infrared region encompasses wavelengths between 4000-200 cm^{-1} [5,15]. Solid samples were finely dispersed in potassium bromide (KBr) (100mg KBr : 1mg catalyst) prior to analysis. Characterisation was achieved by observation of functional group absorption frequencies, associated with the vibrations from the interaction of one or more atoms comprising the group.

2.7 Thermogravimetric Analysis (TGA)

This technique is used for measuring the precise weight change when a material is exerted to a temperature increase under controlled conditions [5,15-17]. For example, this technique can be used in calculating the amount of water or organic template bound to the catalyst (chapter 5, section 5.3.2.5). For this research weight loss was recorded as a function of temperature and time. Approximately 2mg of the catalyst were used for each experiment.

2.8 Temperature Programmed Desorption (TPD)

Pyridine absorption and then subsequent desorption at elevated temperatures was used to probe materials in order to gain information concerning the number and strength of acid sites (chapter 5, section 5.3.2.3). Pyridine interacts with Brønsted and Lewis acid sites of different strengths. The low temperature desorption of pyridine is attributed to weak Brønsted or Lewis acid sites, whereas desorption of pyridine at

higher temperatures is attributed to stronger Brønsted acid sites [5,15,17]. Approximately 80mg of the catalyst were used for each experiment.

2.9 Specific surface Area

Specific surface area is used in determining the surface area per unit mass of powdered samples. The specific surface area of a powder is achieved by physical adsorption of a gas on the surface of the solid and by measuring the amount of adsorbate gas corresponding to a mono-/multi-molecular layer on the surface (chapter 5, section 5.3.2.4) [5,15]. In a typical experiment, 15mg of catalyst was analysed. Firstly the material is pre-treated by a combination of vacuum and a flowing gas at cryogenic temperature to remove adsorbed contaminants obtained from atmosphere exposure. An adsorbate, in this case nitrogen, is then exposed to the solid in controlled increments. After each exposure of adsorbate, the pressure within the apparatus is left to equilibrate and the quantity of adsorbed gas calculated. The resulting data is plotted as volume of gas adsorbed versus pressure and defines an adsorption isotherm. From this, the quantity of gas necessary to form a mono- (Langmuir) /multi-layer (BET) is determined and the surface area also deduced.

2.10 References

(1) Inui, T.; Matsuda, H.; Okaniwa, H.; Miyamoto, A. *Applied Catalysis* **1990**, *58*, 155-163.

(2) Kang, M. *J. Mol. Catal. A-Chem,* **2000**, *160*, 437-444.

(3) IZA Structure Database Website, http://www.iza-structure.org/databases, **2004**

(4) Kettle, S. F. A. *Physical Inorganic Chemistry - A Coordination Chemistry Approach*; Oxford University Press, **1998**.

(5) Skoog, D. A.; Leary, J. J. *Principles of Instrumental Analysis*; Saunders College Publishing, **1992**.

(6) Atkins, P. W. *Physical Chemistry*; 4th Edition ed.; Oxford University Press, **1990**.

(7) Clegg, W. *Journal of the Chemical Society Dalton Transactions,* **2000**, 3223.

(8) Catlow, C. R. A.; Sankar, G. *Synchrotron Radiation and Solid State Science - Microscopic Properties and Processes in Minerals*, Kluwer Academic Publishers, **1999**.

(9) Beale, A. M. Thesis: *Novel low temperature preparation methods for mixed oxide catalysts and their characterisation using in situ SR techniques*, PhD Thesis, University of London, **2003**.

(10) Teo, B. K. *EXAFS Basic Principles and Data Analysis*; Springer Verlag, **1986**.

(11) Koningsberger, D. C.; Prins, R. *X-ray Absorption Spectroscopy, Principles and Applications*; New York Press, **1992**.

(12) Wong, J.; Lytle, F. W.; Messmer, R. P.; Maylotte, D. H. *Phys. Rev. B* **1984**, *30*, 5596-5610.

(13) Nabavi, M.; Taulelle, F.; Sanchez, C.; Verdaguer, M. *J. Phys. Chem. Solids* **1990**, *51*, 1375-1382.

(14) Iwasawa, Y. *X-ray Absoption Fine Structure for Catalysts and Surfaces*; World Scientific Publishing Co. Pte. Ltd, **1996**.

(15) Skoog, D. A.; West, D.M.; Holler, F.J. *Fundamentals of Analytical Chemistry*; 7th Edition ed.; Saunders College Publishing, **1996**.

(16) West, A. R. *Basic Solid State Chemistry*; John Wiley & Sons, **1991**.

(17) Aramendia, M. A.; Borau, V.; Jimenez, C.; Marinas, J. M.; Romero, F. J. *J. Colloid Interface Sci.* **2004**, *269*, 394-402.

Chapter 3

Study of the shape selective and redox properties of several framework metal substituted aluminophosphates for the Methanol to Olefin (MTO) reaction

3.1 Chapter Overview

This chapter discusses the results obtained from investigations into the shape selective and redox properties associated firstly with the substitution of different metal ions within individual aluminophosphate frameworks, and secondly the substitution of the same metal ion within different aluminophosphate frameworks. Information into the phase purity and crystallinity of the materials has been achieved with the use of X-ray diffraction (XRD) analysis. In addition, catalytic studies into the methanol to olefin (MTO) reaction have been carried out to demonstrate how selective the different frameworks were for the production of light and higher olefins. Overall, the results showed that the manganese substituted AlPO-18 material was in fact the most active species at 350°C (TOS = 30 minutes) for the production of lower olefins. Whilst conversely, the cobalt substituted AlPO-5 material was the more active species at 350°C (TOS = 30 minutes) for the production of higher olefins. The comparisons observed for the MTO reaction between the substitution of cobalt ions into the AlPO-5, -18, -36 and -39 materials, found that at 350°C (TOS = 30minutes), the most active and selective framework for the production of lower olefins was AlPO-18.

3.2 Methanol to Olefin (MTO) reaction

The result of the energy crisis during the 1970's brought about a renewed interest in the use of alternative materials, such as natural gas, as base stocks for the production of fuels.

LeBel first reported the formation of hydrocarbons from methanol in molten $ZnCl_2$ back in 1880 [1]. Then in the 1970's Mobil scientists reported their research into the use of ZSM-5 for the selective production of gasoline (higher olefins) aromatics from methanol [2].

In 1979, the New Zealand government built the first methanol to gasoline plant (MTG) from the use of natural gas as a base stock and Mobil's ZSM-5 catalyst and more recently UOP/ Norsk Hydro have developed a methanol to olefin (MTO) plant using the NiSAPO-34 catalyst. Both plants have had commercial success, although the limiting factor for the MTO process is that it needs to be located close to natural gas reserves.

Methanol can be easily formed via several reactions from natural gas, coal and crude oil. In more recent years, most interest has concentrated on the environmentally friendly method of methanol production from natural gas, otherwise known as synthesis gas, and the further reaction of the methanol over solid acid catalysts for the production of hydrocarbons/ olefins [3]. Synthesis gas ($CO + H_2$) can be produced in a number of ways. The UOP process uses reformed natural gas, although other ways of obtaining synthesis gas include steam reforming of naphtha, coal gasification and partial oxidation of natural gas and petroleum.

The conversion of methanol to olefins involves the formation of carbon-carbon (C-C) bonds. When methanol is absorbed onto the surface of the catalyst, the first product to form is dimethyl ether. The formation of the first C-C bond, is a hot topic of discussion, with many theoreticians proposing possible mechanistic solutions. Such mechanisms include the most favoured solution proposed by Van den Berg et al. This involves the oxonium ylide mechanism, which predicts that the interaction between dimethyl ether and an acid site on the solid acid catalyst forms a dimethyl oxonium ion, which further reacts with dimethyl ether resulting in the production of a trimethyl oxonium ion. This ion then de-protonates forming a surface-associated dimethyl oxonium ion, which is then transformed into either methylethyl ether by Stevens re-

arrangement or an ethyldimethyl oxonium ion by methylation, both subsequently form ethylene via β-elimination [4].

The mechanistic solution that Gale et al proposed is shown below in figure 3.1 [5]. After the equilibrium mixture containing un-reacted methanol, dimethyl ether and water has formed, light olefins are then produced. Dependent on the catalysts being used, the light olefins can react further with each other by hydrogen transfer, alkylation and polycondensation reactions to produce higher olefins, paraffins, aromatics and naphthenes [4].

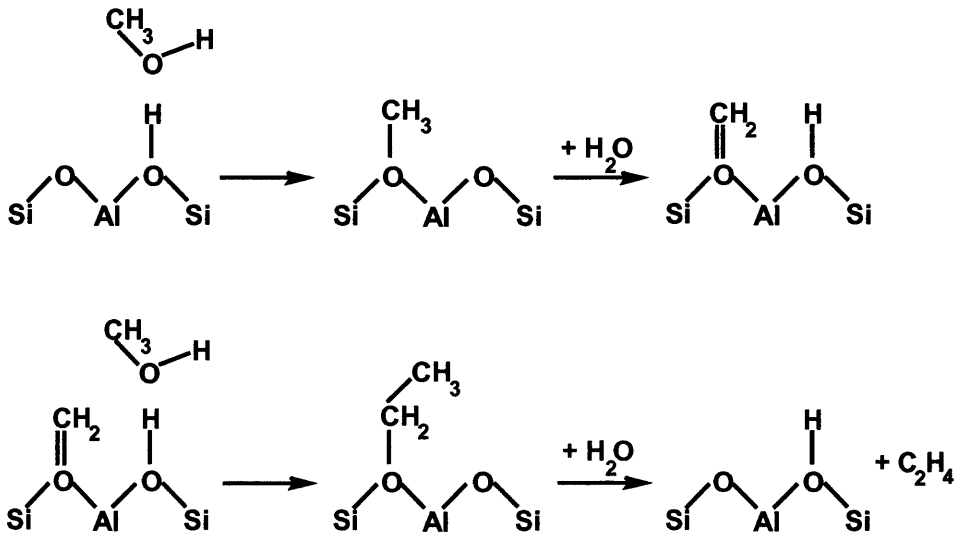

Figure 3.1 *Reaction scheme for the conversion of methanol to olefins over an aluminosilicate catalyst* [5]

Deactivation of the catalyst occurs via a process known as coking. This occurs when the hydrocarbons that are formed inside the pores do not or cannot exit back out through the pores, thereby getting stuck inside the catalyst and blocking the way for other molecules to access and break away from the acid sites of the material. Coke formation cannot be avoided during the MTO process however the catalyst can be

regenerated by calcination where the coke is 'burnt off' and the acid sites are once again free for further catalytic reactions to take place. A lot of research has taken place into understanding why this diffusion and deactivation process occurs so that in the future more efficient catalysts may be developed. In particular Chen *et al* have studied the deactivation of dimethyl ether in SAPO-34 and developed a kinetic model based on the assumption that coke was randomly deposited inside the pores [6].

3.3 Use of aluminophosphates for shape selective catalysis

It has been well established in recent years that heteroatom substituted small pore microporous aluminophosphate materials are extremely efficient shape selective catalysts [4,7]. For example, it is well known that SAPO-34 (structure related to chabazite), and its nickel substituted analogue are very effective in converting methanol to both ethylene and propylene [4,8-10]. Similarly, it has been established in our laboratory that the transition metal ion substituted AlPO-18 and AlPO-34 materials, in particular manganese or cobalt, can be employed to selectively oxidise the terminal carbon atoms in n-hexane and other linear alkanes [11]. In light of these unique catalytic properties there is considerable interest in the study of heteroatom substituted, small pore aluminophosphates for a variety of reactions. Among the various small pore structures, AlPO-18 and AlPO-34 (the main difference being the way in which the double six rings are stacked, otherwise their pore dimensions are identical) based systems have shown good thermal stability upon calcination, and excellent activity and selectivity towards the conversion of methanol to light olefins [4,7,12,13].

The majority of synthesis and catalytic studies in the literature are concerned with SAPO-34 and a variety of metal substituted analogues, such as CoAlPO-34, NiSAPO-34 and FeSAPO-34 [14,15]. Only a few studies have been devoted to the heteroatom substituted AlPO-5, AlPO-18, AlPO-36 and AlPO-39 structures. Although the overall architecture and thermal stability of both AlPO-34 and AlPO-18 related structures are very similar, a greater number of different heteroatom compositions are possible for AlPO-18. For example, it has been shown that SAPO-18 can be prepared with Si/Al ratio ranging from 0.0 to at least 0.1, whereas in contrast SAPO-34 can only be prepared over a much smaller composition range of between 0.09 and 0.11 [16,17].

Previous work by Popova *et al* on several cobalt and silicon substituted AlPO-5 catalysts showed good conversion of methanol to olefins, with the best performance being observed for the cobalt substituted material [18]. Very little research into the MeAlPO-36 and MeAlPO-39 frameworks has taken place. Akolekar *et al*, showed that the magnesium substituted AlPO-36 material possessed the most acidity and was therefore the most active catalyst in the conversion of ethanol, pentane and cyclohexane. This activity was then further enhanced by the incorporation of silicon into the framework, producing the MgAPSO-36 catalyst [19,20]. Whereas Sinha *et al* have reported that substitution of silicon and magnesium into the AlPO-39 structure, produced reasonably active catalysts at 450-500°C, with SAPO-39 being the most active of the two for the MTO reaction [21].

3.3.1 Acidity of aluminophosphates

Substitution of different metal ions within the framework of an AlPO or SAPO brings about a change in the chemical properties of the material. Upon heating cobalt, manganese and iron in oxygen, a change is observed in their oxidation states, 2+ to 3+. Electroneutrality is maintained as you are substituting Al(III) with Me(III) and removing the charge balancing SDA (figure 3.2). However reduction back to 2+ (in a reducing gas) will create a charge imbalance, which is compensated by protons and hence a solid acid catalyst is formed (figure 3.3).

The active acid sites are hydroxyl groups and are located throughout the framework where each of the structural units are linked.

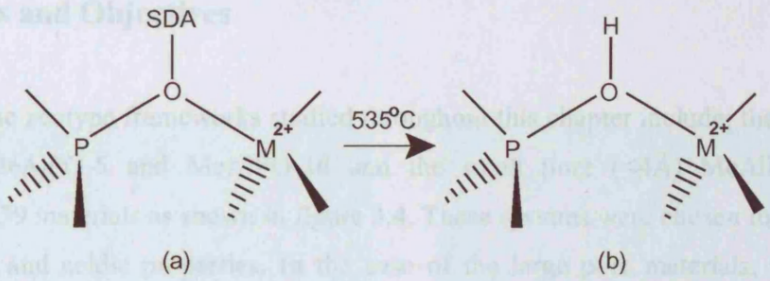

Figure 3.2 *Schematic depicting the formation of Brønsted acid sites in an aluminophosphate (a) before and (b) after calcination (Where Me = Zn, Mg)*

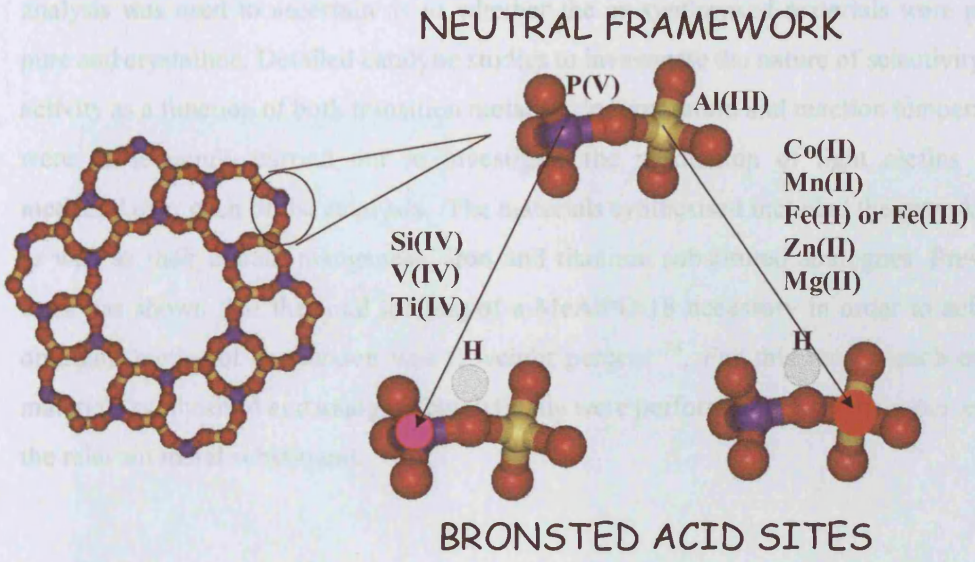

Figure 3.3 *Schematic depicting the Brønsted acid sites in an aluminophosphate*

3.4 Aims and Objectives

The zeotype frameworks studied throughout this chapter include; the large pore (6-8Å) MeAlPO-5 and MeAlPO-36 and the small pore (<4Å) MeAlPO-18 and MeAlPO-39 materials as shown in figure 3.4. These systems were chosen for both their structural and acidic properties. In the case of the large pore materials, the area of interest was the differences between the activity of the two materials since MeAlPO-36 has been found to possess stronger –OH bonds than MeAlPO-5 as studied by Barrett *et al* [22]. Whereas for the small pore materials, interest was concentrated around studying what significance, if any, the cage and channel variations of the two frameworks had on the activity and selectivity for the MTO reaction.

Due to the flexibility in the composition of the MeAlPO structures, several transition metal ion substituted materials were prepared. X-ray diffraction (XRD) analysis was used to ascertain as to whether the as synthesised materials were phase pure and crystalline. Detailed catalytic studies to investigate the nature of selectivity and activity as a function of both transition metal ion incorporation and reaction temperature were subsequently carried out to investigate the production of light olefins from methanol over each of the catalysts. The materials synthesised included the pure AlPOs as well as their cobalt, manganese, iron and titanium substituted analogues. Previous work has shown that the total loading of a MeAlPO-18 necessary in order to achieve optimum methanol conversion was 2 weight percent [23]. For this reason each of the materials synthesised and analysed catalytically were performed using 2 atom percent of the relevant metal substituent.

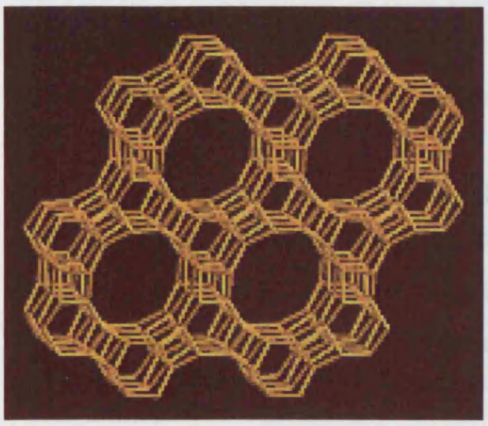

AlPO-5 (AFI)

1-dimensional/ 12-membered ring

7.3 x 7.3Å

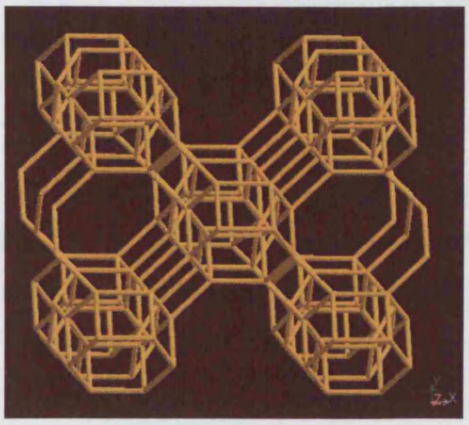

AlPO-18 (AEI)

3-dimensional/ 8-membered ring

3.8 x 3.8Å

AlPO-36 (ATS)

1-dimensional/ 12-membered ring

7.5 x 6.5Å

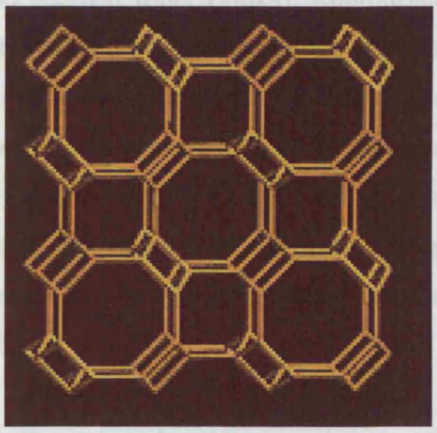

AlPO-39 (ATN)

1-dimensional/ 8-membered ring

4.0 x 4.0Å

Figure 3.4 *Representation of the four aluminophosphate frameworks investigated throughout this chapter, projected along the [001] axis* [24]

3.5 Experimental

3.5.1 Preparation of the MeAlPO materials

Hydrothermal treatment was employed to prepare each of the transition metal substituted aluminophosphate materials. Each material was prepared using aluminium, phosphorous and metal ion sources in addition to a template and water. Further detailed information on the preparation of the materials is given below.

3.5.1.1 Preparation of MeAlPO-5 (where Me = Co/ Mn/ Fe/ Ti)

AlPO-5 and its transition metal ion substituted analogues were synthesised using tetraethyl ammonium hydroxide (TEAOH) (Aldrich) as the structure-directing agent (SDA). In a typical synthesis, aluminium hydroxide hydrate (Aldrich) was added to a solution of phosphoric acid (85%) (Aldrich) and distilled water (Fluka). Appropriate amounts of the Me(II) acetate (Aldrich) were then added prior to the addition of the SDA and vigorous stirring was employed in order to form a homogeneous mixture. The final gel, with a pH of approximately 4.5, was introduced into a Teflon lined stainless steel autoclave and subjected to hydrothermal treatment at 175°C for 3 hours. The recovered solid was filtered, washed with distilled water then dried in air at approximately 100°C overnight. Molar compositions for the preparation of the MeAlPO-5 materials can be seen below in table 3.1.

Metal (x)	$Al(OH)_3$	H_3PO_4	TEAOH (y)	Water
0.02	0.98	1.5	0.8	25

Table 3.1 *Molar compositions used for the preparation of the MeAlPO-5 materials, with structure* $Me_{(x)}Al_{(1-x)}PO_4.TEAOH_{(y)}$

3.5.1.2 Preparation of MeAlPO-18 (where Me = Co/ Mn/ Fe/ Ti)

Both AlPO-18 and its transition metal ion substituted analogues were synthesised using a previously reported procedure [7] employing N,N-diisopropylethylamine (DIPE) (Aldrich) as the structure-directing agent (SDA). In a typical synthesis aluminium hydroxide hydrate (Aldrich) was added to a solution of phosphoric acid (85%) (Aldrich) and distilled water (Fluka). Appropriate amounts of the Me(II) acetate (Aldrich) were then added prior to the addition of the SDA with vigorous stirring in order to form a homogeneous mixture. The final gel, with a pH of 8, was introduced into a Teflon lined stainless steel autoclave and subjected to hydrothermal treatment at 150°C for 96 hours. The recovered solid was filtered, washed with distilled water then dried in air at approximately 100°C overnight. Molar compositions for the preparation of the MeAlPO-18 materials can be seen below in table 3.2.

Metal (x)	$Al(OH)_3$	H_3PO_4	DIPE (y)	Water
0.02	0.98	1.0	0.85	30

Table 3.2 *Molar compositions used for the preparation of the MeAlPO-18 materials, with structure* $Me_{(x)}Al_{(1-x)}PO_4.DIPE_{(y)}$

3.5.1.3 Preparation of CoAlPO-36

Cobalt substituted AlPO-36 was synthesised using N-ethyldicyclohexylamine (ECHA) (Aldrich) as the structure-directing agent (SDA). In a typical synthesis, aluminium hydroxide hydrate (Aldrich) was added to a solution of phosphoric acid (85%) (Aldrich) and distilled water (Fluka). Co(II) acetate (Aldrich) was then added prior to the addition of the SDA. Vigorous stirring was employed throughout the whole synthesis in order to form a homogeneous mixture. The final gel, with a pH of approximately 6.5, was introduced into a Teflon lined stainless steel autoclave and subjected to hydrothermal treatment at 160°C for 16 hours. The recovered solid was filtered, washed with distilled water then dried in air at approximately 100°C overnight.

Molar compositions for the preparation of the CoAlPO-36 material can be seen below in table 3.3.

Cobalt (x)	$Al(OH)_3$	H_3PO_4	ECHA (y)	Water
0.02	0.98	1.0	0.8	10

Table 3.3 *Molar compositions used for the preparation of the CoAlPO-36 material, with structure* $Co_{(x)}Al_{(1-x)}PO_4.ECHA_{(y)}$

3.5.1.4 Preparation of CoAlPO-39

Cobalt substituted AlPO-39 was synthesised using diisobutylamine (DBA) (Aldrich) as the structure-directing agent (SDA). In a typical synthesis, aluminium hydroxide hydrate (Aldrich) was added to a solution of phosphoric acid (85%) (Aldrich) and distilled water (Fluka). Co(II) acetate (Aldrich) was then added prior to the addition of the SDA. Vigorous stirring was employed throughout the whole synthesis in order to form a homogeneous mixture. The final gel, with a pH of approximately 6.5, was introduced into a Teflon lined stainless steel autoclave and subjected to hydrothermal treatment at 160°C for 16 hours. The recovered solid was filtered, washed with distilled water then dried in air at approximately 100°C overnight. Molar compositions for the preparation of the CoAlPO-39 material can be seen below in table 3.4.

Cobalt (x)	$Al(OH)_3$	H_3PO_4	DBA (y)	Water
0.02	0.98	1.0	0.8	10

Table 3.4 *Molar compositions used for the preparation of the CoAlPO-39 material, with structure* $Co_{(x)}Al_{(1-x)}PO_4.DBA_{(y)}$

3.5.2 Characterisation

The as-prepared materials were characterised for phase purity and crystallinity by X-ray diffraction (XRD). The analysis was carried out at room temperature using a Siemens D500 diffractometer equipped with copper target. The degree of reaction for the gaseous conversion of methanol to olefins was recorded by on-line gas chromatography analysis, using the apparatus previously discussed in chapter 2, section 2.10.

3.5.2.1 XRD measurements

Phase purity and crystallinity of the as synthesised materials were accounted for by X-ray diffraction (XRD) analysis, measured using a Siemens D500 employing Cu-$K\alpha_1$ radiation. In a typical experiment, the sample was pressed onto a plate and smoothed prior to the plate being loaded into position. The materials were subsequently analysed over a range of 5 - 40 degrees (2θ) at a rate of 0.02 degrees a second.

3.5.2.2 Catalytic analysis

One major part of this research focused on the design of a new catalytic reactor. The gaseous experiments were carried out on a catalytic rig built by myself for the specific purpose of running the methanol to olefin (MTO) reaction. The set-up essentially comprised a gas flow, reactant feed, reactor and gas chromatograph (GC) as shown in figure 3.5. The aim was to link each of the pieces of equipment in series so that during the catalytic reaction, the products could be characterised by on-line analysis. Stainless steel Swagelok was used for all piping and connections. The methanol (Aldrich, 99.5%) feed was injected into the flowing gas stream (nitrogen, 20

ml/min) at a fixed flow rate of 0.05ml/min, WHSV – 11.9 h^{-1}, using a syringe pump[1]. The pipe-work around this area, prior to the furnace and between the furnace and GC was heated using a variac variable transformer and heating tape (approximately 70°C), so that the feed would vaporise and be transported forward with the pressure of the gas flow. The reactor was a Carbolite furnace equipped with eurotherm controls and the GC was a Perkin Elmer 8410 equipped with a FID detector and fitted with a Porapak N column.

In a typical experiment, 200mg of the as-prepared catalyst was pelletized then crushed using a 20 micron mesh sieve prior to being loaded into a tubular quartz reactor, and held in place using plugs of quartz wool. The gas flow was monitored prior to and post the catalyst slug to check for back pressure, none was observed throughout the entire series of experiments. The catalyst was activated by removal of the organic template (an important process carried out prior to the catalytic testing, which frees the channels and pores making them available for shape selective catalysis) via calcination. This was achieved by heating the catalyst in a nitrogen atmosphere at 5°C/min to 530°C, then with the temperature maintained, the gas was changed to oxygen for a further 16 hours. The sample was then cooled to a specific temperature, again in a nitrogen atmosphere, ready for catalytic investigation. Catalytic activity was tested over a temperature range of 350-500°C, using a fresh catalyst sample for each temperature[2].

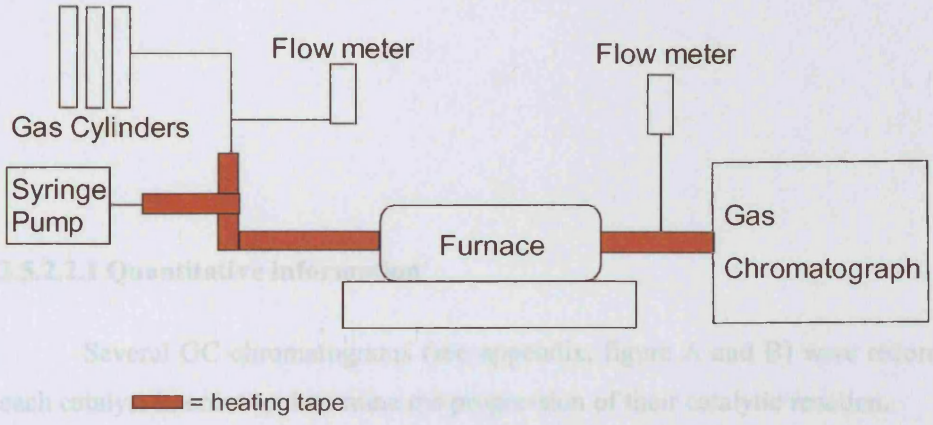

Figure 3.5 *Schematic of the gaseous reactor set-up, built essentially for investigating the MTO reaction*

[1] Weight hourly space velocity (WHSV) is the mass flow rate of methanol divided by the mass of the catalyst in the reactor, i.e. 0.05 x 0.791 x 60 / 0.2 = 11.9 h^{-1}.
[2] The actual temperature of the reactor, as tested using a thermocouple, was 15 °C below the reading given by the eurotherm.

The size of the catalyst particles would be in the range of 20-100μm, as previously investigated by other members of the research group using EDAX analysis.

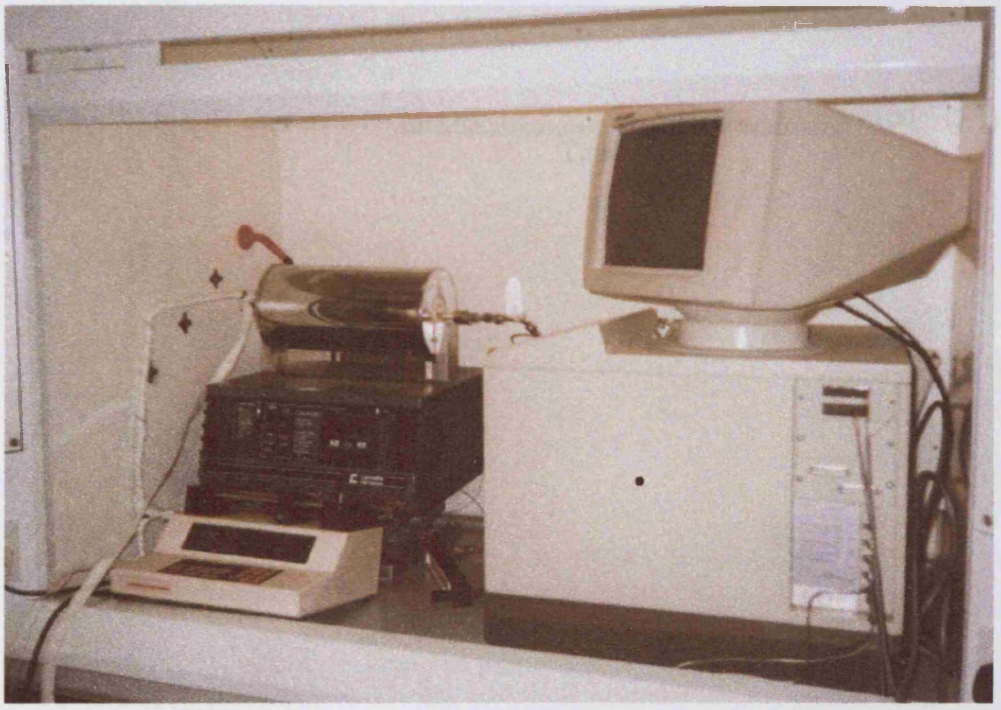

Figure 3.6 *Methanol to olefin catalytic reactor set-up*

3.5.2.2.1 Quantitative information

Several GC chromatograms (see appendix, figure A and B) were recorded for each catalyst in order to determine the progression of their catalytic reaction.

Apart from DME, relative response factors of the products were determined with respect to methane (which produces a linear response and can be easily resolved), using standardised gas canisters (Aldrich) (see Appendix, tables A, B and C for the data obtained from these tests). From this information, product formation could be calculated using the area counts. As there were no standards for the calibration of DME, the

relative response factor was approximated. Since there are two carbon atoms in both ethane and DME it was considered that the RF for DME would also be approximately 0.58.

Methanol conversion was calculated with respect to the difference in area prior to and after the catalytic reaction, equation 3.1.

$$\% \text{ MeOH conversion} = \frac{\text{MeOH}_{(\text{prior to reaction})} - \text{MeOH}_{(\text{after reaction})}}{\text{Total Area}} \times 100 \quad (3.1)$$

3.6 Results and Discussion

3.6.1 XRD study of the as synthesised catalysts

The X-ray diffraction patterns of the as-synthesised MeAlPO-5/ -18/ -36/ and -39 materials can be seen in figures 3.6, 3.7, 3.8 and 3.9 respectively.

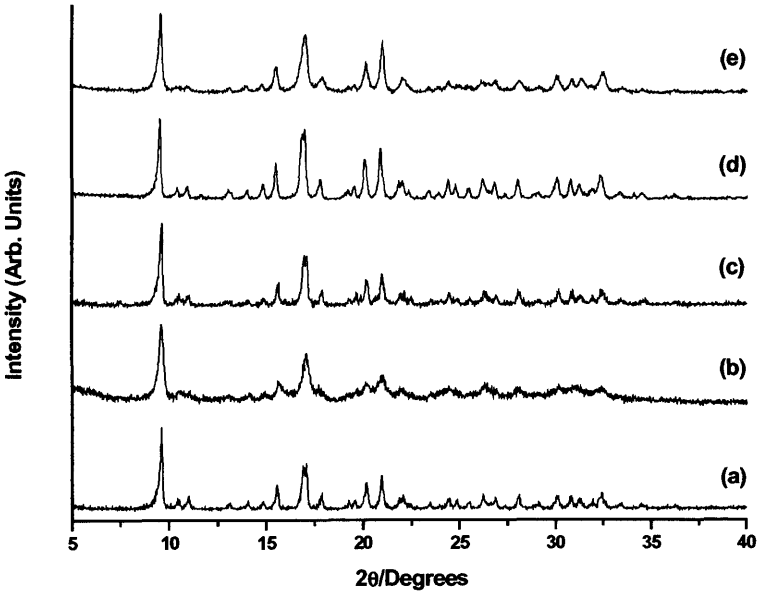

Figure 3.7 *XRD patterns of the as synthesised MeAlPO-5 materials, where (a) is the pure AlPO-5, (b) is the CoAlPO-5, (c) is the MnAlPO-5, (d) is the FeAlPO-5 and (e) is the TiAlPO-5 material*

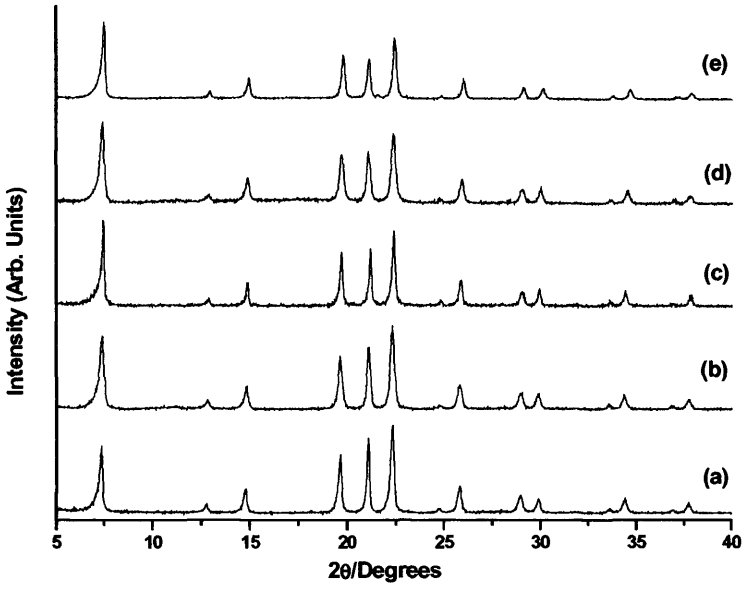

Figure 3.8 *XRD patterns of the as synthesised MeAlPO-18 materials, where (a) is the pure AlPO-18, (b) is the CoAlPO-18, (c) is the MnAlPO-18, (d) is the FeAlPO-18 and (e) is the TiAlPO-18 material*

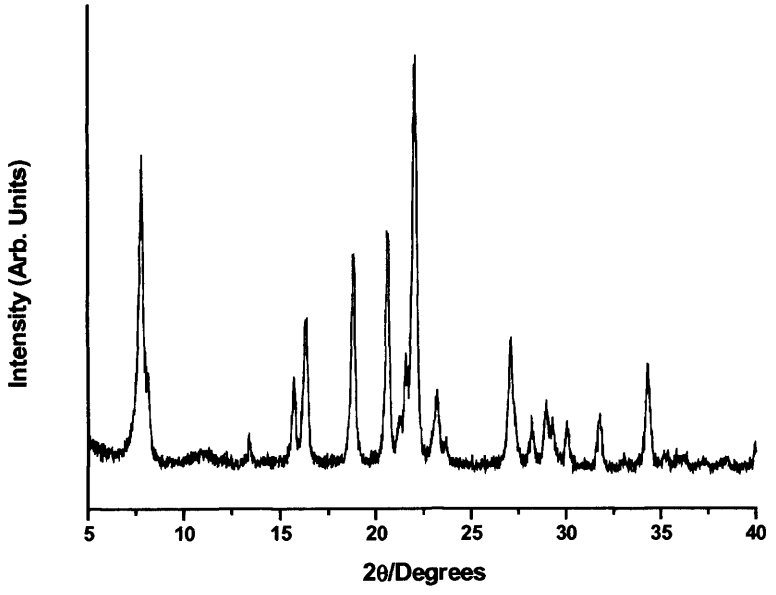

Figure 3.9 *XRD pattern of the as synthesised CoAlPO-36 material*

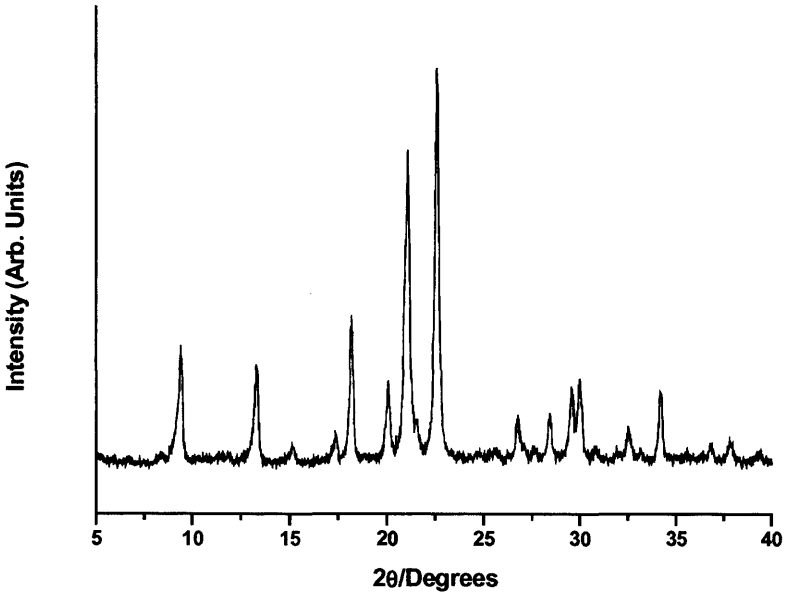

Figure 3.10 *XRD pattern of the as synthesised CoAlPO-39 material*

The patterns indicate that the materials obtained were crystalline. On comparison with previously reported patterns, found on the IZA-structure database [24], they were found to correlate exactly with each of the framework topologies, indicating that they are indeed phase pure. Previously reported XAS data obtained within our research group has shown that the majority of the transition metal ions had been successfully substituted within the frameworks [23,29]. Also reported were the oxidation states of the metal ions and the co-ordination geometry of the materials and therefore there was no need to do any further analysis around this area [22,25-29].

Salient features of the previous studies are as follows. Both cobalt and manganese are substituted into the AlPO frameworks in the 2+ oxidation state. Upon removal of the structure-directing agent (SDA) they are oxidised to the 3+ state distinctive structure. They can easily be reduced back to a 2+ state in oxygen, hydrogen or methanol resulting in the generation of a Brønsted acid site. Iron is substituted mainly as Fe^{3+}. Reduction back to the 2+ state is difficult, however in some cases for example FeAlPO-18 some ions are observed to undergo this change [29]. Titanium on the other hand was found to be very difficult to substitute into the AlPO framework [30,31].

3.6.2 Catalytic investigations for the Methanol to Olefin (MTO) reaction using the as synthesised catalysts

The results for the MTO reaction over each of the calcined catalysts are shown and discussed below. Although mass transfer resistance's weren't investigated further, it is fair to say that a reduction in particle size would increase the catalyst life since by-product formation would be reduced [32].

3.6.2.1 Methanol to Olefin reaction over pure and Me substituted AlPO-5 (where Me = Co/ Mn/ Fe/ Ti)

The catalytic conversion of methanol over pure AlPO-5 produces solely dimethyl ether due to its very low acidity. However, the conversion of methanol over MeAlPO-5 catalysts produces a wide range of hydrocarbons including C_1-C_6 alkanes, alkenes and aromatics, the higher hydrocarbons being the most predominant. This is all due to the shape selective nature of the AlPO-5 framework which is 7.5Å x7.5Å in diameter and large enough to allow very bulky molecules to pass through its pores and channels. The results obtained from the investigation into the catalytic activity of pure and Me substituted AlPO-5 (where Me = Co/ Mn/ Fe/ Ti) for the methanol to olefin reaction are shown in table 3.5.

	AlPO-5	CoAlPO-5	MnAlPO-5	FeAlPO-5		TiAlPO-5	
Temperature (°C)	350	350	350	350	400	350	400
Methanol Conversion (%)	77.54	95.19	97.06	14.07	46.71	18.75	62.57
Product Selectivity (%) (exclusive of H_2O)							
$(CH_3)_2O$	100	2.61	9.00	99.07	99.15	94.13	94.27
CH_4		0.91	0.76	0.10	0.81	0.24	0.03
C_2H_4		17.70	9.45	0.14	0.04	0.08	0.34
C_2H_6		0.16					0.06
C_3H_6		40.62	39.17	0.27		5.55	5.30
C_3H_8		10.3	13.61				
C_4H_8							
C_4H_{10}		4.09	4.63				
C_4 others							
C_{5+}		23.61	23.38	0.42			

Table 3.5 *Results for the catalytic conversion of methanol over pure and Me substituted AlPO-5 (where Me = Co/ Mn/ Fe/ Ti)*

The results in Table 3.5 show that, at 350°C and TOS = 30 minutes, slightly more methanol was converted to hydrocarbons over MnAlPO-5 than for any other MeAlPO-5 catalyst. In addition MnAlPO-5 was the best catalyst for the selective production of C_3-C_5 olefins. A large amount of methane was produced when methanol was reacted over MnAlPO-5.

The production of methane has been observed when catalysts have been analysed at higher temperatures [33]. Deactivation and the consecutive formation of methane occur due to the diffusion constraints within narrow pores. With respect to the reaction mechanism, methane may have been produced via one of two methods. Firstly, the methoxy groups that are initially formed on interaction of the methanol with the acid sites, interact with other methanol molecules absorbed around the acid sites forming not only carbon-carbon bonds but also transformations, ultimately leading to the desorption of gaseous methane [34]. On the other hand, in the absence of diffusional constrains, methane may have been produced via a secondary reaction of the C_{2+} hydrocarbons on the acid sites within the catalyst.

The least active of the transition metal substituted catalysts studied at 350°C, were FeAlPO-5 and TiAlPO-5. On increasing the reaction temperature to 400°C, the percentage of methanol catalytically converted also increased. However, the selectivity

to products was once again greatly in favour of dimethyl ether, with >99% formed on reaction with FeAlPO-5 and >94% formed on reaction with TiAlPO-5.

The trend observed for the activity of the materials studied for the selective conversion of methanol to C_3-C_5 hydrocarbons at 350°C and TOS = 30 minutes can be deduced as:

MnAlPO-5 > CoAlPO-5 > FeAlPO-5 > TiAlPO-5 > AlPO-5

3.6.2.2 Methanol to Olefin reaction over pure and Me substituted AlPO-18 (where Me = Co/ Mn/ Fe/ Ti)

Previously published work has shown that increasing the reaction temperature for methanol conversion over MeAlPO-18 catalysts to 400°C increases their selectivity for the production of ethylene [7]. Time constraints predominantly limited the research to reactions at 350°C. The results obtained from the investigation into the catalytic activity of pure and Me substituted AlPO-18 (where Me = Co/ Mn/ Fe/ Ti) for the methanol to olefin reaction are shown below in table 3.6.

	AlPO-18	CoAlPO-18	MnAlPO-18	FeAlPO-18		TiAlPO-18	
Temperature (°C)	350	350	350	350	400	350	400
Methanol Conversion (%)	68.59	99.05	98.80	53.57	73.31	43.33	69.37
Product Selectivity (%) (exclusive of H_2O)							
$(CH_3)_2O$	100	2.04	1.83	89.36	83.24	99.62	93.64
CH_4		0.40	0.70	0.43	2.51	0.38	3.86
C_2H_4		35.40	31.79	3.15	5.49		0.91
C_2H_6		0.15	0.10		1.00		0.13
C_3H_6		42.85	44.10	5.56	6.41		1.25
C_3H_8							
C_4H_8		4.27	4.66		0.10		
C_4H_{10}		7.69	8.26		0.93		0.16
C_4 others		4.10	5.06	1.50	0.32		
C_{5+}		3.10	3.50				0.05

Table 3.6 *Results for the catalytic conversion of methanol over pure and Me substituted AlPO-18 (where Me = Co/ Mn/ Fe/ Ti)*

Due to its low acidity, the pure AlPO-18 catalyst was found to catalytically convert methanol solely to dimethyl ether, similar to AlPO-5, and has been previously reported by IR analysis [16]. Conversely, all the MeAlPO-18 materials catalysed methanol to other olefins as well as dimethyl ether. For example, at 350°C and time on stream (TOS) = 30mins, the selectivitys for methanol conversion to olefins other than dimethyl ether, are predominantly in favour of ethylene and propylene. The overall conversion to these predominant hydrocarbons is due to the shape selective nature of the MeAlPO-18 material, as well as the increase in acid strength of the materials after substitution of the particular transition metal ion. The pore size of the AlPO-18 material is just 3.8Å x

3.8Å and therefore this aluminophosphate framework is selective for the production of mainly C_1-C_5 olefins.

The trend observed for the acidity of the materials, correlates perfectly with the selective conversion of methanol to ethylene and propylene at 350°C, this activity is in the order of:

CoAlPO-18 > MnAlPO-18 > FeAlPO-18 > TiAlPO-18 > AlPO-18

In particular, CoAlPO-18 and MnAlPO-18 showed very good methanol conversions, 99.05% and 98.80% respectively at 350°C and TOS = 30 minutes. Additionally both catalysts achieved over 75% selectivity to C_2-C_4 alkenes. The catalysts were assessed for up to two hours on stream, in comparison with pure AlPO-18, in order to determine the extent to which the catalysts continued to convert the methanol feed, the results of which are shown below in figure 3.10. None of the catalysts showed any significant decline in either activity or selectivity over the two hour period, however CoAlPO-18 did deactivate at a marginally faster rate than MnAlPO-18.

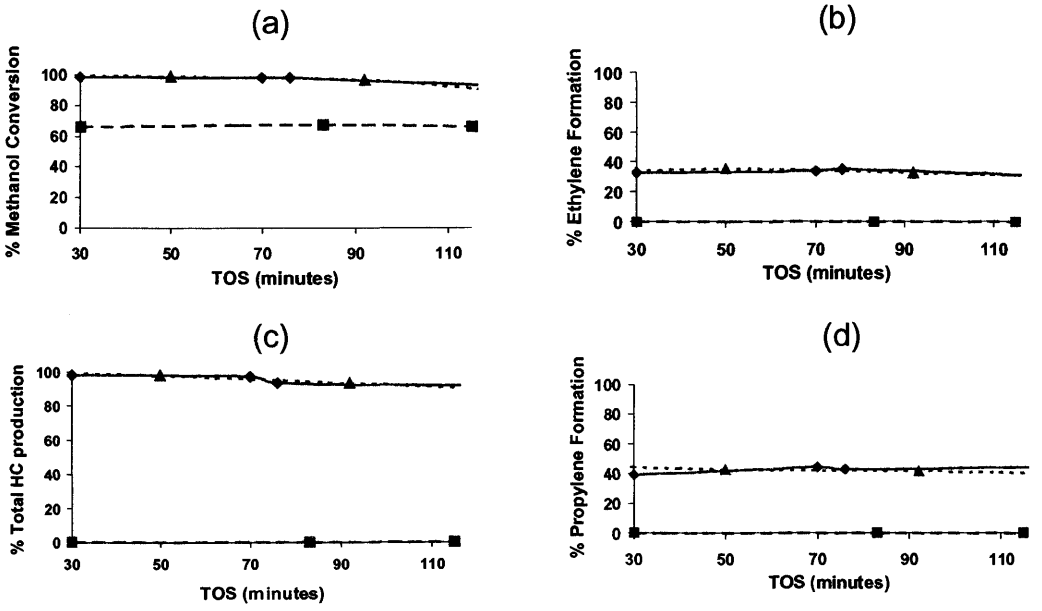

Figure 3.11 *Effect of TOS on the (a) methanol conversion, (b) selectivity to ethylene, (c) total hydrocarbon production and (d) selectivity to propylene, for the MTO reaction over pure AlPO-18 (■), CoAlPO-18 (▲) and MnAlPO-18 (♦) at 350°C*

The catalytic performance was also tested after regeneration of the catalyst. Recyclability of the MnAlPO-18 catalyst was studied, at 350°C and TOS = 30 minutes, to show how effective the catalyst was after three consecutive methanol conversion reactions. In a typical experiment the as synthesised catalyst was calcined and subjected to the MTO reaction at 350°C for seventy minutes. The same catalyst was then re-calcined at 530°C to regenerate its original activity and again subjected to the MTO reaction. This procedure was repeated three times and the results are given in Table 3.7. The results show that over the two-hour period only a very slight decrease in the conversion of methanol was observed, likely to be due to the formation of coke which is known to occur in these materials over time [4,17]. Based on the initial conversion after each cycle and under the conditions employed in this study, it can be proposed that there is no significant leaching of the active metal centres during reaction [23]. With respect to the methanol conversion observed in table 3.7, the information also clearly shows how successfully reproducible the GC analysis and data interpretation is over successive reactions.

Run	TOS (minutes)	Methanol Conversion (%)
1	30	98.80
	70	98.16
2	30	100.00
	70	100.00
3	30	96.30
	70	91.74

Table 3.7 *Recyclability study showing the effect of three consecutive methanol conversion reactions and regeneration's over MnAlPO-18 at 350°C*

Also observed in table 3.6 is a trend for the catalytic conversion of methanol at 400°C and TOS = 30 minutes, for the less acidic materials FeAlPO-18 and TiAlPO-18. It was observed that more methanol was converted to hydrocarbons, with the selectivitys for the production of ethylene and propylene both increasing in unison in comparison to the methanol reaction at 350°C. However, they are still very poor catalysts for this reaction.

3.6.2.3 Methanol to Olefin reaction over CoAlPO-36

Results obtained from the investigation into the catalytic activity over CoAlPO-36 for the methanol to olefin reaction are shown below in table 3.8.

	CoAlPO-36		
Temperature (°C)	350	450	500
Methanol Conversion (%)	50.50	55.19	58.78
Product Selectivity (%) (exclusive of H_2O)			
$(CH_3)_2O$	54.66	90.69	79.90
CH_4	3.85	9.31	20.10
C_2H_4	7.44		
C_2H_6			
C_3H_6	19.67		
C_3H_8			
C_4H_8			
C_4H_{10}	7.07		
C_4 others	4.32		
C_{5+}	2.99		

Table 3.8 *Results for the catalytic conversion of methanol over CoAlPO-36*

The structure of the AlPO-36 framework, 7.5 x 6.5Å in diameter, allows for the production and diffusion of large hydrocarbons as previously observed with the AlPO-5 framework material. It was therefore proposed that the cobalt substituted AlPO-36 catalyst should on reaction at 350°C (TOS = 30 minutes), as observed earlier in table 3.5 for CoAlPO-5, convert high levels of methanol and in addition be selective towards the formation of C_3-C_5 olefins. This however was not the case. 350°C was observed to be the most desired temperature for the production of higher olefins, although >60% of the products formed were dimethyl ether. When the reaction temperature was increased to 450°C, a small increase in the conversion of methanol was observed. However, greater than 90% of the products formed on reaction over the CoAlPO-36 catalyst were dimethyl ether with the remaining fraction being methane. Similarly when the reaction temperature was increased still further, to 500°C, although there was an additional few percent more methanol converted, the products formed during the reaction were once again predominantly dimethyl ether with the remaining being methane. Yet again methane levels were observed to increase with increasing reaction temperature on

analysis of the reaction after just 30 minutes. As proposed early in section 3.6.2.1, this is most likely observed due to the de-activation (coking) of the catalyst.

3.6.2.4 Methanol to Olefin reaction over CoAlPO-39

The framework of AlPO-39 has pores/channels that are 4.0 x 4.0Å in diameter. On comparison with the widely studied AlPO-18 material it was hoped that substitution of cobalt into the AlPO-39 framework would produce a selective catalyst towards the production of C_2-C_3 olefins from the catalytic reaction with methanol. More over, it was hoped that the one-dimensional AlPO-39 material would show more selectivity than the three-dimensional framework observed for the AlPO-18 material since there should be less chance of the reactant and product molecules getting trapped within the framework. The results obtained for the methanol to olefin reaction, examining the catalytic activity of CoAlPO-39, are shown below in table 3.9.

	CoAlPO-39		
Temperature (°C)	350	450	500
Methanol Conversion (%)	39.02	63.06	54.37
Product Selectivity (%) (exclusive of H_2O)			
$(CH_3)_2O$	100	36.59	49.67
CH_4		5.32	9.50
C_2H_4		5.88	5.13
C_2H_6			
C_3H_6		43.47	24.24
C_3H_8			
C_4H_8		4.24	2.25
C_4H_{10}		2.82	1.93
C_4 others			
C_{5+}		1.68	7.28

Table 3.9 *Results for the catalytic conversion of methanol over CoAlPO-39*

From the results depicted in table 3.9, it is shown that on comparison of the reaction at 350°C (TOS = 30 minutes), CoAlPO-39 was observed to convert just 39% methanol, with 100% selectivity towards the formation of dimethyl ether. Upon further

increasing the reaction temperature to 450°C, only around 36% dimethyl ether was produced and the methanol conversion had almost doubled to >60%. At this temperature it was noticed that the selectivity to products other than dimethyl ether were predominantly in favour of C_2-C_3 olefins, with just over 8% C_4-C_5 olefins also being produced. On further increase of the reaction temperature to 500°C, although a large percentage of the products being formed are still C_2-C_3 hydrocarbons, methanol conversion had once again decreased and in addition the levels of methane being formed had increased.

One reason as to why the CoAlPO-39 catalyst behaved so poorly could be that the one-dimensional system proved too restrictive towards the diffusion of the hydrocarbons out of the pores and channels after reaction on the catalyst surface. This would in turn lead to rapid coking of the catalyst and the eventual deactivation [35]. Previous work by Sinha *et al* correlate with these findings in observing that at high methanol conversions and temperatures greater than 350°C, the catalysts deactivate more quickly throughout the reaction. This work however does not identify as to which specific hydrocarbons were formed [21].

3.6.2.5 Comparison of the Methanol to Olefin reaction over cobalt substituted AlPO-5/ -18/ -36 and -39

Overall, the cobalt substituted AlPO-5, -18, -36 and -39 materials showed the best catalytic performance in comparison to other metal substituents for the methanol to olefin (MTO) reaction at 350°C, TOS = 30 minutes. On comparison of the different framework activities, table 3.10 below, several observations can be deduced.

	CoAlPO-5	CoAlPO-18	CoAlPO-36	CoAlPO-39
Temperature (°C)	350	350	350	350
Methanol Conversion (%)	95.19	99.05	50.50	39.02
Product Selectivity (%) (exclusive of H_2O)				
$(CH_3)_2O$	2.61	2.04	54.66	100
CH_4	0.91	0.40	3.85	
C_2H_4	17.70	35.40	7.44	
C_2H_6	0.16	0.15		
C_3H_6	40.62	42.85	19.67	
C_3H_8				
C_4H_8	10.3	4.27		
C_4H_{10}	4.09	7.69	7.07	
C_4 others		4.10	4.32	
C_{5+}	23.61	3.10	2.99	

Table 3.10 *Results for the catalytic conversion of methanol over cobalt substituted AlPO-5/ -18/ -36 and -39 catalysts*

The most active framework for the catalytic conversion of methanol was CoAlPO-18, converting greater than 99% methanol, with just 2% dimethyl ether being produced. In comparison, CoAlPO-5 was also observed to be a very active catalyst with more than 95% methanol conversion and with dimethyl ether production being less than 3%. On the other hand the CoAlPO-36 and CoAlPO-39 catalysts were less active and only managed to convert approximately 50% and 39% of the methanol respectively.

The observed trend of the activity for the catalysts analysed in the conversion of methanol is:

CoAlPO-18 > CoAlPO-5 > CoAlPO-36 > CoAlPO-39

As was expected, the selectivity towards the production of particular olefins was directly related to the pore/channel size of the materials under investigation. For this reason the large pore CoAlPO-5 and CoAlPO-36 catalysts were observed to be selective in the formation of C_3-C_5 olefins. Whereas the small pore CoAlPO-18 catalyst was selective in producing more than 75% C_2-C_3 olefins.

The reason for this activity trend is probably due to the presence of different amounts of Brønsted and Lewis acid centres within these materials [7,36]. Barrett *et al.* observed that Co(II) when substituted in an AlPO framework does not undergo complete oxidation upon removal of the template molecule after reduction [22].

Depending on the framework type, it has been observed that the concentration of Brønsted acid sites varies and they follow this order,

CoAlPO-18 > CoAlPO-36 > CoAlPO-5

(there is no complete data on CoAlPO-39 and hence it is not included here in the discussion) [22]. The creation of Lewis sites are believed to be due to the presence of certain Co(II) ions which could not be raised to the 3+ and then reduced to the 2+ states on reduction. Thus the trend in activity is closely similar to the above trend in the Brønsted acid site concentration. However, the catalytic results suggest that CoAlPO-36 should be better than CoAlPO-5 which is not in complete agreement with the observed trend. It has been noted for Zn(II) substituted AlPO-36 that the activity is very high in the first few minutes of the reaction and deactivates due to a large amount of coke formation and hence in this study our results may not reflect the appropriate result.

3.7 Summary and Conclusions

In summary, two atom percent transition metal were successfully substituted into the microporous framework of the MeAlPO-5 (where Me = Co, Mn, Fe, Ti), MeAlPO-18 (where Me = Co, Mn, Fe, Ti), CoAlPO-36 and CoAlPO-39 structures.

The X-ray diffraction (XRD) patterns of the as-synthesised aluminophosphates were shown to be phase pure. Although the patterns could not reveal directly the extent of incorporation of the metal ions, previously reported XAS data obtained within our research group has shown that the majority of the transition metal ions were successfully incorporated within the framework materials [23,33]. Also reported were the oxidation states of the metal ions and the co-ordination geometry of the materials and therefore no analysis was needed to investigate this matter [22,25-29].

Studies into the catalytic activity of the as synthesised materials for the methanol to olefin (MTO) reaction were performed. Results found the same trend for each of the frameworks studied, both the cobalt and manganese substituted materials converted the greatest amount of methanol and were the most active catalysts. Catalytic selectivitys varied dependent on the use of catalysts. The trend shown, as expected, found that the small-pore materials were more selective for the production of light olefins in contrast to the higher hydrocarbons produced on reaction over the large-pore catalysts. In particular MnAlPO-5 was the best catalyst for the selective production of C_3.C_5 olefins at 350°C and TOS = 30 minutes, with methanol conversion > 97%. Whereas CoAlPO-18 showed very good methanol conversions > 99% at 350°C and TOS = 30 minutes, achieving over 82% selectivity to C_2-C_4 alkenes.

Overall, the trend observed for the catalytic activity of the transition metal ion substituted aluminophosphates for the MTO reaction at 350°C is deduced as:

$$Co > Mn > Fe > Ti$$

This activity can be further explained on comparison with XAS data [29-31]. The extent to which the substituted ions undergo oxidation and reduction during calcination, plays a vital role in the acidic nature and hence activity of the catalyst. For example, it has been found that both cobalt and manganese are substituted into the AlPO frameworks in the 2+ oxidation state, after removal of the SDA they are easily reduced back to a 2+ state generating a Brønsted acid site. Iron on the other hand is substituted

mainly as 3+ with reduction back to the 2+ state a more difficult process. Similarly, it has been discovered that titanium ions are extremely difficult to successfully substitute into the AlPO framework.

In order to determine the extent to which the Co and Mn substituted AlPO-18 catalysts continued to convert methanol feed [15], a time on stream (TOS) study was carried out. The results found that there was no significant decline in either activity or selectivity for both catalysts, for up to two hours. The performance of the catalyst was also tested after regeneration. Once again the results suggested that there was no significant decline in the conversion level after two hour reaction. The slight decrease that was noticed is likely to be due to the formation of coke, which is known to occur in these materials. Based on the initial conversion after each cycle and under the conditions employed in this study, it was proposed that over a two-hour reaction period there is no significant leaching of the active metal centres.

To determine as to which cobalt-substituted framework was most active, a comparative study of the cobalt substituted AlPO-5, AlPO-18, AlPO-36 and AlPO-39 catalysts was carried out at 350°C, TOS = 30minutes. The trend observed for the catalytic activity in terms of amount methanol converted was:

CoAlPO-18 > CoAlPO-5 > CoAlPO-36 > CoAlPO-39

Comparing this information to previous XAS studies into the co-ordination and geometry of the cobalt substituted ions within these different framework topologies, one explanation that could be drawn as to why the above trend is observed is that whereas the cobalt ion in CoAlPO-18 undergoes complete oxidation upon removal of the SDA (Co(II) to Co(III)), the cobalt ion in CoAlPO-5 and CoAlPO-36 are only observed to partially oxidise (no data has yet been collected for CoAlPO-39 and therefore it is not possible to discuss how this may affect the catalytic performance of this material [22]). Therefore although the selectivity to products varies in consideration to the pore size of the material under investigation, if all the cobalt ions were to have oxidised in the CoAlPO-36 framework, then this one-dimensional material may have been more active towards the methanol to olefin reaction.

3.8 References

(1) Olah, G. A.; Molnar, A. *Hydrocarbon Chemistry*, Wiley, New York, **1995.**

(2) Chang, C. D.; Silvestri, A. J. *Journal of Catalysis*, **1977**, *47*, 249-259.

(3) Djieugoue, M. A.; Prakash, A. M.; Kevan, L. *Journal of Physical Chemistry B*, **2000**, *104*, 6452-6461.

(4) Stocker, M. *Microporous and Mesoporous Materials*, **1999**, *29*, 3-48.

(5) Gale, J.D.; Shah, R.; Payne, M. C.; Stich, I.; Terakura, K. *Catalysis Today*, **1999**, *50*, 525-532.

(6) Chen, D.; Rebo, H. P.; Moljord, K; Holman, A. *Natural Gas Conversion V*, **1998**, 521-526.

(7) Chen, J. S.; Thomas, J. M. *Journal of the Chemical Society-Chemical Communications*, **1994**, *5*, 603-604.

(8) Inui, T.; Matsuda, H.; Okaniwa, H.; Miyamoto, A. *Applied Catalysis*, **1990**, *58*, 155-163.

(9) Inui, T.; Phatanasri, S.; Matsuda, H. *Journal of the Chemical Society-Chemical Communications*, **1990**, *3*, 205-206.

(10) Thomas, J. M.; Xu, Y.; Catlow, C. R. A.; Couves, J. W. *Chemistry of Materials*, **1991**, *3*, 667-672.

(11) Thomas, J. M.; Raja, R.; Sankar, G.; Bell, R. G. *Accounts of Chemical Research*, **2001**, *34*, 191-200.

(12) Wendelbo, R.; Akporiaye, D.; Andersen, A.; Dahl, I. M.; Mostad, H. B. *Applied Catalysis A-General*, **1996**, *142*, 197-207.

(13) Wilson, S.; Barger, P. *Microporous and Mesoporous Materials*, **1999**, *29*, 117-126.

(14) Inoue, M.; Dhupatemiya, P.; Phatanasri, S.; Inui, T. *Microporous and Mesoporous Materials*, **1999**, *28*, 19-24.

(15) Kang, M., *Journal of Molecular Catalysis A-Chemical*, **2000**, *160*, 437-444.

(16) Chen, J. S.; Thomas, J. M.; Wright, P. A.; Townsend, R. P. *Catalysis Letters*, **1994**, *28*, 241-248.

(17) Chen, J. S.; Wright, P. A.; Thomas, J. M.; Natarajan, S.; Marchese, L.; Bradley, S. M.; Sankar, G.; Catlow, C. R. A.; Gaiboyes, P. L.; Townsend, R. P.; Lok, C. M. *Journal of Physical Chemistry*, **1994**, *98*, 10216-10224.

(18) Popova, M.; Minchev, C; Kanazirev, V. *Reaction Kinetics and Catalysis Letters*, **1998**, *63*, 379-384.

(19) Akolekar, D. B., *Journal of the Chemical Society-Faraday Transactions*, **1994**, *90*, 1041-1046.

(20) Akolekar, D. B., *Zeolites*, **1994**, *14*, 53-57.

(21) Sinha, A. K.; Hegde, S. G.; Jacob, N. E.; Sivasanker, S. *Zeolites*, **1997**, *18*, 350-355.

(22) Barrett, P. A., et al., *Journal of Physical Chemistry*, **1996**, *100*, 8977-8985.

(23) Franklin, I. L.; Beale, A. M.; Sankar, G. *Catalysis Today*, **2003**, *81*, 623-629.

(24) IZA Structure Database Website, http://www.iza-structure.org/databases, **2004**

(25) Cora, F.; Catlow, C. R. A.; D'Ercole, A. *Journal of Molecular Catalysis A-Chemical*, **2001**, *166*, 87-99.

(26) Sankar, G.; Gleeson, D.; Catlow, C. R. A.; Thomas, J. M.; Smith, A. D. *Journal of Synchrotron Radiation*, **2001**, *8*, 625-627.

(27) Thomas, J.M.; Catlow, C. R. A.; Sankar, G. *Chemical Communications*, **2002**, 2921-2925.

(28) Thomas, J.M.; Sankar, G. *Journal of Synchrotron Radiation*, **2001**, *8*, 55-60.

(29) Zenonos, C.; Sankar, G.; Cora, F.; Lewis, D. W.; Pankhurst, Q. A.; Catlow, C. R. A.; Thomas, J. M. *Physical Chemistry Chemical Physics*, **2002**, *4*, 5421-5429.

(30) Akolekar, D. B.; Ryoo, R. *Journal of the Chemical Society-Faraday Transactions*, **1996**, *92*, 4617-4621.

(31) Zahedi-Niaki, M. H.; Beland, F.; Bonneviot, L.; Kaliaguine, S. *Impact of Zeolites and Other Porous Materials on the New Technologies at the Beginning of the New Millennium, Pts A and B,* **2002**, 125-133.

(32) Wilson, S.; Barger, B., *Microporous and Mesoporous Materials,* **1999**, *29*, 117-126

(33) Beale, A. M., *Novel low temperature preparation methods for mixed oxide catalysts and their characterisation using in situ SR techniques*, PhD Thesis, University of London, **2003**.

(34) Popova, M.; Minchev, C; Kanazirev, V. *Applied Catalysis A-General*, **1998**, *169*, 227-235.

(35) Li, J.; Xiong, G.; Feng, Z.; Liu, Z.; Xin, Q.; Li, C. *Microporous and Mesoporous Materials*, **2000**, *39*, 275-280.

(36) Hocevar, S.; Batista, J.; Kaucic, V. *Journal of Catalysis*, **1993**, *139*, 351-361.

Chapter 4

Investigation into the influence of transition metal ion exchange in zeolites and aluminophosphates for the hydroxylation of phenol

4.1 Chapter Overview

Iron, cobalt and titanium containing zeolites and aluminophosphates were synthesised, characterised and subsequently tested for the hydroxylation of phenol. Preparation of the aluminophosphate was carried out under hydrothermal conditions, whereas the ammonium zeolite Beta catalyst was bought from Zeolist International. In both cases, subsequent incorporation of the metal centres was achieved via ion-exchange methods with the total metal loading for each catalyst being about two atom percent. Characterisation was achieved using X-ray diffraction (XRD) and X-ray absorption spectroscopy (XAS) for phase purity, crystallinity and local structure of the metal centres. Energy Dispersive Analysis using X-rays (EDAX) was also used for investigations into the quantity of substituents successfully exchanged within the frameworks. Catalytic studies were undertaken to investigate the influence of different metal substituents and temperature on the conversion of phenol and selectivities to catechol, hydroquinone and 1,4-benzoquinone. Reactions were carried out at atmospheric pressure in liquid phase at both 40°C and 60°C. The results found that preferential exchange of metal substituents occurred contrary to previously reported work [1] and therefore the overall performance of the catalysts was poorer than had been expected. These investigations concluded that CoFeNH4-β showed to be the most active catalyst for the hydroxylation of phenol at 40°C, converting >12% phenol with selectivities to products being >48% catechol, >37% hydroquinone and 14% 1,4-benzoquinone, whereas although no reaction was observed for FAPO-5 at 40°C, this catalyst was found to be the most active at 60°C, converting >13% phenol with selectivities to products being 50% catechol, >36% hydroquinone and > 13% 1,4-benzoquinone.

4.2 Dihydroxybenzenes

Catechol (CAT) and hydroquinone (HQ) are valuable chemicals used extensively as antioxidant and polymerisation inhibitors in pesticides, flavouring agents, medicines and within the photographic industries [1]. Recent interest has concentrated on the use of heterogeneous catalysts for their production since they are easily recoverable from the reaction mixture. These include metal oxides, metallosilicalites, hydrotalcites-type catalysts and metal substituted mesoporous materials [2-6]. The most successful catalyst to date is the titanosilicalite TS-1, however each of the best performance catalysts are either expensive, entail complex preparations and/ or involve the use of high temperatures and pressures.

4.2.1 Application of zeolites and aluminophosphates (AlPOs) for the hydroxylation of phenol

Transition metal framework substituted zeolites for the hydroxylation of phenol has been researched at length [6-10] however, not a lot of attention has been paid to ion-exchanged zeolites for this reaction [1].

Zeolites were previously discussed in Chapter 1 section 1.3.1. Throughout this research, metal ion exchanged zeolite-β (figure 4.1) was studied and its activity for the phenol hydroxylation reaction investigated. Zeolite-β has a tetragonal structure with straight 12-membered ring channels (7.6 x 6.4Å) crossed with 10-membered ring channels (5.5 x 6.5Å) [11,12].

Similarly, little work has looked into the activity of metal exchanged and substituted aluminophosphates for this reaction either. Aluminophosphates were previously discussed in chapter 1 section 1.3.1.3 and chapter 3 section 3.3. Here AlPO-5 and its transition metal exchanged analogues were studied, this material has large pores and possesses 12-membered rings (7.3 x 7.3Å) [11].

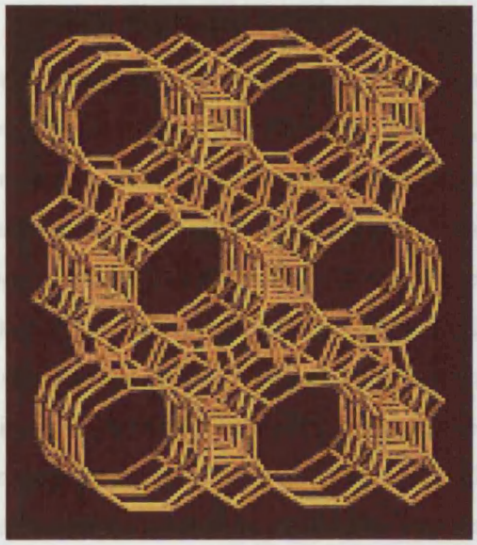

Zeolite Beta (BEA)

3-dimensional

Figure 4.1 *Representation of zeolite-β projected along the [100] axis* [11]

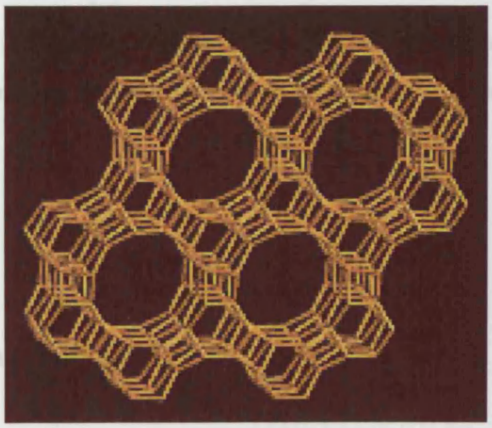

AlPO-5 (AFI)

1-dimensional

Figure 4.2 *Representation of AlPO-5 projected along the [001] axis* [11]

4.2.2 Acidity of zeolites and aluminophosphates (AlPOs)

A zeolite can be designed to exhibit acidity by a number of different methods, including substitution or exchange of metal ions. In essence, substitution of Al(III) for Si(IV) imparts a negative charge on the neutral framework which can then be compensated by charge balancing and exchangeable cations (chapter 3 section 3.3.1). Similarly for aluminophosphates, substitution of lower valent ions (for example cobalt and iron) for Al(III) or P(V) or both generates a negative charge imbalance. In both cases Brønsted acid sites are created and hence a solid acid catalyst is formed [13].

An increase in the Si/Al ratio of a zeolite reduces the total number of acid sites present, however the number of strong Brønsted acid sites also increases which has an impact on the overall catalytic performance of the material [13,14]. The nature of the compensating cation can also have an effect on the acid strength of the materials, although it is a lot less than the framework composition [15].

4.2.3 Synthesis of aluminophosphates (AlPOs)

Synthesis of aluminophosphates was performed using conventional hydrothermal techniques as outlined by Wilson *et al* [16,17] and followed in chapter 3, section 3.5.1.1.

4.2.3.1 Ion exchange methods

Ion exchange of both the zeolites and MeAlPO-5 materials was performed as outlined by Wang *et al* [1]. The sequential exchange of the two ions involved mixing of the zeolite or MeAlPO-5 and metal substituent for eight hours followed by filtration and subsequent calcination in air.

4.2.4 Hydroxylation of phenol

The favoured method for the production of dihydroxybenzenes is from the environmentally 'green' process concerning the direct hydroxylation of phenol with hydrogen peroxide (figure 4.3) [1,18]. Titanosilicalite (TS-1), first reported in 1983 by Taramasso *et al* [19], is a very active and selective catalyst for the production of dihydroxybenzenes from phenol using aqueous hydrogen peroxide, so much so that Enichem [20] built a commercial plant for this process. Van der Pol *et al* [21] have suggested that the phenol hydroxylation reaction is controlled by intracrystalline diffusion in large crystals of TS-1, whereas Tuel *et al* [22] concluded that it was the external surface acidity which controlled the product ratio of HQ to CAT. HQ was thought to be the preferred reaction product in the micropores of the titanosilicalite catalyst TS-1 whereas CAT was thought to be the preferred reaction product on the external surface titanium sites [7,22]. Wilkenhoner *et al* however disagree with this last summation in that they have proved CAT to be formed both on the external sites and also those in the pores [23].

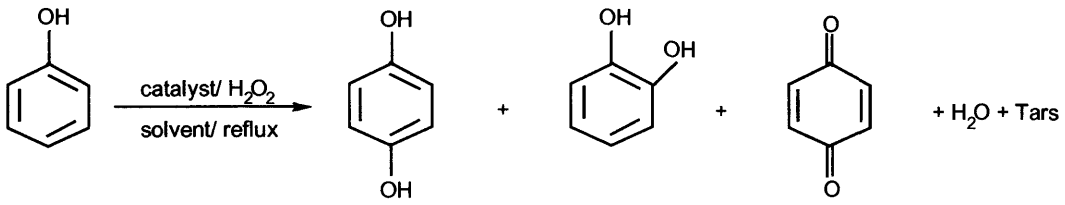

Figure 4.3 *Schematic depicting the products formed during the phenol hydroxylation reaction*

4.2.4.1 Hydrogen peroxide versus *tert*-butylhydroperoxide (TBHP) as oxidant for the hydroxylation of phenol

Phenol hydroxylation over TS-1 and Ti-β are only possible with the use of hydrogen peroxide as the oxidant. This is not thought to be due to the size of the TBHP molecule as there is still room inside the pores for the Ti species to be activated as in epoxidation reactions [24]. Rather, it is thought that a different reaction mechanism is observed. Wilkenhoner *et al* have proposed that it is the terminal hydroxyl of the titanium hydroperoxo group which is the electrophile that attacks the aromatic ring, as proffered by Reddy and Jacobs [25] for the hydroxylation of amines. Other routes offered include the formation of radicals.

4.2.5 Aims and Objectives

The aim of this study was to investigate the activity of the Co(II), Fe(II) and Ti(II) ion exchanged zeolite-β and AlPO-5 catalysts for the phenol hydroxylation reaction at 40°C and 60°C are compare the results to previous studies [1].

4.3 Experimental

4.3.1 Preparation of the catalysts

The materials were prepared as denoted by the sequence in which the metal substituents are written in the catalyst name. For example, for $FeCoNH_4$Beta, iron was firstly exchanged, filtered and calcined then subsequently followed by the repetition of the exchange procedure except this time with cobalt ions.

4.3.1.1 Preparation of Me exchanged zeolite-β (where Me = Co/ Fe/ Ti)

NH_4-β (Si/Al=25) was mixed with an aqueous solution (0.005 M) of metal sulphate at room temperature overnight. The weight ratio of zeolite to aqueous metal substituent was 1:100. The solution was then filtered, washed with distilled water (Aldrich) and dried for two hours at 100°C. The material was subsequently calcined in air from room temperature to 450°C at 5°C/min and held for approximately two hours prior to cooling the catalyst back to room temperature. For the double metal exchanged materials the process was repeated, except this time the second metal sulphate substituent was applied [1].

4.3.1.2 Preparation of pure and Me exchanged AlPO-5 (where Me = Co/ Fe)

AlPO-5 was synthesised using tetraethyl ammonium hydroxide (TEAOH) (Aldrich) as the structure-directing agent (SDA). In a typical synthesis, aluminium hydroxide hydrate (Aldrich) was added to a solution of phosphoric acid (85%) (Aldrich) and distilled water (Fluka). The SDA was subsequently added and vigorous employed in order to form a homogeneous mixture. The final gel, with a pH of approximately 4.5,

was introduced into a Teflon lined stainless steel autoclave and subjected to hydrothermal treatment at 175°C for 3 hours. The recovered solid was filtered, washed with distilled water then dried in air at approximately 100°C overnight.

Ion exchange was undertaken using identical conditions as those for the ion exchanged zeolites as detailed in 4.3.1.1, except this time pure AlPO-5 was mixed with the aqueous metal sulphate solution.

4.3.2 Characterisation

The as synthesised materials were characterised for phase purity and crystallinity using X-ray diffraction (XRD) techniques and X-ray Absorption Spectroscopy (XAS) was employed to investigate the co-ordination of the metal centres within the topology of the zeolites. Energy Dispersive Analysis using X-rays (EDAX) was used to detect the degree of exchange of metal ions within the materials and the catalytic activity for the hydroxylation of phenol to dihydroxybenzenes and other by-products was investigated and analysed using High Performance Liquid Chromatography (HPLC) techniques.

4.3.2.1 XRD measurements

Phase purity and crystallinity of the as synthesised materials were confirmed by X-ray diffraction (XRD) analysis, measured using a Siemens D500 employing Cu-$K\alpha_1$ radiation. In a typical experiment, the sample was pressed onto a plate, smoothed then loaded into position. The materials were subsequently analysed over a range of 5 - 40 degrees (2θ) at a rate of 0.02 degrees a second.

4.3.2.2 XAS measurements

X-ray Absorption Spectroscopy (XAS) measurements were carried out to ascertain the co-ordination of the calcined materials. Co and Fe K-edge XAS measurements were carried out on DUBBLE at the European Synchrotron Radiation Service (ESRF), France. The station is equipped with a Si(111) double crystal monochromator, two ion chambers (one for measuring the incident beam intensity, the other for measuring the transmitted beam intensity) and a nine element Canberra fluorescence detector for collecting information on dilute samples. In a typical experiment, approximately 100mg of the sample was pressed into a 20mm disc and placed into an *in situ* cell (chapter 2, figure 2.7). The sample was calcined by heating at 5°C/min to 535°C in oxygen, changing to nitrogen for an hour to reduce the catalyst then cooling back to room temperature. XAS spectra were recorded by placing the cell in the beam and taking a series of measurements over a one hour period. The data was then analysed using a suite of programs available at the Daresbury Laboratories, namely EXCALIB, EXBROOK and EXCURV98.

4.3.2.3 EDAX measurements

Measurements were carried out using a Philips EDAX machine, at UCL archaeology department. The EDAX was linked to a scanning electron microscope, and X-rays were used to identify trace amounts of elements on the surface of the samples. EDAX also determines the relative amounts of the detected elements present on the scanned area. This is a very useful technique for providing information about the surface composition of a material.

4.3.2.4 Catalytic analysis

Liquid phase phenol hydroxylation batch reactions were carried out in a 100ml three-necked round bottomed flask equipped with a magnetic stirrer, thermometer and water-cooled reflux condenser. The reaction temperature was controlled using an oil-bath located within a fume cupboard. In a typical experiment, 2.0g phenol (Aldrich, 99.5%) was dissolved in approximately 45ml of distilled water (Aldrich) then 200mg of the calcined powder catalyst (particle sizes where approximately 0.5-2μm) and 0.5g 4-fluorophenol (internal standard) (Aldrich) were added. On reaching the desired reaction temperature (40/60°C), 0.75g of aqueous hydrogen peroxide (H_2O_2) (35% Aldrich) was charged dropwise into the reactor using a pipette (phenol to H_2O_2 mole ratio was 3 [1,26]). To avoid any photocatalytic effect on the reaction, the reactor was covered in aluminium foil.

Representative samples were taken after a 10-hour reaction and analysed for catechol (CAT), hydroquinone (HQ) and 1,4-benzoquinone (BQ). Trace amounts of catalyst were removed from the samples using a 0.25μm millipore filter prior to analysis. The aliquots were analysed using an autosampler attached to a Varian Prostar 210 HPLC equipped with a Hichrom KR1005C18 250mm x 2.1mm column using acetonitrile in water as the mobile phase and a 320 detector operating at 225nm. HPLC analysis was carried out by Michael Pilkington-Miksa at UCL chemistry department. Successive analysis of the standard calibration standard proved that the results were reproducible and that sampling and analysis errors were marginal to +/-0.5% (see appendix, figure C and table E).

4.3.2.4.1 High performance liquid chromatography (HPLC) versus gas chromatography (GC) for analysis of the reaction products

Previous work has noted discrepancies in the detection of 1,4-benzoquinone when using gas chromatography (GC) to analyse the reaction products [21]. This is due to GC injection temperatures initiating further reaction between hydroquinone and hydrogen peroxide leading to abnormally high levels of 1,4-benzoquinone being detected. In comparison, only low levels of 1,4-benzoquinone are observed, as expected

for this reaction, when using high performance liquid chromatography (HPLC). For this reason HPLC was the preferred analytical technique for the analysis of the reaction products as demonstrated by other research groups including Wang *et al* [1].

4.4 Results and Discussion

4.4.1 XRD study of the as synthesised catalysts

Figures 4.4 and 4.5 show the XRD patterns acquired for the as synthesised materials. The results indicate that all the catalysts were crystalline and phase-pure on comparison with reported literature for the pure BEA and AFI topologies, obtained from the IZA structure database [11].

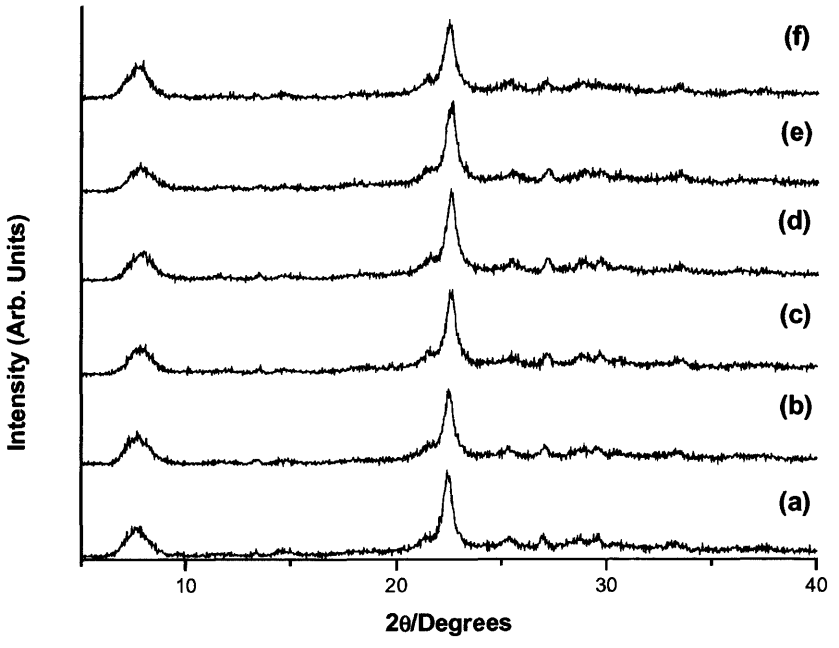

Figure 4.4 *XRD patterns of the as synthesised (a) NH_4-β, (b) $FeCoNH_4$-β, (c) $CoFeNH_4$-β, (d) $FeNH_4$-β, (e) $CoNH_4$-β and (f) TiAl-β catalysts*

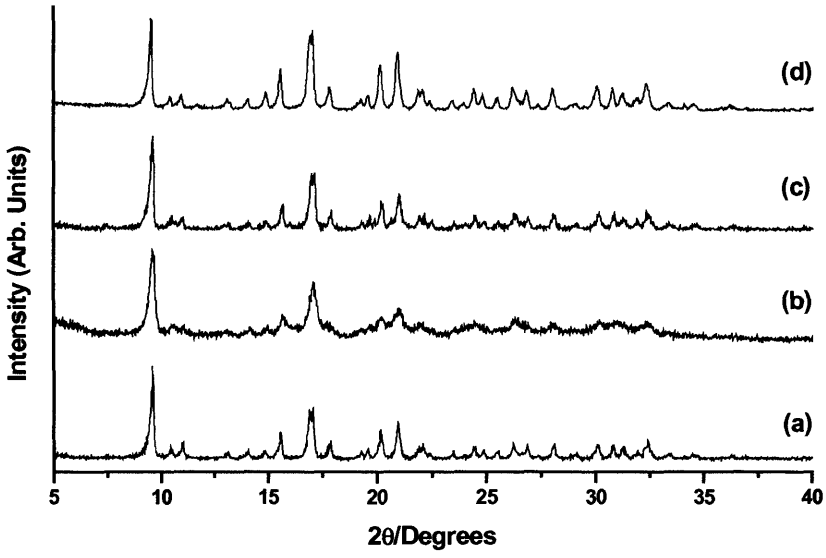

Figure 4.5 *XRD patterns of the as synthesised (a) AlPO-5, (b) FeCoAlPO-5, (c) FeAlPO-5, and (d) CoAlPO-5 catalysts*

4.4.2 XAS study of the calcined catalysts

Results from EXAFS investigations into the cobalt and iron co-ordination within the calcined materials can be seen in table 4.1 and figures 4.6 and 4.7. Data collected for the cobalt and iron exchanged aluminophosphates was found to be too noisy and unfortunately no reasonable information was achievable.

Material	K-edge	Atom pair	N	R (Å)	$2\sigma^2$ (Å^2)
$FeCoNH_4$-β	Fe	Fe-O	1.88	1.89	0.016
	Co	Co-O	5.79	2.08	0.022
$CoFeNH_4$-β	Fe	Fe-O	1.46	1.86	0.016
	Co	Co-O	5.68	2.08	0.02
$FeNH_4$-β	Fe	Fe-O	1.55	1.89	0.016
$CoNH_4$-β	Co	Co-O	5.27	2.07	0.02

Table 4.1 *Structural parameters obtained from EXAFS analysis performed on the cobalt and iron exchanged zeolite-β materials (where: N = co-ordination number, R (Å) = bond length and $2\sigma^2$ (Å^2) = Debye-Waller factor)*

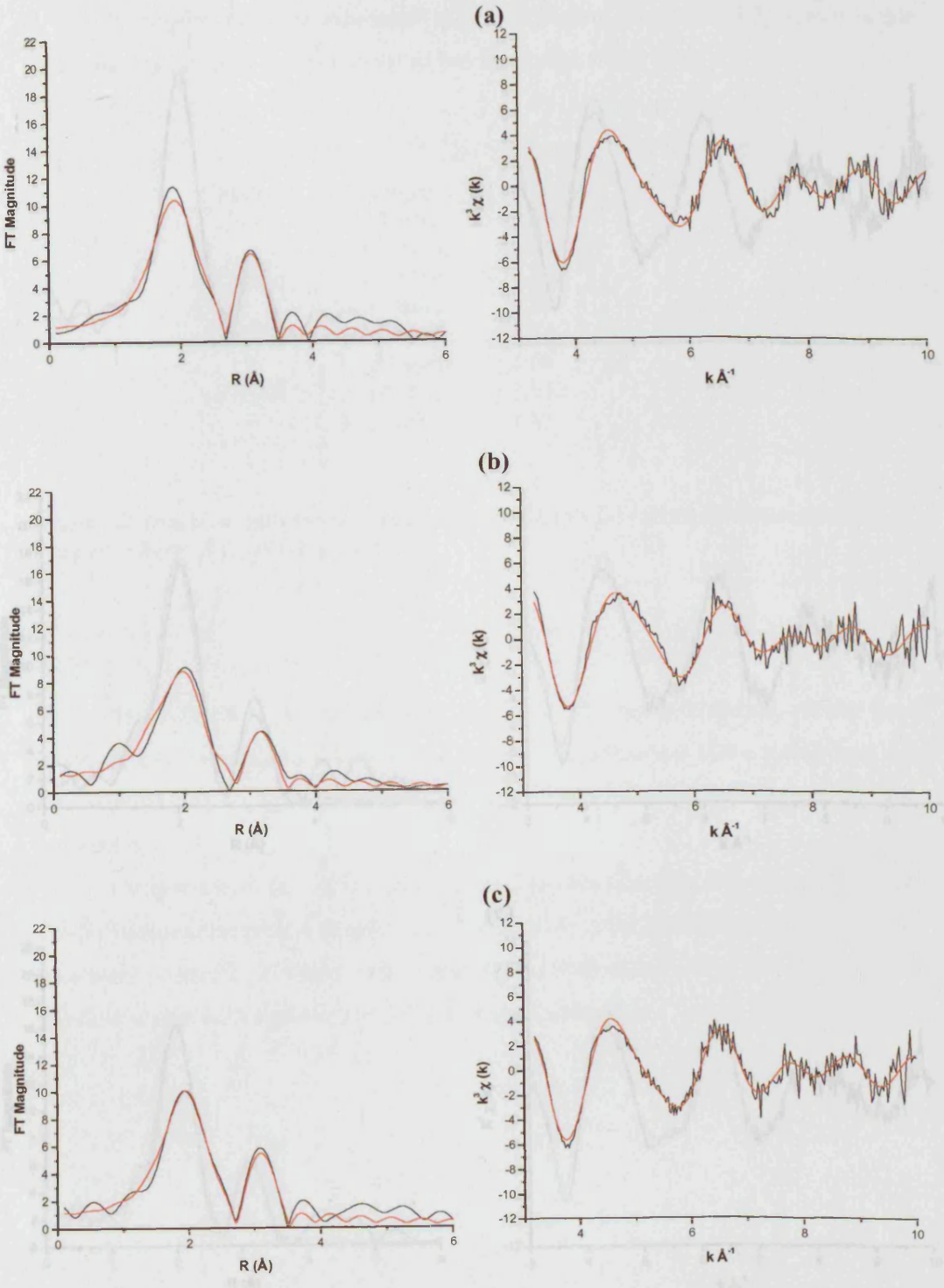

Figure 4.6 *Best fit Fe K-edge EXAFS (left) and Fourier Transform (right) data for the calcined iron exchanged zeolite-β materials, namely (a) $FeCoNH_4$-β, (b) $CoFeNH_4$-β and (c) $FeNH_4$-β (the red line represents the experimental data whilst the black line represents the calculated data)*

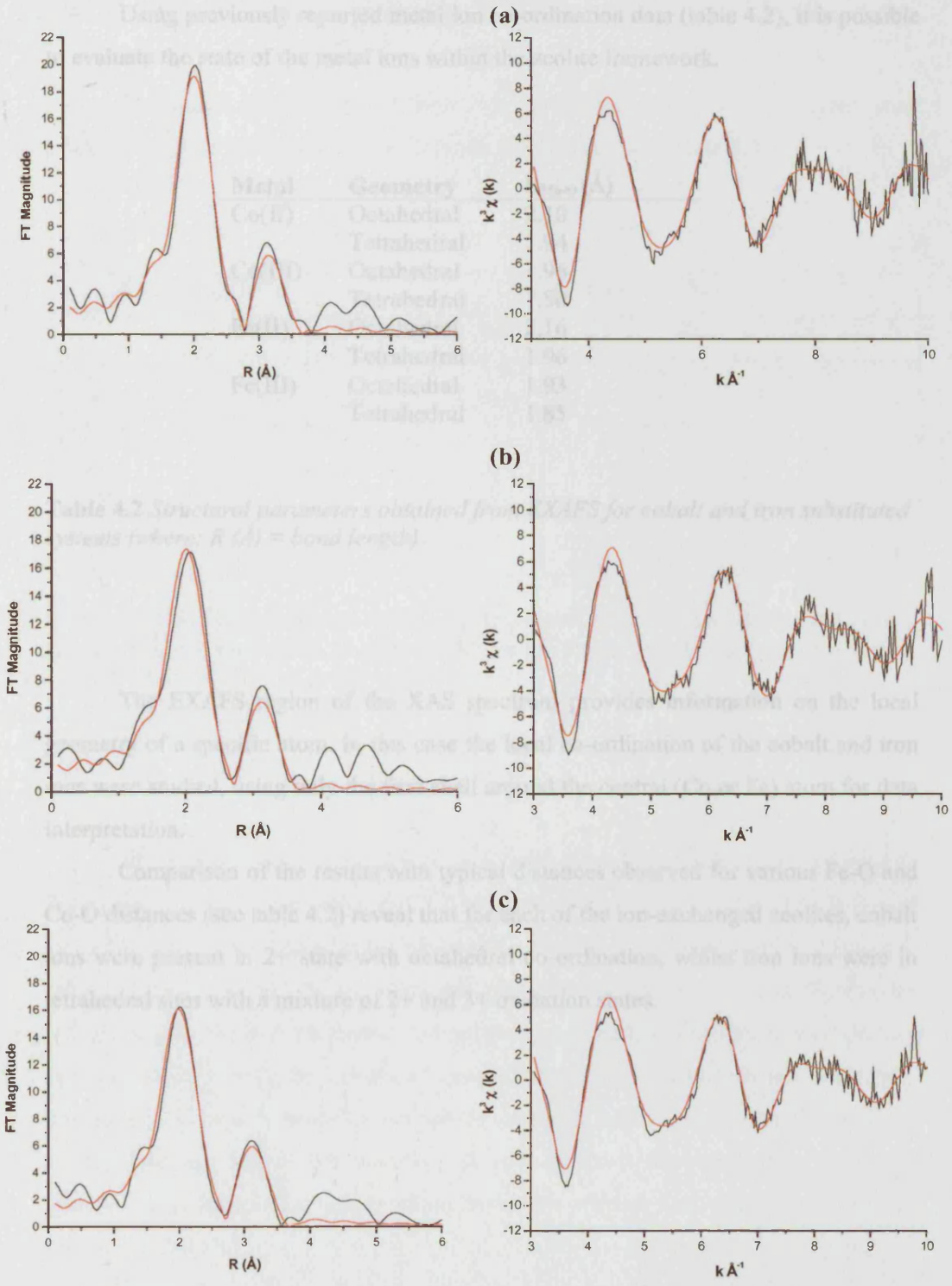

Figure 4.7 *Best fit Co K-edge EXAFS (left) and Fourier Transform (right) data for the calcined cobalt exchanged zeolite- β materials, namely (a) $FeCoNH_4$-β, (b) $CoFeNH_4$-β and (c) $CoNH_4$-β (the red line represents the experimental data whilst the black line represents the calculated data)*

Using previously reported metal ion co-ordination data (table 4.2), it is possible to evaluate the state of the metal ions within the zeolite framework.

Metal	Geometry	R_{Me-O} (Å)
Co(II)	Octahedral	2.10
	Tetrahedral	1.94
Co(III)	Octahedral	1.96
	Tetrahedral	1.80
Fe(II)	Octahedral	2.16
	Tetrahedral	1.96
Fe(III)	Octahedral	1.93
	Tetrahedral	1.85

Table 4.2 *Structural parameters obtained from EXAFS for cobalt and iron substituted systems (where: R (Å) = bond length)*

The EXAFS region of the XAS spectrum provides information on the local geometry of a specific atom. In this case the local co-ordination of the cobalt and iron ions were studied, using only the first shell around the central (Co or Fe) atom for data interpretation.

Comparison of the results with typical distances observed for various Fe-O and Co-O distances (see table 4.2) reveal that for each of the ion-exchanged zeolites, cobalt ions were present in 2+ state with octahedral co-ordination, whilst iron ions were in tetrahedral sites with a mixture of 2+ and 3+ oxidation states.

4.4.3 EDAX study of the as synthesised catalysts

The composition of each of the as synthesised materials was investigated using EDAX analysis. The results of this study are detailed below in table 4.3.

CATALYST	Elements (mass %)						
	Si	Al	Si/Al	P	Fe	Co	Ti
FeCoNH$_4$-β	92.13	5.58	15:1		1.89 (1.12)	0.40 (1.26)	
CoFeNH$_4$-β	94.44	3.32	28:1		1.85	0.40	
FeNH$_4$-β	91.19	6.52	14:1		2.30 (1.15)		
CoNH$_4$-β	92.21	7.66	12:1			0.13 (1.14)	
NH$_4$-β	96.33	3.67	25:1				
TiAl-β	93.47	6.08	15:1				0.45
FeCoAlPO-5		39.64		58.55	1.03	0.79	
FeAlPO-5		38.42		59.99	1.59		
CoAlPO-5		39.31		60.00		0.69	

Table 4.3 *Molecular composition of the as synthesised materials characterised using EDAX analysis (numbers in brackets represent the results Wang et al. obtained via ICP-AES analysis of their prepared materials)*

These results do not completely agree with those found in the work reported by Wang et al [1]. They found through ICP-AES analysis that the quantities of both Fe and Co in all their ion-exchanged materials were approximately 1% (see bracketed values in table 4.3 above). EDAX is a surface analysis technique, whereas ICP-AES provides information on the bulk elemental composition of a catalyst. For this reason, the two sets of results cannot be compared quantitatively, as observed by the erratically changing Si/Al ratio in table 4.3, but can be used as a suggestion of approximate levels of each element within the materials. It appears from the results that there was preferential exchange of iron ions within the zeolite whether it was exchanged firstly or secondly to cobalt.

4.4.4 Catalytic investigations for the hydroxylation of phenol over Me exchanged zeolite-β and AlPO-5 (where Me = Co/ Fe/ Ti)

The catalytic performance of the metal exchanged zeolite-β and AlPO-5 materials were compared for the conversion of phenol and selectivities to products CAT, HQ and BQ, the results of which can be seen in table 4.4 below. Particle size investigations weren't undertaken to ascertain what difference it would have on the reaction. It can however be said that a reduction in particle size would shorten the diffusional path and therefore the probability of by-products formation would decrease, hence the catalyst should have a longer lifetime.

CATALYST	TEMP (°C)	Phenol Conversion (wt%)	Selectivity (wt%)		
			CAT	HQ	BQ
FeCoNH$_4$-β	60	11.68	44.66	40.05	15.29
FeCoNH$_4$-β	40	11.64	46.70	38.88	14.42
CoFeNH$_4$-β	60	11.81	46.99	38.53	14.48
CoFeNH$_4$-β	40	12.22	48.48	37.51	14.00
FeNH$_4$-β	60	8.68	44.92	37.88	17.21
FeNH$_4$-β	40	11.23	66.43	20.84	12.91
CoNH$_4$-β	60	8.45	43.84	39.55	16.61
CoNH$_4$-β	40	6.52	41.46	40.80	17.74
NH$_4$-β	60	5.56	44.14	34.77	21.08
NH$_4$-β	40	5.45	50.46	31.56	17.98
TiAl-β	60	11.56	48.70	36.59	14.71
TiAl-β	40	0			
FeCoAlPO-5	60	0			
FeCoAlPO-5	40	0			
FeAlPO-5	60	13.43	50.00	36.81	13.19
FeAlPO-5	40	0			
CoAlPO-5	60	0			
CoAlPO-5	40	0			
AlPO-5	60	0			
AlPO-5	40	0			
Blank	60	0			
Blank	40	0			

Table 4.4 *Catalytic results for the hydroxylation of phenol over the as synthesised catalysts (reaction conditions: feed = 200mg of catalyst, 2.0g phenol, 45 ml distilled water, 0.5g 4-fluorophenol and 0.75g H_2O_2. reaction temperature = 40/60°C, TOS = 10 hrs)*

Maximum conversions for this reaction over several catalysts have been previously reported in the region of 25%, TOS = 120 minutes. In general, phenol conversions decreased on increase of the reaction temperature.

The exchange of cobalt, iron and titanium transition metal cations into the framework materials significantly improved the conversion of phenol. Catalytic investigations observed no reaction over pure AlPO-5, whereas <6% phenol was converted over pure NH_4-β at both 40°C and 60°C indicating that the non-metal exchanged AlPO was not active for the reaction, whereas the pure zeolite was slightly active.

Selectivities to CAT, HQ and BQ for each of the catalysts were in the main approximately 0.45: 0.4: 0.15 respectively. All catalysts favoured the production of CAT, which correlates with the findings of Wilkenhoner *et al*, who states that the zeolite pore size is the parameter which controls the product formation [23]. Selectivity of these reactions were perhaps not governed by diffusional restraints as the CAT: HQ ratio is relatively low, however the pore size of both the zeolite-β and aluminophosphate catalysts are larger than those of TS-1 leading to less interaction of the reactants with the active sites [6,10] and therefore one reason as to why these catalysts where less active for the conversion of phenol. In addition one should also bear in mind that both zeolite-β and AlPO-5 are more hydrophobic than TS-1.

Of all the exchanged materials, $CoFeNH_4$-β was observed to be the most active at 40°C. On closer examination of the EDAX data, it can be observed that the Si/Al ratio for this material was greater than that of the other exchanged zeolites. One possible reason for the larger ratio is that some of the aluminium leached out during ion exchange. If this were the case, the ion exchange of $FeCoNH_4$-β was incomplete in comparison to $CoFeNH_4$-β. However, the total percentage of iron and cobalt exchanged looks to be similar for both.

At 60°C, no significant difference was observed between the activity for either the $FeNH_4$-β or $CoNH_4$-β catalysts, however on decrease of the reaction temperature, the iron exchanged catalyst was found to be more active. These results are comparable to the conversion of phenol observed for the TiAl-Beta catalyst at 60°C.

No reaction was observed for any of the exchanged AlPO-5 catalysts at 40°C, however at 60°C FeAlPO-5 was observed as being the most active of all the catalysts investigated, with product ratios similar to those observed for the exchanged zeolite-β catalysts.

The observed order of catalytic activity expressed in terms of phenol conversion at 40°C was:

$$CoFeNH_4\text{-}\beta > FeCoNH_4\text{-}\beta > FeNH_4\text{-}\beta > CoNH_4\text{-}\beta > NH_4\text{-}\beta$$

and at 60°C was:

$$FeAlPO\text{-}5 > CoFeNH_4\text{-}\beta > FeCoNH_4\text{-}\beta > TiAl\text{-}\beta > FeNH_4\text{-}\beta > CoNH_4\text{-}\beta > NH_4\text{-}\beta$$

One reason as to why these catalysts were not very reactive could be due to the production of tars. Tar was observed to form during the reactions due to over oxidation, however It was not possible to quantify as to how much had been produced (thermal analysis would have been the preferred technique for this analysis). As the tar was not soluble in the solvent (water) it would most likely have built up on the catalyst surface leading to the de-activation of active sites and pore and channel mouth blockages. The deposition of tar on the external surfaces of some catalysts, for example TS-1, has been found to aid in the conversion of phenol [23]. Here, the tar de-activation of active sites is used as an alternative external surface inertization, lending the catalyst more active for the phenol hydroxylation reaction this however does not seem to have been the case with the materials that were studied.

Another possible reason for the deactivation of the catalysts is framework leaching by solvolysis. Here, polar molecules (e.g. water) react with the metal-oxygen framework bond resulting in the removal of metal atoms. This may occur in defective sites, where the metal is not properly co-ordinated to the framework.

Leaching of the metal ions from the catalysts were investigated. Firstly the catalyst was filtered out of the reaction liquor prior to the liquor minus catalyst being re-heated back to the reaction temperature and the catalytic investigation continued for a further two hours. At this point the liquor was re-analysed using HPLC to see if any further reaction had taken place. For example with the FeAlPO-5 catalyst, as shown in table 4.5 below, no further reaction had proceeded on removal of the catalyst. It was therefore concluded that no metal ions had leached out of the catalyst during the reaction and therefore it was the catalyst itself that was active for the reaction.

Catalyst	Temperature (°C)	Phenol Conversion (wt%)	Selectivity (wt%)					
			CAT		HQ		BQ	
			TOS (hours)					
			10	12	10	12	10	12
FeAlPO-5	60	13.43	50.0	49.9	36.8	36.9	13.2	13.2

Table 4.5 *Catalytic results for the investigation into leaching of the active metal ions for the hydroxylation of phenol over the as synthesised catalyst FeAlPO-5 (reaction conditions: feed = 200mg of catalyst, 2.0g phenol, 45 ml distilled water, 0.5g 4-fluorophenol and 0.75g H_2O_2; reaction temperature = 60°C)*

4.5 Summary and Conclusions

Several iron, cobalt and titanium substituted zeolite-β and AlPO-5 materials were synthesised via ion-exchange techniques in relation to a paper published by Wang *et al* [1]. X-ray diffraction studies found the materials to be both crystalline and phase-pure, on comparison to previously reported patterns outlined in the IZA structure database.

The EDAX results did not completely agree with those found in the work reported by Wang et al [1] since here surface analysis was employed whereas they had used bulk analysis. For this reason the information in table 3.4 cannot be used quantitatively however it can be used as a suggestion of approximate levels of each element within the materials. The results also show that there was preferential exchange of the metal ions within the zeolite.

Investigations into the local geometry of the ion-exchanged zeolites by EXAFS analysis revealed that for each of the materials, cobalt ions were present in the octahedral 2+ state, whilst the iron ions were in tetrahedral sites with a mixture of 2+ and 3+ oxidation states. Unfortunately poor quality data was acquired for the AlPO-5 exchanged materials due to high background noise and therefore no reasonable information was obtainable.

Overall, the catalytic results demonstrate that the exchange of metal ions into the framework materials significantly improved the conversion of phenol. Catalytic investigations observed no reaction over pure AlPO-5, whereas <6% phenol was converted over pure NH_4-β at both 40°C and 60°C indicating that the non-metal exchanged material was slightly active for the reaction. The studies revealed that of all the exchanged materials, CoFeNH_4-β was observed to be the most active catalyst for the hydroxylation of phenol with H_2O_2 at 40°C and selective towards the production of dihydroxybenzenes at 40°C. In addition, although no reaction was observed for any of the exchanged AlPO-5 catalysts at 40°C, at 60°C FeAlPO-5 was observed as being the most active of all the catalysts investigated. The most preferable catalyst however must be the one which is most active at temperatures as close to ambient as possible.

The observed order of catalytic activity expressed in terms of phenol conversion at 40°C was:

$$CoFeNH_4\text{-}\beta > FeCoNH_4\text{-}\beta > FeNH_4\text{-}\beta > CoNH_4\text{-}\beta > NH_4\text{-}\beta$$

and at 60°C was:

$$FeAlPO\text{-}5 > CoFeNH_4\text{-}\beta > FeCoNH_4\text{-}\beta > TiAl\text{-}\beta > FeNH_4\text{-}\beta > CoNH_4\text{-}\beta > NH_4\text{-}\beta$$

In comparison, $CoFeNH_4$-β and $FeCoNH_4$-β should act in similar ways since EDAX analysis showed almost similar values for metal ion exchange. Taking into account errors in sampling and analysis techniques, the catalytic activity of both materials was found to be in the same order. Unfortunately no studies were performed into the leaching of the metal ions, however it would be interesting to see as to whether these remained stable if successive reactions were performed.

4.6 References

(1) Wang, J.; Park, J. N.; Wei, X. Y.; Lee, C. W. *Chem. Commun.* **2003**, 628-629.

(2) Dubey, A.; Rives, V.; Kannan, S. *J. Mol. Catal. A-Chem.* **2002**, *181*, 151-160.

(3) Lee, C. W.; Ahn, D. H.; Wang, B.; Hwang, J. S.; Park, S. E. *Microporous Mesoporous Mat.* **2001**, *44*, 587-594.

(4) Sun, J. M.; Meng, X. J.; Shi, Y. H.; Wang, R. W.; Feng, S. H.; Jiang, D. H.; Xu, R. R.; Xiao, F. S. *J. Catal.* **2000**, *193*, 199-206.

(5) Goldstein, S.; Czapski, G.; Rabani, J. *J. Phys. Chem.* **1994**, *98*, 6586-6591.

(6) Reddy, J. S.; Sivasanker, S.; Ratnasamy, P. *Journal of Molecular Catalysis* **1992**, *71*, 373-381.

(7) Thangaraj, A.; Kumar, R.; Ratnasamy, P. *J. Catal.* **1991**, *131*, 294-297.

(8) Perego, C.; Carati, A.; Ingallina, P.; Mantegazza, M. A.; Bellussi, G. *Appl. Catal. A-Gen.* **2001**, *221*, 63-72.

(9) Grieneisen, J. L.; Kessler, H.; Fache, E.; Le Govic, A. M. *Microporous Mesoporous Mat.* **2000**, *37*, 379-386.

(10) Klaewkla, R.; Kulprathipanja, S.; Rangsunvigit, P.; Rirksomboon, T.; Nemeth, L. *Chem. Commun.* **2003**, 1500-1501.

(11) IZA Structure Database Website, http://www.iza-structure.org/databases, **2004**.

(12) Higgins, J. B.; LaPierre, R.B.; Schlenker, J.L.; Rohrman, A.C.; Wood, J.D.; Kerr, G.T.; Rohrbaugh, W.J. *Zeolites* **1988**, *8*, 446-452.

(13) Ribeiro, F. R.; Alvarez, F.; Henriques, C.; Lemos, F.; Lopes, J. M.; Ribeiro, M. F. *J. Mol. Catal. A-Chem.* **1995**, *96*, 245-270.

(14) Corma, A.; Miguel, P.J.; Orchilles, A.V.; Koermer, G. *J. Catal.* **1994**, *145*, 181-186.

(15) Chen, Y. S.; Guisnet, M.; Kern, M.; Lemberton, J.L. *New Journal of Chemistry* **1987**, *11*, 623-626.

(16) Flanigen, E. M.; Lok, B.; Patton, R.; Wilson, S. *Pure and Applied Chemistry* **1986**, *58*, 1351-1358.

(17) Wilson, S. T.; Flanigen, E. M. US Patent No. 4 567 029,**1986**.

(18) Tatsumi, T. *Curr. Opin. Solid State Mat. Sci.* **1997**, *2*, 76-83.

(19) Taramasso, M.; Perego, G; Notari, B. US Patent No. 4 410 501, **1983**.

(20) Notari, B. *Studies in Surface Science and Catalysis* **1987**, *47*, 413-418.

(21) van der Pol, A.; ver Duyn, A. J.; van Hooff, J. H. C. *Appl. Catal. A-Gen.* **1993**, *96*, 13-20.

(22) Tuel, A. Moussa-Khouzami, S.; Ben Taarit, Y.; Naccache, C. *Journal of Molecular Catalysis* **1991**, *68*, 45-52.

(23) Wilkenhoner, U.; Langhendries, G.; van Laar, F.; Baron, G. V.; Gammon, D. W.; Jacobs, P. A.; van Steen, E. *J. Catal.* **2001**, *203*, 201-212.

(24) Blasco, T.; Camblor, A.; Corma, A.; Esteve, P.; Guil, J.M.; Martinez, A.; Perdigon-Melon, J.A.; Valencia, S. *J. Phys. Chem.* **1998**, *102*, 75-88.

(25) Reddy, J. S.; Jacobs, P.A. *Catalysis Letters* **1996**, *37*, 213-218.

(26) Mal, N. K.; Ramaswamy, A. V. *J. Mol. Catal. A-Chem.* **1996**, *105*, 149-158.

(27) Camblor, M. A.; Constantini, A.; Corma, A.; Gilbert, L.; Esteve, P.; Martinez, A.; Valuncia, S. *Journal of the Chemistry Society Chemical Communications* **1996**, 1339-1344.

(28) van der Waal, J. C.; van Bekkum, H. *J. Mol. Catal. A-Chem.* **1997**, 137-146.

Chapter 5

Study into the acidic and shape-selective nature of platinum impregnated silicoaluminophosphates and metal substituted aluminophosphates, and their catalytic activity for the hydroisomerisation of n-heptane

5.1 Chapter Overview

A series of bifunctional platinum impregnated silicoaluminophosphate (Pt/SAPO) and metal substituted aluminophosphate (Pt/MeAlPO) catalysts containing 0.5 weight percent platinum and 10 weight percent Co(II), Mg(II) or Zn(II) metal ions were synthesised by ion exchange and hydrothermal techniques. The materials were characterised for phase purity and crystallinity using X-ray diffraction (XRD) whilst X-ray absorption spectroscopy (XAS) was applied for investigating the co-ordination geometry of the platinum centres. The acidic nature of the materials were investigated by temperature programmed desorption (TPD) of pyridine, specific surface area using the BET method and thermogravimetric analysis (TGA) to quantify the amount of organics or chemically bonded water held within the systems. The influence of reaction temperature, 275-350°C, as well as pore size and acid/metal properties of the MeAlPOs were examined to study the catalytic activity and selectivity for the hydroisomerisation of n-heptane at atmospheric pressure using 60ml/min hydrogen. The investigations found that the performance of the Pt/Co-AlPO-5 catalyst was initially comparable to previously reported literature for zeolite-β for the hydroisomerisation of n-heptane, with conversion of n-heptane > 48% and selectivity to isomers > 94%, at 350°C.

5.2 Gasoline manufacture

Over the last 100 years there have been many developments within the petrochemical industries to improve the efficiency, quality and environmental risks associated with the everyday use and production of gasoline. More recently, the enforcement of new laws and legislation's governing the quantity of lead, sulphur and aromatic compounds present in gasoline have seen trends towards the use of more unsaturated and branched hydrocarbons being favoured due to their high octane numbers [1-4].

5.2.1 Past and present issues associated with health concerns of gasoline manufacture within petroleum industries

The gasoline/air mix within a spark ignition engine has a tendency to spontaneously ignite or "knock" prematurely rather than burn smoothly upon compression. This ultimately damages the engine and decreases the fuel economy. For this reason anti-knocking agents, developed back in the 1920's, were blended with gasoline to overcome the problem. It was in 1921 that Thomas Midgley developed a very effective anti-knocking agent, tetraethyl lead, although unfortunately it was found to be a major air pollutant and a very poisonous, carcinogenic material [5]. Consequently, during the 1900's, the levels of lead in the air gradually rose as the number of cars using leaded petrol increased. High levels of lead in the blood were found to have dangerous side affects on the brain and digestive system, with children being found to be more at risk due to their size and the fact that lead is more easily absorbed through their respiratory and digestive systems than that of adults [6,7].

In the 1970's, methyl t-butyl ether (MTBE) replaced lead as an octane enhancer. It is still used in the America today as an additive to increase the anti-knocking performance of gasoline and reduce CO and O_3 emissions, although the United Kingdom has banned its use. Unfortunately there were also problems observed with the use of MTBE, these included leaking into groundwater, disguised due to the fact that it is a colourless liquid that dissolves easily in water, as well as being a possible

carcinogen [8]. Instead, toxic compounds for example benzene and toluene are presently added to gasoline as anti-knocking agents.

5.2.1.1 Octane number

The octane number indicates how smoothly a gasoline burns; the higher it is the more efficiently it will burn. Commercial fuels for spark-ignition engines have a research octane number (RON[1]), typically between 88 and 101 [9,10].

The octane number of gasoline is a standard test designed to measure the resistance to knocking and is determined by comparing the properties of a gasoline to isooctane (2,2,4-trimethylpentane) and heptane. Iso-octane has an octane number of 100 (table 5.1), is highly branched and burns smoothly, with little knock. In comparison, heptane has an octane number of zero, is not branched and knocks badly [6,11].

Straight-run gasoline possesses an octane number of around 70. In the 1920's-1980's anti-knocking agents (for example, tetraethyl lead, $Pb(C_2H_5)_4$) were used to increase the octane number, whereas more recently cracking, isomerisation, and other such industrial processes have been used, raising the octane number of gasoline to around 90. Lately, changes to unleaded gasoline have required more costly compounds such as aromatics and highly branched alkanes to be used in order to maintain high octane numbers.

[1] RON is the measure of the antiknock quality of a fuel.

FUEL	RON
n-heptane	0
Iso-octane	100
Iso – octane + 1 g/L $PbEt_4$	108
n-pentane	62
n-hexane	25
2-methylbutane	92
2-methylpentane	73
2-methylhexane	42
1-pentene	91
1-hexene	76
1-heptene	55
Toluene	124
Ethylbenzene	124
Benzene	106
Ethanol	130
MTBE	116

Table 5.1 *Research octane numbers (RON) for hydrocarbons found within gasoline*

5.2.2 Zeolites as a possible solution

In the last decade, more intense European laws regarding the limitation of aromatic compounds, sulphur and other potentially hazardous components within gasoline, have been issued to the petrochemical industries [1-4]. This has led to many new investigations within the petrochemical industry into alternative compounds that could be used with a similar high octane number. Currently being widely investigated as a solution to this problem is the isomerisation of parrafins, for example n-heptane, to mono and multi-branched products.

Zeolites (as previously discussed in chapter 1 section 1.3.1) have been found to be very effective in the production of compounds which possess high octane numbers, in particular Pt/mordenite is currently used within industry [12]. However the performance of zeolite-β has also been found to be comparable at 262°C [13,14]. Numerous studies have established that the isomerisation and cracking of C_7 and C_8 paraffins, particularly n-heptane (RON=0), over zeolites produces mono- (RON=42-65) and preferentially multi-branched (RON=81-112) products enhancing the performance of gasoline.

However, it is still unknown as to how the acidic sites and pore structure affects the product selectivitys [15-17,30]. Several platinum impregnated SAPO and MeAlPO frameworks have been studied to date including Pt/SAPO-5, Pt/SAPO-11, Pt/MeAlPO-5, Pt/MeAlPO-11, Pt/MeAlPO-31 and Pt/MeAlPO-41 [16-19]. Here, several of these frameworks with different metal substituents as well as other previously unpublished framework species Pt/SAPO-36 and Pt/MeAlPO-36, have been studied.

5.2.3 Introduction to aluminophosphates

The three framework materials studied within this chapter include the large pore AlPO-5 and AlPO-36 catalysts, and the small pore AlPO-34 catalyst. Aluminophosphates were previously discussed in chapter 1 section 1.3.1.1 and chapter 3 section 3.3, however one different framework topology, AlPO-34, was not defined.

AlPO-34 is closely related to AlPO-18, the only difference being the stacking of the double six ring units. Crystallographically the structures are different however they both possess similar cages.

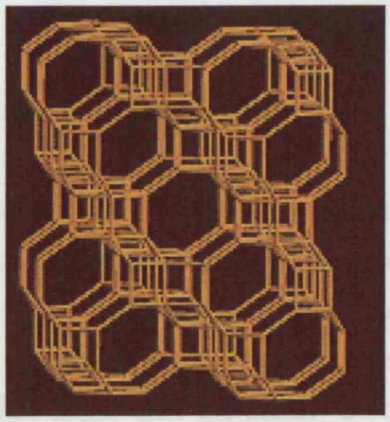

AlPO-34 (CHA)
3-dimensional/ 8-membered ring
3.8 x 3.8Å

Figure 5.1 *Representation of AlPO-34 projected along the [001] axis* [20]

5.2.4 Synthesis of platinum impregnated aluminophosphates (Pt/AlPOs), silicoaluminophosphates (Pt/SAPOs) and their metal substituted analogues

Aluminophosphate and silicoaluminophosphate development and preparation were previously discussed in Chapter 3, section 3.2.2.

Platinum impregnated aluminophosphates (Pt/AlPOs) and silicoaluminophosphates (Pt/SAPOs) are generally prepared via ion exchange methods, the first platinum-zeolite catalysts having been prepared over three decades ago [21,22]. This procedure was shown to be a simple method for the introduction of metal ions into AlPO and SAPO frameworks [23,24]. However, some studies have shown this to lead to larger platinum particles being deposited (due to the presence of HCl when using $Pt(NH_3)(Cl)_2$ complex as the platinum source) than if wet impregnation methods were used [25]. Generally, the size and dispersion of the platinum particles is indicative to the source used in the preparation of the material [23].

If the acid sites and the hydrogenation sites are balanced then the dehydrogenation reaction is not the rate-determining step, hence the selectivity depends on the porosity of the catalyst in question [26-28].

5.2.5 Hydroisomerisation of n-heptane

The challenge faced within the petroleum industry is to achieve a high-octane range by rearrangement of the structure of the hydrocarbons within gasoline. C_5 and C_6 paraffins are currently used in isomerisation units to obtain high octane number components since C_7 and C_8 paraffins have a higher tendency to be cracked. Isomerisation of paraffins larger than C_6, namely n-heptane, towards higher octane number isomers without substantial cracking would be the ideal solution. Selectivity to branched products increases with increased Brønsted acid site strength of the catalyst, and consequently hydroisomerisation is favoured at the expense of cracking under such conditions.

Isomerisation of n-alkanes over bifunctional metal-acid catalysts is a multi-step process as suggested by Weisz *et al* [29] (figure 5.2). Firstly, the paraffin is de-

hydrogenated at the metallic catalytically active sites and then the olefin migrates to the acidic catalytically active sites where it is adsorbed to form a carbenium ion. The carbenium ion undergoes re-arrangements to form either a branched or smaller carbenium ion and an olefin via cracking. Next, desorption of the carbenium takes place and the olefins are hydrogenated once again at the metallic sites [16,17,30].

Hydrocarbon	Hydrocarbon
C_5- (cracking products)	*C_6 aromatics*
Methane	Benzene
Ethane	*C_7 alkanes (n-heptane isomers)*
Propane	n-Heptane
Isobutane	2-Methylhexane
n-Butane	3-Methylhexane
Isopentane	2,2-Dimethylpentane
n-Pentane	2,3-Dimethylpentane
C_6 alkanes (n-hexane isomers)	2,4-Dimethylpentane
n-Hexane	3,3-Dimethylpentane
2-Methylpentane	2,2,3-Trimethylbutane
3-Methylpentane	*C_7 aromatics*
2,2-Dimethylbutane	Toluene
2,3-Dimethylbutane	
C_6 cycloalkanes	
Cyclohexane	
Methylcylopentane	

Table 5.2 *Isomer and cracking product distribution upon hydroisomerisation of n-heptane over solid acid catalysts* [31]

Benzene is an n-hexane isomer, produced only when the reaction temperature is high. It is produced by a process known as dehydrocyclization, not isomerisation and is an undesirable product as it can cause the catalyst to deactivate via coking. Cyclohexane is another undesirable product as this can easily dehydrogenate to form benzene, but can itself also cause deactivation of the catalyst.

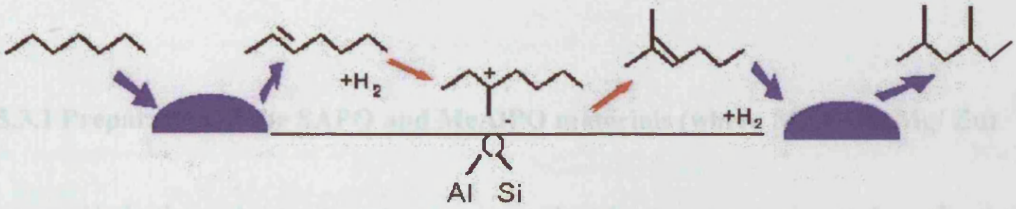

Figure 5.2 *Schematic depicting the hydroisomerisation of n-heptane over a bifunctional catalyst, (De) hydrogenation (and cracking) activity occurs on the platinum sites, whilst isomerisation occurs on the acid sites*

5.2.6 Aims and Objectives

The aim of this study was to synthesise several platinum impregnated SAPO and MeAlPO catalysts, of varying framework topologies, and to determine how the surface acidity and pore structure affected the catalytic activity and selectivity towards the hydroisomerisation of n-heptane.

5.3 Experimental

5.3.1 Preparation of the SAPO and MeAlPO materials (where Me = Co/ Mg/ Zn)

Hydrothermal treatment was employed to prepare each of the silicoaluminophosphate and metal substituted aluminophosphate materials. Preparation was achieved using a silicon and/or a phosphorous source as well as an aluminium source, and if required a metal ion source, followed by a template plus the required amount of water. Further detailed information on the preparation of the materials is given below.

5.3.1.1 Preparation of SAPO-5 and MeAlPO-5 (where Me = Co/ Mg/ Zn)

AlPO-5 and its metal substituted analogues were synthesised using n-methyldicyclohexylamine (MCHA) (Aldrich) as the structure-directing agent (SDA). In a typical synthesis, aluminium hydroxide hydrate (Aldrich) was added to a solution of phosphoric acid (85%) (Aldrich) and distilled water (Fluka). Appropriate amounts of the Me(II) acetate (Aldrich) were then added prior to the addition of the SDA. Vigorous stirring was employed in order to achieve a homogeneous gel, with a final pH of ~ 4.5. The gel was then introduced into a Teflon lined stainless steel autoclave and subjected to hydrothermal treatment at 175°C for 4 hours. The recovered solid was filtered, washed with distilled water then dried in air at approximately 100°C overnight.

The silicoaluminophosphate material, SAPO-5, was prepared using the same experimental procedures as above except that fumed silica (Aldrich) was used in place of some of the phosphoric acid and a longer reaction time of 13 hours was needed to synthesise the pure material.

The gel compositions for the preparation of the MeAlPO-5 and SAPO-5 materials can be seen in table 5.3.

Catalyst	Gel Composition	SDA	Hydrothermal Synthesis Time (hrs)/ Temperature (°C)
MeAlPO-5	0.9Al:1.0P:0.1Me:0.8MCHA:25H_2O	N-methyldicyclohexylamine (MCHA)	4/ 175
SAPO-5	1.0Al:0.9P:0.1Si:0.8MCHA:25H_2O	N-methyldicyclohexylamine (MCHA)	13/ 175

Table 5.3 *Molar compositions used for the preparation of MeAlPO-5 and SAPO-5 (where Me = Co/ Mg/ Zn)*

5.3.1.2 Preparation of SAPO-34 and MeAlPO-34 (where Me = Co/ Mg/ Zn)

The chabazite framework materials were synthesised using tetraethylammonium hydroxide (TEAOH) (Aldrich) as the structure-directing agent (SDA). In a typical SAPO-34 synthesis, phosphoric acid (85%) (Aldrich) was mixed with the required amount of distilled water (Fluka) prior to the addition of aluminium hydroxide hydrate (Aldrich), fumed silica (Aldrich) and TEAOH. Vigorous stirring was employed after each addition and for four hours prior to formation of the final homogeneous gel, pH ~9. The gel was then placed into a Teflon lined stainless steel autoclave and subjected to hydrothermal treatment at 160°C for 148 hours.

The MeAlPO-34 catalysts were synthesised by the addition of aluminium hydroxide hydrate (Aldrich) to a solution of phosphoric acid (85%) (Aldrich) and distilled water (Fluka). Appropriate amounts of the Me(II) acetate (Aldrich) were then added prior to the addition of the SDA, with continuous stirring to ensure a homogeneous mix. The gel, pH ~8, was introduced into a Teflon lined stainless steel autoclave and subjected to hydrothermal treatment at 175°C for 4 hours. The recovered solid was filtered, washed with distilled water then dried in air at approximately 100°C overnight. The gel compositions for the preparation of the SAPO-34 and MeAlPO-34 catalysts can be seen in table 5.4.

Catalyst	Gel Composition	SDA	Hydrothermal Synthesis Time (hrs)/ Temperature (°C)
MeAlPO-34	0.9Al:1.5P:0.1Me:0.8TEAOH:30H_2O	Tetraethyl ammonium hydroxide (TEAOH)	4/ 175
SAPO-34	1.0Al:0.9P:0.1Si:1.0TEAOH:30 H_2O	Tetraethyl ammonium hydroxide (TEAOH)	148/ 160

Table 5.4 *Molar compositions used for the preparation of the MeAlPO-34 and SAPO-34 materials (where Me = Co/ Mg/ Zn)*

5.3.1.3 Preparation of ZnSAPO-36 and MeAlPO-36 (where Me = Co/ Mg/ Zn)

The MeAlPO-36 substituted materials were synthesised using N-ethyldicyclohexylamine (ECHA) (Aldrich) as the structure-directing agent (SDA). In a typical synthesis, aluminium hydroxide hydrate (Aldrich) was added to a solution of phosphoric acid (85%) (Aldrich) and water (Fluka). Me(II) acetate (Aldrich) was then added prior to the addition of the SDA with vigorous stirring to ensure a homogeneous gel. The final gel, pH ~6.5, was then introduced into a Teflon lined stainless steel autoclave and subjected to hydrothermal treatment at 160°C for 16 hours.

The ZnSAPO-36 catalyst was also prepared using N-ethyldicyclohexylamine (ECHA) (Aldrich) as the structure-directing agent (SDA). Typically, phosphoric acid (85%) (Aldrich) was mixed with the required amount of distilled water (Fluka) prior to the addition of aluminium hydroxide hydrate (Aldrich). Next fumed silica (Aldrich), zinc acetate dihydrate (Aldrich) and ECHA (Aldrich) were added with vigorous stirring after each addition. The final gel, pH ~7.5, was then placed into a Teflon lined stainless steel autoclave and subjected to hydrothermal treatment at 155°C for 15 hours. The recovered solid was filtered, washed with distilled water then dried in air at approximately 100°C overnight. Gel compositions for the preparation of the ZnSAPO-36 and the MeAlPO-36 catalysts are shown in table 5.5.

The presence of divalent cations favours the formation of the ATS structure. For this reason zinc was included in the preparation of the silicoaluminophosphate framework material producing ZnSAPO-36. Of course this also produced double acidity within the framework as Zn^{2+} was substituted in the Al^{3+} sites and Si^{4+} substituted in the P^{5+} sites.

Catalyst	Gel Composition	SDA	Hydrothermal Synthesis Time (hrs)/ Temperature (°C)
MeAlPO-36	0.9Al:1.0P:0.1Me:0.8ECHA:10H_2O	N-ethyldicyclohexylamine (ECHA)	16/ 160
ZnSAPO-36	0.9Al:0.9P:0.1Zn:0.1Si:0.8ECHA:10H_2O	N-ethyldicyclohexylamine (ECHA)	15/ 155

Table 5.5 *Molar compositions used for the preparation of the MeAlPO-36 and ZnSAPO-36 materials (where Me = Co/ Mg/ Zn)*

5.3.1.4 Preparation of platinum impregnated catalysts

Each of the materials were firstly calcined by heating in a nitrogen atmosphere at 5°C/ min to 530°C and held for two hours. The gas was then changed to oxygen and heated for a further hour in order to remove the SDA. Platinum loading was accomplished by ion exchanging 0.5 weight percent Pt onto each of the calcined catalysts prior to catalysis. In a typical experiment, 1.5g of the calcined sample was mixed with 7.8ml aqueous $Pt(II)(NH_3)(NO_3)_2$. The solution was stirred at room temperature on a rotary evaporator for one hour prior to evaporation of the liquor at approximately 45°C over one to two hours. The resulting impregnated material was dried in air at 120°C overnight.

5.3.2 Characterisation

The as-prepared materials were characterised for phase purity and crystallinity by X-ray diffraction (XRD). Whilst X-ray absorption fine structure (XAFS) measurements were undertaken to ascertain the co-ordination of the platinum metal within the systems. Temperature programmed desorption (TPD) of pyridine was carried out to determine the acidity of each of the catalysts and the specific surface area of the catalysts was calculated using the BET method. Thermogravimetric analysis (TGA) was used to ascertain the amount of organics or chemically attached water within each catalyst. The degree of reaction and selectivity towards the hydroisomerisation of n-heptane was undertaken using a gaseous reactor set-up in the laboratories at Cordoba University, Spain.

5.3.2.1 XRD measurements

Phase purity and crystallinity of both the as synthesised, calcined and platinum impregnated materials were proven for by X-ray diffraction (XRD). Data was measured using a Siemens D500 employing Cu-$K\alpha_1$ radiation. In a typical experiment, the sample was pressed onto a plate and smoothed prior to the plate being loaded into position. The materials were subsequently analysed over a range of 5 - 40 degrees (2θ) at a rate of 0.02 degrees a second.

5.3.2.2 XAS measurements

X-ray absorption fine structure (XAFS) measurements were carried out to ascertain the co-ordination of the platinum centres within the impregnated materials.

Pt L(III)-edge EXAFS measurements were carried out on station 9.2 at the Daresbury Laboratories. The station is equipped with a Si(220) double crystal monochromator, two ion chambers (one for measuring the incident beam intensity, the

other for measuring the transmitted beam intensity) and a 32 element Canberra fluorescence detector for collecting information on dilute samples. Measurements were recorded on the reduced Pt/CoAlPO-5 and Pt/MgAlPO-5 catalysts since these were observed to be the most catalytically active and the Pt/CoAlPO-34 catalyst to investigate the lack of catalytic hydroisomerisation. In a typical experiment, approximately 100mg of the impregnated sample was pressed into a 20mm disc, placed into an *in situ* cell (chapter 2, figure 2.7). The sample was then subjected to a ramped heating programme, 5°C/min to 535°C in oxygen. The gas was subsequently changed to nitrogen for an hour to reduce the catalyst and then changed once more, to pure hydrogen for a further hour to reduce the platinum species. After the sample had cooled back to room temperature under the hydrogen atmosphere, measurements were recorded in the beam for one hour. The data was then analysed using a suite of programs available at the Daresbury Laboratories, specifically EXCALIB, EXBROOK and EXCURV98.

5.3.2.3 TPD measurements

Qualitative measurements to characterise the acidity of each of the catalysts were determined using temperature programmed desorption (TPD) of pyridine. Typically, 80mg of the calcined/ non-impregnated sample was placed into a vertical stainless steel tubular reactor on top of a metal frit. The sample was pre-calcined (10°C/min in nitrogen (40ml then cooled cooling down to 140°C in nitrogen) prior to analysis. Absorption of pyridine was achieved by injecting 1 µl of the material approximately every fifteen minutes onto the GC column. This was continued until all the peaks for the injection of pyridine observed on the GC computer programme were of equal height, approximately 2-3 hours. Desorption was achieved by subsequent heating of the pyridine absorbed sample from 140°C to 650°C at 5°C /min over a two hour period.

The pyridine absorption and desorption data were collected using a reactor made at the Instituto de Catálisis y Petróleoquímica (CSIC) in Madrid. The gas chromatograph used was a Fisons 8000 series GC equipped with a FID detector.

Modifications to the GC meant that no column was used, instead a 20cm metal pipe had been fitted to conduct the products to the FID.

5.3.2.4 BET measurements

The specific surface area of the catalysts was determined by nitrogen physisorption, calculated using the BET method. In a typical investigation, 15mg of the calcined/ non-impregnated sample was loaded into a glass sample holder and loaded into the Micromeritics ASAP 2010 analyser. The samples were firstly degassed overnight at 300°C in nitrogen prior to the surface area measurements being recorded, using liquid nitrogen (-196°C) as the adsorbate.

5.3.2.5 TGA measurements

The amount of organic material or chemically attached water within each catalyst was ascertained using thermogravimetric analysis (TGA). Firstly, the machine was calibrated using an empty platinum sample holder, then approximately 2mg of the uncalcined/ non-impregnated sample was placed into a platinum sample holder and loaded into the Setaram Setsys 12 TGA machine. The sample was heated from room temperature to 700°C in a flowing argon atmosphere (40ml/min), at a rate of 5°C/min, and the data recorded.

5.3.2.6 Catalytic analysis

The hydroisomerisation reactions were carried out individually using a continuous flow reactor with on-line gas chromatographic analysis, as seen in figure 5.3, made in the Instituto de Catálisis y Petróleoquímica (CSIC), Madrid. In a typical experiment, 500mg of the impregnated sample (powder, 20-100μm) was loaded into a

¼" I.D. vertical stainless steel tubular reactor, on top of a metal frit. The catalyst was then activated by firstly heating the material under a flow of nitrogen (40ml/min), at a rate of 10°C/min from room temperature to 400°C. This temperature was held, whilst the gas was changed to oxygen (20ml/min) for 30mins, then nitrogen for 10mins (40ml/min). Reduction of the catalyst was achieved by further heating at 400°C in hydrogen for 60mins (20ml/min). The temperature was next reduced to 275°C and the hydrogen flow increased to 60ml/min ready for analysis to begin. The hydrocarbon (n-heptane) was injected using a syringe pump at a rate of 5.4ml/h (WHSV = 7.4 h^{-1}) and a period of 30 minutes was allowed before data was collected to ensure equilibrium had firstly been attained within the system. One chromatograph was recorded at temperatures of 275 °C, 290 °C, 310 °C, 330 °C, and 350 °C, then the temperature increased, ready for the next sample acquisition. The products were analysed using a methyl silicone 100 m x 0.25 mm ID fused silica capillary column (Programme: 60 to 115°C at 2°C/min^{-1}) in a Fisons 8000 series gas chromatograph equipped with a FID detector.

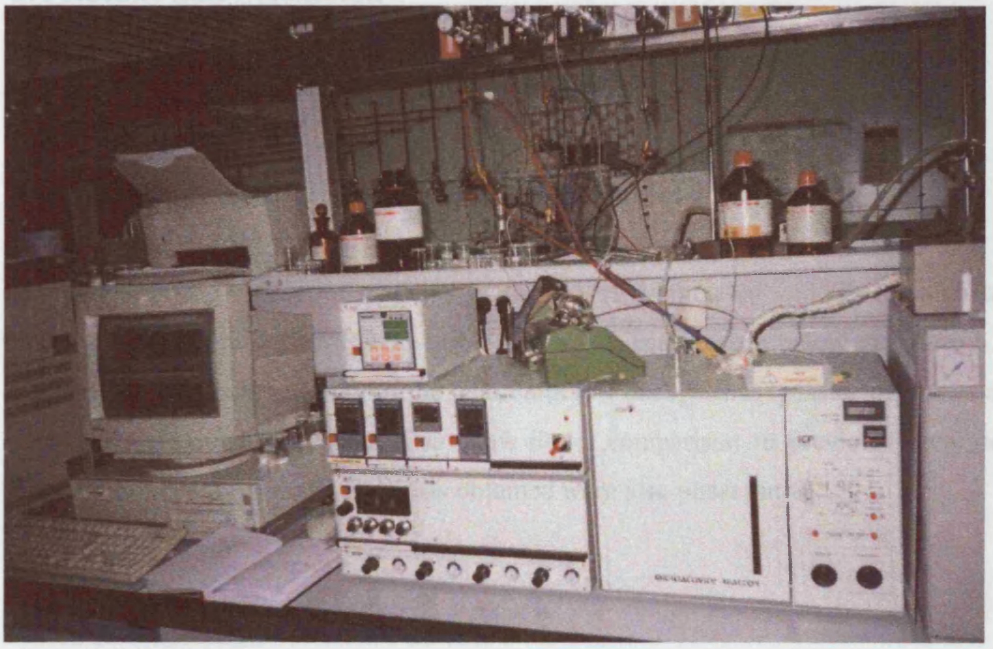

Figure 5.3 *Reactor set-up used for the hydroisomerisation of n-heptane*

5.4 Results and Discussion

5.4.1 XRD study of the as synthesised and impregnated catalysts

The X-ray diffraction patterns of the (1) as synthesised and (2) impregnated SAPO-5/ -36/ -34 and MeAlPO-5/ -36/ -34 materials can be seen below in figures 5.4, 5.5 and 5.6. The high intensity of the peaks and low background indicate the materials prepared were crystalline. They also show direct comparison to previously reported patterns, confirming that the materials obtained were also phase-pure.

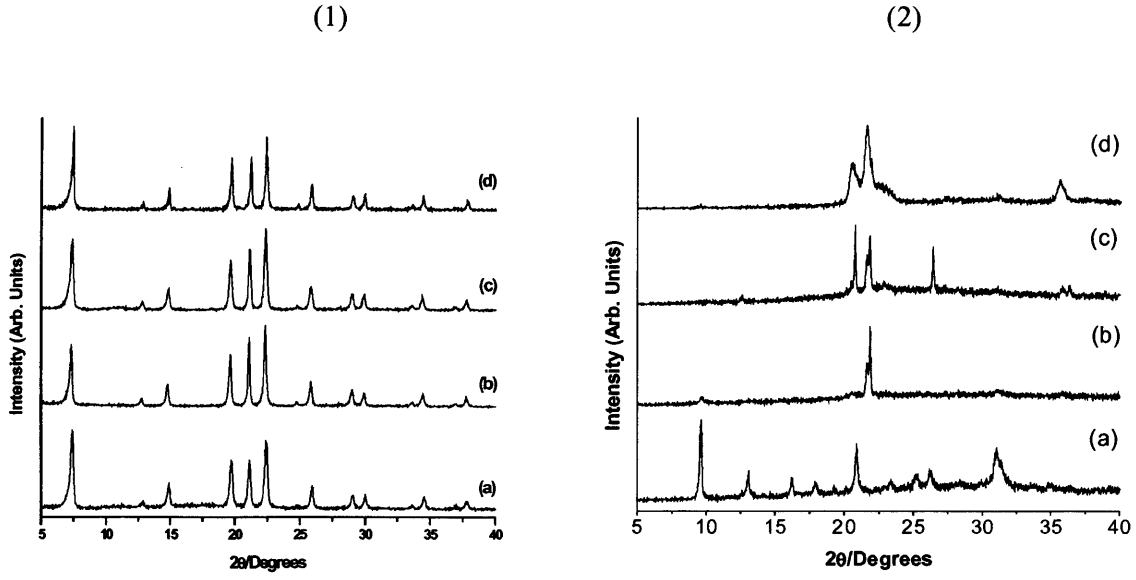

Figure 5.4 *XRD patterns of the (1) as synthesised and (2) impregnated (a) SAPO –5 and MeAlPO-5 materials, where (b) is the CoAlPO-5 material, (c) is the MgAlPO-5 material and (d) is the ZnAlPO-5 material*

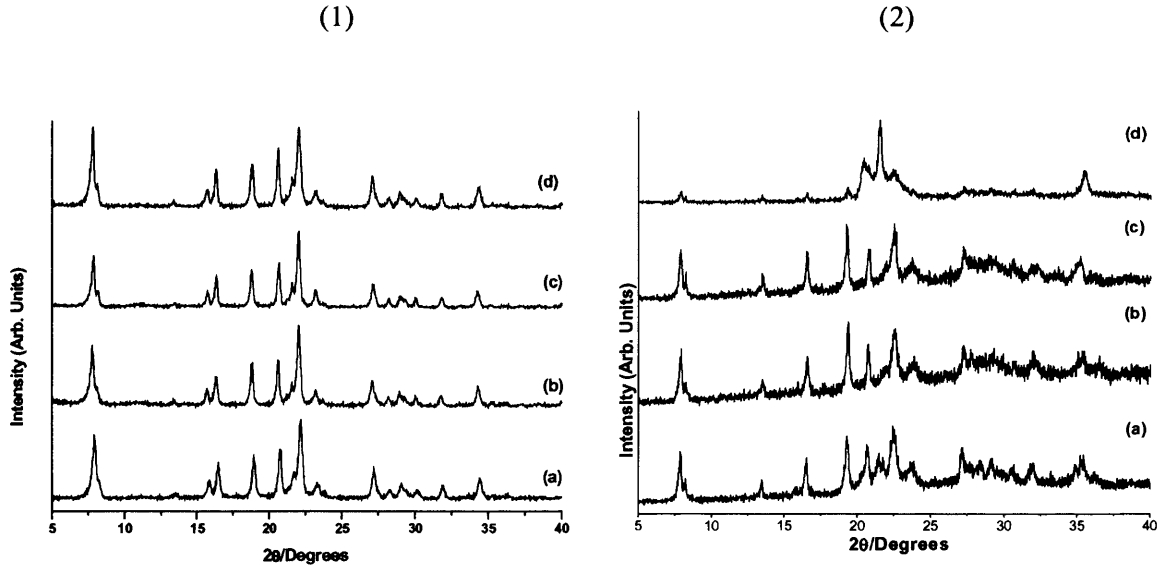

Figure 5.5 *XRD patterns of the (1) as synthesised and (2) impregnated (a) ZnSAPO –36 and MeAlPO-36 materials, where (b) is the CoAlPO-36 material, (c) is the MgAlPO-36 material and (d) is the ZnAlPO-36 material*

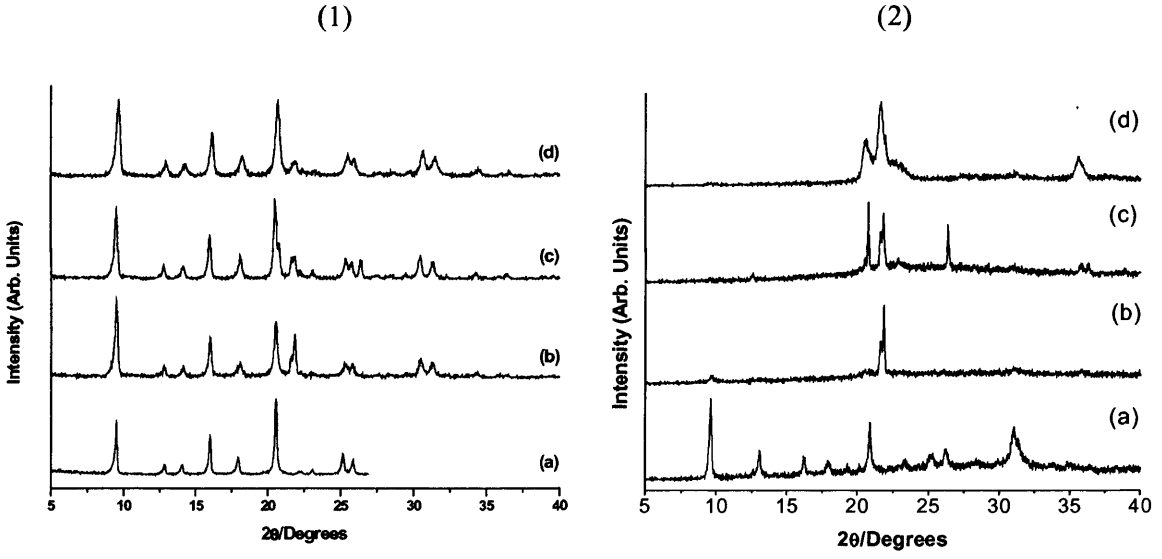

Figure 5.6 *XRD patterns of the (1) as synthesised and (2) impregnated (a) SAPO –34 and MeAlPO-34 materials, where (b) is the CoAlPO-34 material, (c) is the MgAlPO-34 material and (d) is the ZnAlPO-34 material*

On impregnation of the platinum species no change was observed in the structure for most of the framework materials, as shown in figures 5.3, 5.5 and 5.6. The exceptions to this were all of the zinc substituted topologies and the MeAlPO-34 structures, which were observed to collapse during calcination, prior to impregnation.

5.4.2 XAS study of the as synthesised and impregnated catalysts

Results from EXAFS investigations into the platinum co-ordination within the calcined and reduced materials can be seen in table 5.6 and figure 5.7. Only three of the catalysts were studied. Pt/CoAlPO-5 was chosen as it was the most active catalyst for the hydroisomerisation reaction, Pt/MgAlPO-5 as it was similar in activity to the cobalt substituted material and Pt/CoAlPO-34 to see if there were any other underlying reasons as to why no reaction was observed over this catalyst.

Material	L(III)-edge	Atom pair	N	R (Å)	$2\sigma^2$ (Å^2)
Pt/CoAlPO-5	Pt	Pt-Pt	3	2.75	0.01
		Pt-O	0.6	2.02	0.004
Pt/MgAlPO-5	Pt	Pt-Pt	3	2.77	0.01
		Pt-O	0.6	2.03	0.004
Pt/CoAlPO-34	Pt	Pt-Pt	3	2.77	0.01
		Pt-O	1	2.04	0.005

Table 5.6 *Structural parameters obtained from EXAFS analysis performed on the platinum impregnated aluminophosphates (where: N = co-ordination number, R (Å) = bond length and $2\sigma^2$ (Å^2) = Debye-Waller factor)*

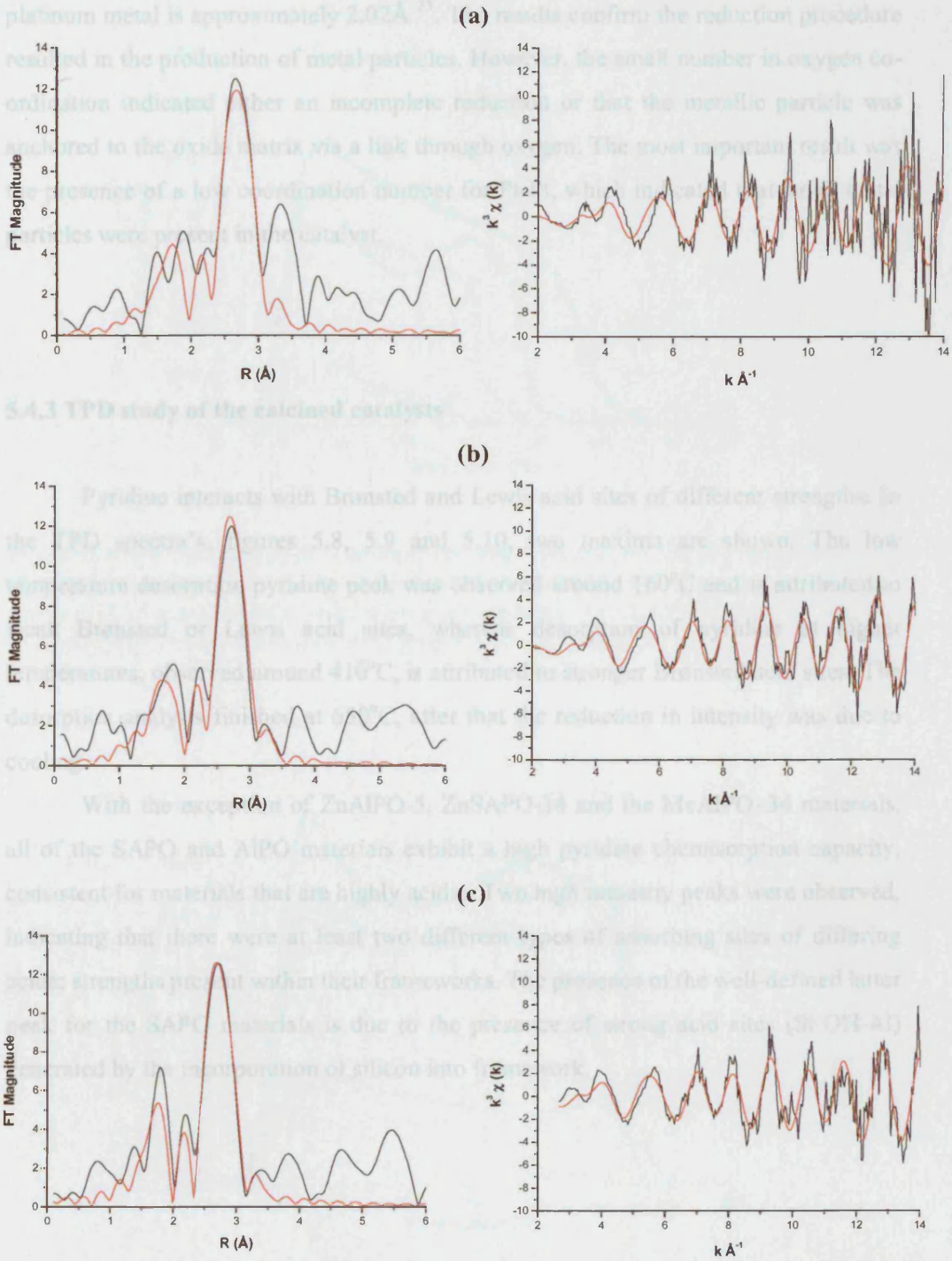

Figure 5.7 *Best fit Pt L(III)-edge EXAFS (left) and Fourier Transform (right) data for the calcined platinum impregnated aluminophosphates, namely (a) Pt/CoAlPO-5, (b) Pt/MgAlPO-5 and (c) Pt/CoAlPO-34 (the red line represents the experimental data whilst the black line represents the calculated data)*

The typical bond length for Pt-Pt in platinum metal is 2.74Å and Pt-O in platinum metal is approximately 2.02Å [23]. The results confirm the reduction procedure resulted in the production of metal particles. However, the small number in oxygen co-ordination indicated either an incomplete reduction or that the metallic particle was anchored to the oxide matrix via a link through oxygen. The most important result was the presence of a low coordination number for Pt-Pt, which indicated that small metal particles were present in the catalyst.

5.4.3 TPD study of the calcined catalysts

Pyridine interacts with Brønsted and Lewis acid sites of different strengths. In the TPD spectra's, figures 5.8, 5.9 and 5.10, two maxima are shown. The low temperature desorption pyridine peak was observed around 160°C and is attributed to weak Brønsted or Lewis acid sites, whereas desorption of pyridine at higher temperatures, observed around 410°C, is attributed to stronger Brønsted acid sites. The desorption analysis finished at 650°C, after that the reduction in intensity was due to cooling.

With the exception of ZnAlPO-5, ZnSAPO-34 and the MeAlPO–34 materials, all of the SAPO and AlPO materials exhibit a high pyridine chemisorption capacity, consistent for materials that are highly acidic. Two high intensity peaks were observed, indicating that there were at least two different types of adsorbing sites of differing acidic strengths present within their frameworks. The presence of the well-defined latter peak for the SAPO materials is due to the presence of strong acid sites (Si-OH-Al) generated by the incorporation of silicon into framework.

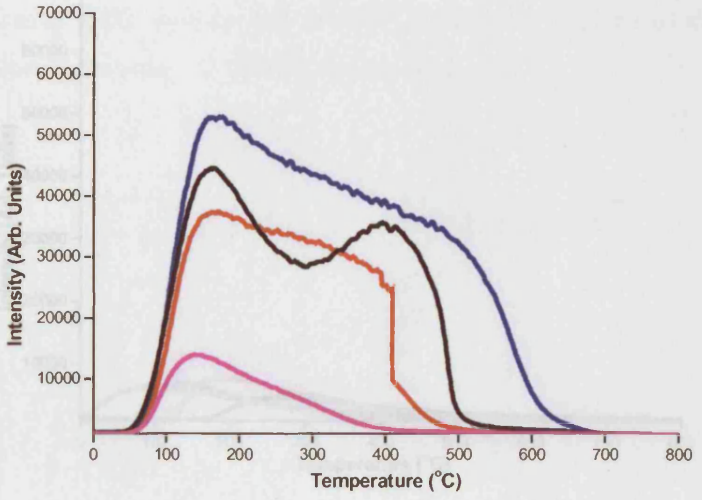

Figure 5.8 *TPD patterns of the calcined/ non-impregnated (-) SAPO-5 and MeAlPO-5 materials, where (-) is the CoAlPO-5 material, (-) is the MgAlPO-5 material and (-) is the ZnAlPO-5 material (N.B. sudden drop observed for the CoAlPO-5 material was due to a technical glitch which caused the temperature to cut out)*

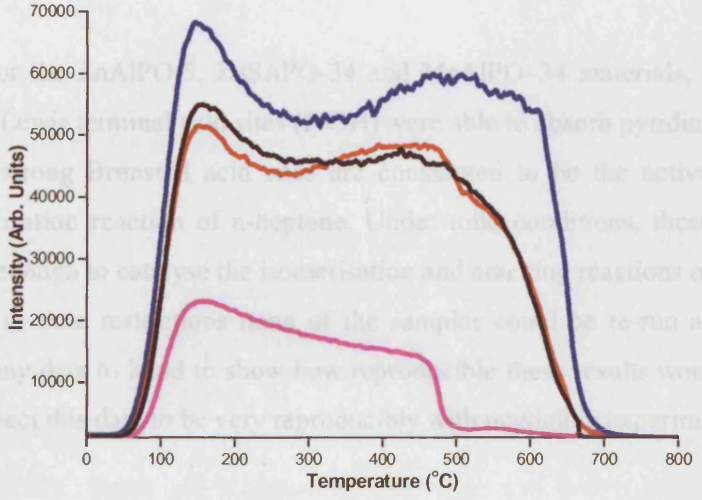

Figure 5.9 *TPD patterns of the calcined/ non-impregnated (-) ZnSAPO –36 and MeAlPO-36 materials, where (-) is the CoAlPO-36 material, (-) is the MgAlPO-36 material and (-) is the ZnAlPO-36 material*

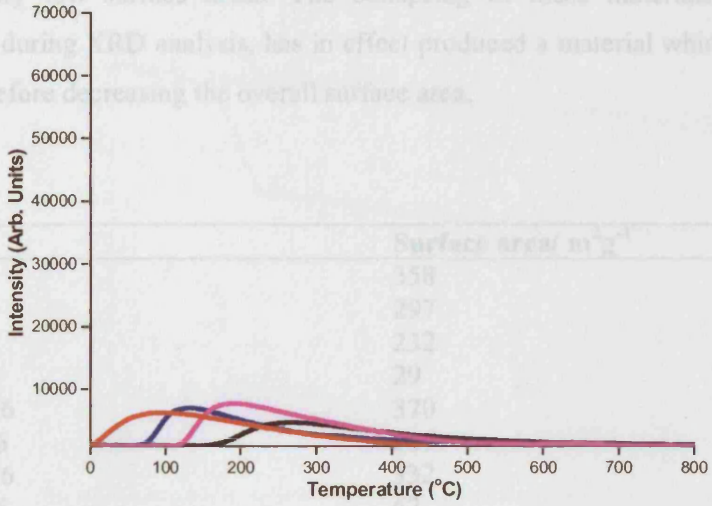

Figure 5.10 *TPD patterns of the calcined/ non-impregnated (-) SAPO –34 and MeAlPO-34 materials, where (-) is the CoAlPO-34 material, (-) is the MgAlPO-34 material and (-) is the ZnAlPO-34 material*

As for the ZnAlPO-5, ZnSAPO-34 and MeAlPO–34 materials, only the weak Brønsted or Lewis terminal acid sites (P-OH) were able to absorb pyridine.

The strong Brønsted acid sites are considered to be the active sites for the hydroisomerisation reaction of n-heptane. Under mild conditions, these are the only sites strong enough to catalyse the isomerisation and cracking reactions of alkanes [32,33].

Due to time restrictions none of the samples could be re-run and therefore I don't have any data to hand to show how reproducible these results would be. I would however expect this data to be very reproducibly with negligible experimental error.

5.4.4 BET study of the as synthesised catalysts

Table 5.7 shows the results obtained from nitrogen physisorption measurements. Apart from the zinc substituted AlPO materials, all the others exhibited high surface

areas typical of these materials. The zinc catalysts on the other hand were found to possess very low surface areas. The collapsing of these materials, as discussed previously during XRD analysis, has in effect produced a material which possesses no pores, therefore decreasing the overall surface area.

Catalyst	Surface area/ m^2g^{-1}
SAPO-5	358
CoAlPO-5	297
MgAlPO-5	232
ZnAlPO-5	29
ZnSAPO-36	370
CoAlPO-36	367
MgAlPO-36	332
ZnAlPO-36	62
SAPO-34	356
CoAlPO-34	370
MgAlPO-34	361
ZnAlPO-34	61

Table 5.7 *Surface area properties of the calcined/ non-impregnated catalysts*

5.4.5 TGA study of the as synthesised catalysts

Thermogravimetric analysis studies were undertaken to determine the nature of various loosely bound species present within the catalyst. Figures 5.11, 5.12 and 5.13 show the TGA data recorded for each of the AFI, ATS and CHA-type as synthesised materials.

Two different weight losses were observed overall, these included an exotherm in the range $T < 180^{\circ}C$ and a second in the range $180 < T < 500^{\circ}C$ (where T = temperature). The first loss is attributed to loss of surface and framework water whereas the second is associated to desorption of the physically occluded template [34]. These multistep losses have been seen many times before for these kind of materials, one example is FeAlPO-18 [35].

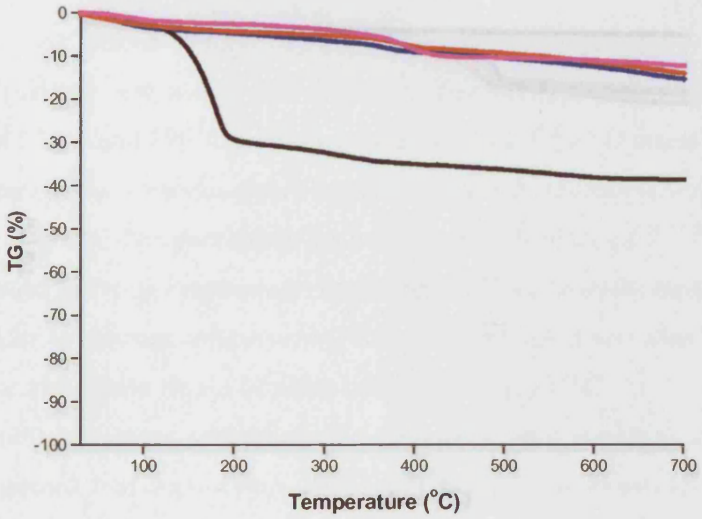

Figure 5.11 *Thermogravimetric measurements of the uncalcined/ non-impregnated (-) SAPO-5 and MeAlPO-5 materials, where (-) is the CoAlPO-5 material, (-) is the MgAlPO-5 material and (-) is the ZnAlPO-5 material*

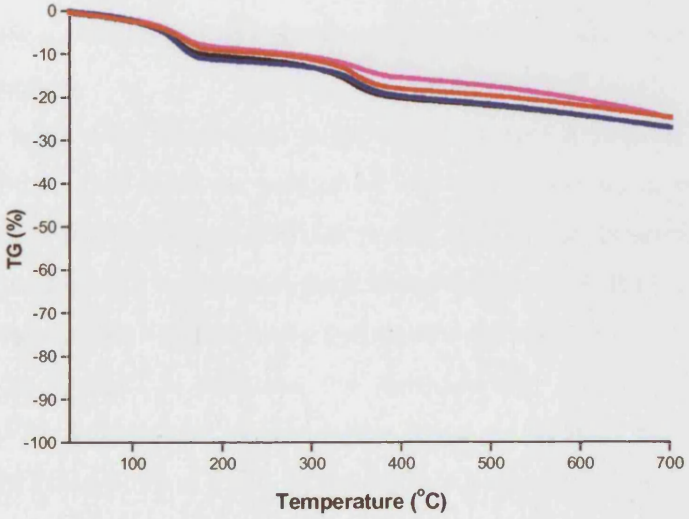

Figure 5.12 *Thermogravimetric measurements of the uncalcined/ non-impregnated (-) ZnSAPO-36 and MeAlPO-36 materials, where (-) is the CoAlPO-36 material, (-) is the MgAlPO-36 material and (-) is the ZnAlPO-36 material*

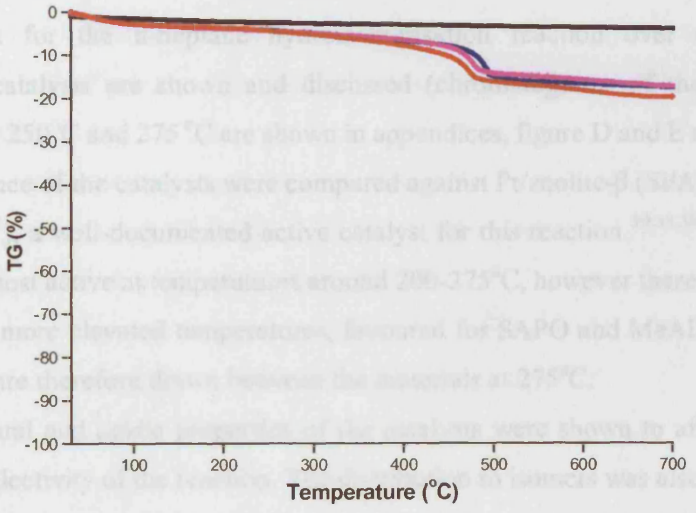

Figure 5.13 *Thermogravimetric measurements of the uncalcined/ non-impregnated (-) SAPO-34 and MeAlPO-34 materials, where (-) is the CoAlPO-34 material, (-) is the MgAlPO-34 material and (-) is the ZnAlPO-34 material*

5.4.6 Catalytic investigation for the hydroisomerisation of n-heptane over the platinum impregnated catalysts

Results for the n-heptane hydroisomerisation reaction over each of the impregnated catalysts are shown and discussed (chromatograms of the analysis of Pt/Zeolite-β at 250°C and 275 °C are shown in appendices, figure D and E respectively). The performance of the catalysts were compared against Pt/zeolite-β (Si/Al=25, surface area=530m^2g^{-1}), a well-documented active catalyst for this reaction [30,33,36]. Zeolite-β is known to be most active at temperatures around 200-275°C, however these studies were carried out at more elevated temperatures, favoured for SAPO and MeAlPO catalysts. Comparisons are therefore drawn between the materials at 275°C.

Structural and acidic properties of the catalysts were shown to affect both the activity and selectivity of the reaction. The distribution to isomers was also seen to vary greatly depending on the pore size and cavity of the framework catalyst used.

Furthermore, n-Hexene hydroisomerisation reactions were undertaken for the Pt/CoAlPO-5 and PtCoAlPO-34 catalysts to investigate as to whether the pore size of the smaller AlPO-34 framework was the reason as to why no conversion had been observed for the n-heptane hydroisomerisation reaction. Both the n-heptane (C_7) and n-hexene (C_6) hydroconversions involved cracking and isomerisation reactions. The quantity of aromatics and cyclic products formed was negligible and furthermore there was no formation of alkenes or products heavier than C_6 or C_7 with either n-hexene or n-heptane respectively.

Once again time restrictions meant that there was a limit to the quantity of catalytic reactions that could be performed. For this reason no investigations were carried out as to what effect particle size would have on the catalytic reaction. It is however fair to say that a reduction in particle size would lead to the formation of fewer by-products and hence a decrease in the deactivation of the catalyst since the diffusional path would be shorter. In addition, the reproducibility of the investigation was confirmed by the achievement of similar data (error < 1%) from that of past analysis undertaken for Pt/Zeolite-β at 250°C by the research group in Cordoba.

5.4.6.1 Hydroisomerisation of n-heptane over Pt/SAPO-5 and Pt/MeAlPO-5 (where Me = Co/ Mg/ Zn)

Figure 5.14 below shows the effect of temperature on the hydroisomerisation of n-heptane over Pt/SAPO-5 and Pt/MeAlPO-5 (where Me = Co/ Mg/ Zn) under identical reaction conditions.

The aromatics and cyclic products produced during these studies accounted for <0.5% for the reaction over the Pt/MgAlPO-5 catalyst at 330°C and 350°C and <2% for the reaction over the Pt/CoAlPO-5 catalyst at 275°C.

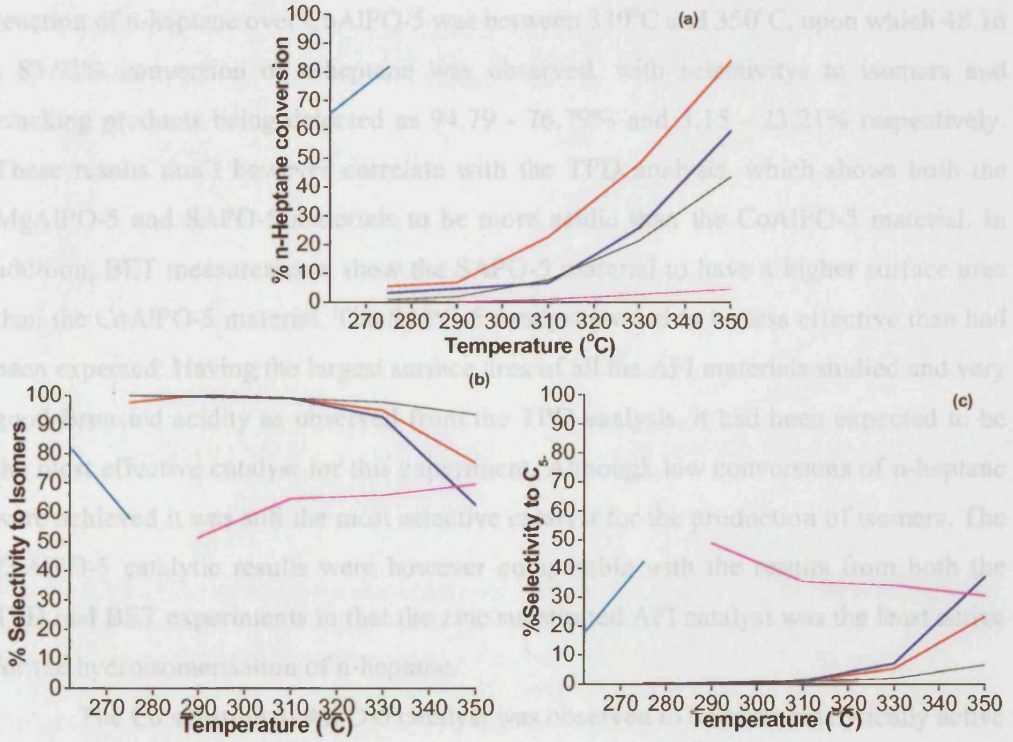

Figure 5.14 *Effect of temperature on the (a) conversion of n-heptane, (b) selectivity to mono- and multi-branched isomers and (c) selectivity to C_{5-} (cracking products), for the hydroisomerisation of n-heptane over (-) Pt/ zeolite-β, (-) Pt/SAPO-5 and Pt/MeAlPO-5 catalysts, where (-) is the Pt/CoAlPO-5 catalyst, (-) is the Pt/MgAlPO-5 catalyst and (-) is the Pt/ZnAlPO-5 catalyst (reaction conditions: H_2 flow=60ml/min, WHSV=5.4ml/h, catalyst weight=500mg)*

The graphs show that the more active material under these reaction conditions was the CoAlPO-5 catalyst at 350°C. On comparison with Zeolite-β at 275°C, both catalysts converted similar amounts of n-heptane, however CoAlPO-5 was more selective in the production of isomers with 76.79% and 57.8% being produced for CoAlPO-5 and Zeolite-β respectively. In addition, selectivies to cracking products for the Zeolite-β catalyst were almost double that produced by the CoAlPO-5 catalyst.

On increasing the reaction temperature, all catalysts exhibited better conversions of n-heptane, although as demonstrated in graphs 5.14b and 5.14c, higher temperatures meant that the selectivity to isomers decreased and simultaneously the amount of cracking products increased. In conclusion, the best temperature observed for the reaction of n-heptane over CoAlPO-5 was between 330°C and 350°C, upon which 48.16 - 83.93% conversion of n-heptane was observed, with selectivitys to isomers and cracking products being detected as 94.79 - 76.79% and 5.15 - 23.21% respectively. These results don't however correlate with the TPD analysis, which shows both the MgAlPO-5 and SAPO-5 materials to be more acidic than the CoAlPO-5 material. In addition, BET measurements show the SAPO-5 material to have a higher surface area than the CoAlPO-5 material. The SAPO-5 catalyst proved to be less effective than had been expected. Having the largest surface area of all the AFI materials studied and very good Brønsted acidity as observed from the TPD analysis, it had been expected to be the most effective catalyst for this experiment. Although low conversions of n-heptane were achieved it was still the most selective catalyst for the production of isomers. The ZnAlPO-5 catalytic results were however comparable with the results from both the TPD and BET experiments in that the zinc substituted AFI catalyst was the least active for the hydroisomerisation of n-heptane.

The Co substituted AlPO-5 catalyst was observed to be more catalytically active for this reaction, this may be due to the location of the acid sites within the pores and cavities of the framework and their accessibility by reactant molecules.

5.4.6.2 Hydroisomerisation of n-heptane over Pt/ZnSAPO-36 and Pt/MeAlPO-36 (where Me = Co/ Mg/ Zn)

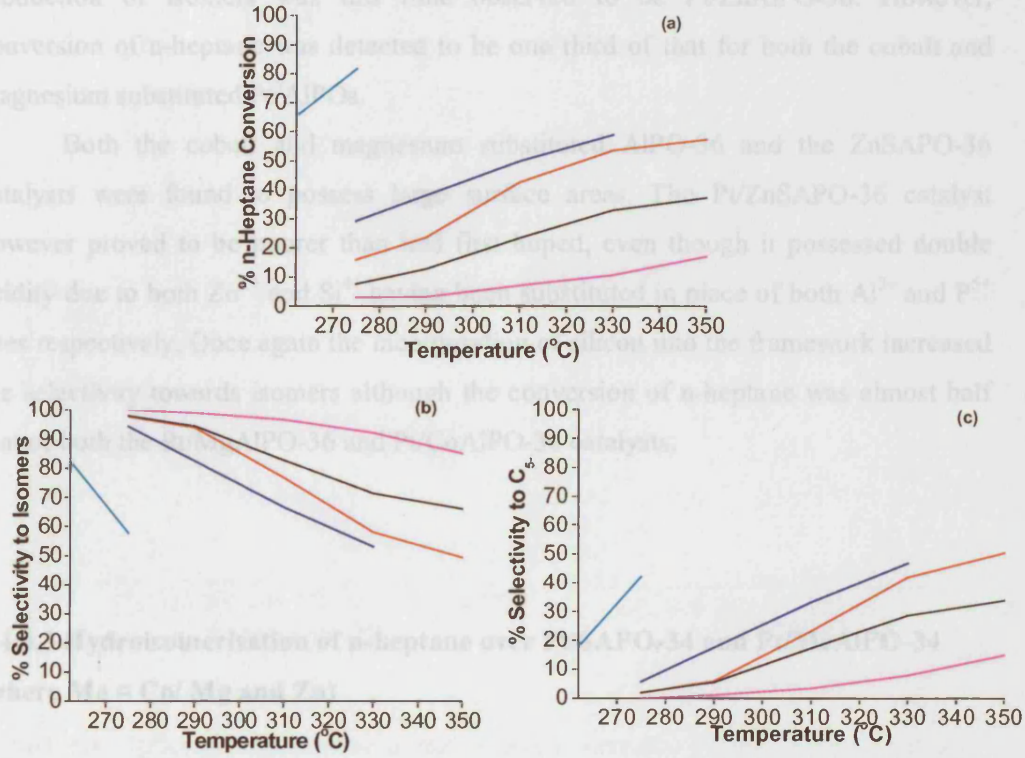

Figure 5.15 *Effect of temperature on the (a) conversion of n-heptane, (b) selectivity to mono- and multi-branched isomers and (c) selectivity to C_{5-} (cracking products), for the hydroisomerisation of n-heptane over (-) Pt/ zeolite-β, (-) Pt/ZnSAPO-36 and Pt/MeAlPO-36 catalysts, where (-) is the Pt/CoAlPO-36 catalyst, (-) is the Pt/MgAlPO-36 catalyst and (-) is the Pt/ZnAlPO-36 catalyst (reaction conditions: H_2 flow=60ml/min, WHSV=5.4ml/h, catalyst weight=500mg)*

Aromatics and cyclic products produced during these studies were observed solely for the reaction over Pt/CoAlPO-36 catalyst, as <0.5% at 275°C and <0.2% at 350°C.

As seen in figure 5.15 above, the Pt/MgAlPO-36 catalyst exhibited higher catalytic activity. On comparing previously determined TPD of pyridine data, section 5.4.3, with the above results both findings correlate very well. A more defined second

peak proves that there are stronger Brønsted acid sites within the MgAlPO-36 framework than for any of the other materials. However, although Pt/MgAlPO-36 converted more n-heptane overall, it was the Pt/CoAlPO-36 catalyst which showed better selectivity to isomers. The most selective ATS framework catalyst for the production of isomers was this time observed to be Pt/ZnAlPO-36. However, conversion of n-heptane was detected to be one third of that for both the cobalt and magnesium substituted Pt/AlPOs.

Both the cobalt and magnesium substituted AlPO-36 and the ZnSAPO-36 catalysts were found to possess large surface areas. The Pt/ZnSAPO-36 catalyst however proved to be poorer than had first hoped, even though it possessed double acidity due to both Zn^{2+} and Si^{4+} having been substituted in place of both Al^{3+} and P^{5+} sites respectively. Once again the incorporation of silicon into the framework increased the selectivity towards isomers although the conversion of n-heptane was almost half that of both the Pt/MgAlPO-36 and Pt/CoAlPO-36 catalysts.

5.4.6.3 Hydroisomerisation of n-heptane over Pt/SAPO-34 and Pt/MeAlPO-34 (where Me = Co/ Mg and Zn)

The lack of catalytic activity observed for both the Pt/SAPO-34 and Pt/MeAlPO-34 catalysts could have been due to several possible factors. The most likely explanation for the Pt/MeAlPO-34 catalysts was being the collapse of the structure during impregnation. Whereas for the Pt/SAPO-34 catalyst, it may have been due to either the pore size of the three-dimensional CHA microporous framework being too small, thereby not allowing reactants/products to pass, or secondly, that the acid and metal sites were located too far apart from each other, it would limit the reaction and the consequent conversion rate of n-heptane [37-39].

The favoured mono- and multi-branched isomers that are formed upon reaction of n-heptane have molecular diameters of 0.56nm and 0.70nm respectively. As the pore sizes of both the AFI and ATS structures are large, 0.73 x 0.73nm and 0.65 x 0.75nm respectively, no diffusional restraints are present within the materials. Here, the Pt/SAPO-34 catalyst was observed to produce isomers therefore indicating that there is no steric hindrance observed in the formation of these molecules within the structures.

5.4.6.4 Hydroisomerisation of n-hexene over Pt/CoAlPO-5 and Pt/CoAlPO-34

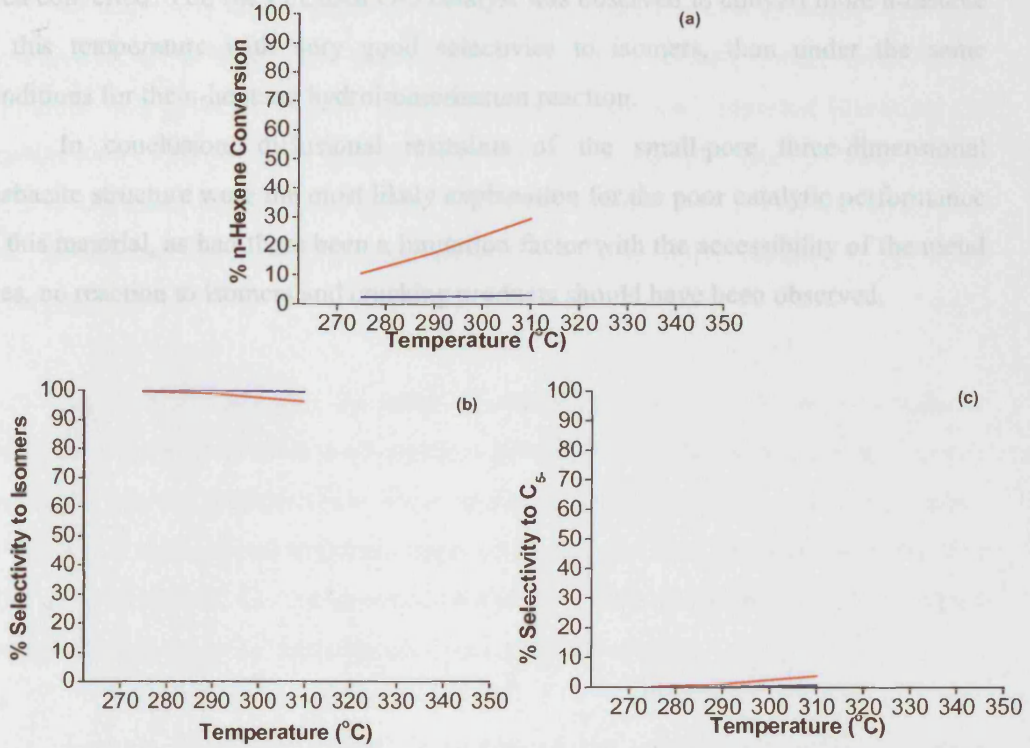

Figure 5.16 *Effect of temperature on the (a) conversion of n-hexane, (b) selectivity to mono- and multi-branched isomers and (c) selectivity to C_{5-} (cracking products), for the hydroisomerisation of n-hexene over (-) Pt/ zeolite-β, (-) Pt/CoAlPO-5 and (-) Pt/CoAlPO-34 (reaction condition: H_2 flow=60ml/min, WHSV=5.4ml/h, catalyst weight=500mg)*

Further investigations were undertaken in order to ascertain as to whether it was a limitation of the metal function or structural/ diffusional restraints that were the cause of no reaction having been observed for the n-heptane hydroisomerisation over the Pt/SAPO-34 and Pt/MeAlPO-34 catalysts.

For this a smaller reactant molecule, namely n-hexene, was used for the hydroisomerisation reaction. Only Pt/CoAlPO-5 and Pt/CoAlPO-34 catalysts were studied, the former as a standard for it was known to readily convert the larger n-heptane molecule under the same reaction conditions, as seen in section 5.4.6.1.

At 310°C, small amounts of isomers and cracking products were observed for the Pt/CoAlPO-34 catalyst, despite only very negligible amounts of n-hexene having been converted. Yet, the Pt/CoAlPO-5 catalyst was observed to convert more n-hexene at this temperature with very good selectivies to isomers, than under the same conditions for the n-heptane hydroisomerisation reaction.

In conclusion, diffusional restraints of the small-pore three-dimensional chabazite structure were the most likely explanation for the poor catalytic performance of this material, as had there been a limitation factor with the accessibility of the metal sites, no reaction to isomers and cracking products should have been observed.

5.5 Summary and Conclusions

In summary, twelve materials of AFI, ATS and CHA-type frameworks were successfully synthesised and characterised by XRD. Results found them to be crystalline and phase-pure upon comparison with previously reported literature. On impregnation of the platinum species within the framework, apart from the exception of the zinc-substituted topologies, all the materials retained their crystalline structures. Zinc substituted materials were observed to collapse upon calcination, prior to impregnation.

An *in situ* study into the local co-ordination of three calcined and reduced platinum impregnated aluminophosphates revealed that in each case the results confirmed that the reduction procedure resulted in the production of platinum metal particles with typical bond lengths of approximately 2.74Å and 2.02Å respectively. The most important result was the presence of a low coordination number for Pt-Pt, which indicated that small metal particles were present in the catalyst.

Analysis into the physical properties of the materials revealed important information leading to further understanding of the catalytic reactions.

The majority of the materials exhibited a high TPD pyridine chemisorption capacity, consistent for materials that are highly acidic. Two high intensity peaks were observed, indicating that there are at least two different types of adsorbing sites of differing acidic strengths present within their frameworks. Specific surface area and thermogravimetric measurements of the materials produced results predictable for these types of materials. The only exception being in the case of the zinc substituted framework materials whose surface areas were found to be very low. This was due to the collapse of the structures during calcination as discovered by XRD.

The catalytic behaviour of the Pt/SAPOs and Pt/MeAlPOs were found to be influenced not only by the strength of the acid sites but also by the size of the pores and location of the catalytically active hydroxyl groups. For example, in the case of Pt/MgAlPO-36, the catalyst was found to be the most acidic out of all the materials studied and indeed was the most active in converting n-heptane. However the catalytic study found the Pt/CoAlPO-5 catalyst was the most active for the selective conversion

of n-heptane to isomers. The trend observed for the overall activity and hence conversion of n-heptane for the hydroisomerisation reaction at 330°C was found to be:

Pt/MgAlPO-36 > Pt/COAlPO-36 > Pt/CoAlPO-5 > Pt/ZnSAPO-36 > Pt/MgAlPO-5 > Pt/SAPO-5 > Pt/ZnAlPO-36 > Pt/ZnAlPO-5

The first three catalysts only differed by around 10% in their activity, converting 59.05%, 53.66% and 48.16% of n-heptane respectively. However, the important factor here is not in the conversion of n-heptane, but in the selectivity to isomers produced during the reaction. Here the trend observed is very different:

Pt/SAPO-5 > Pt/CoAlPO-5 > Pt/MgAlPO-5 > Pt/ZnAlPO-36 > Pt/ZnSAPO-36 > Pt/ZnAlPO-5 > Pt/CoAlPO-36 > Pt/MgAlPO-36

The difference in the selectivity to isomers for the first three catalysts was < 5%. Overall, the most effective catalyst for this reaction was Pt/CoAlPO-5. Lower temperatures are favoured as they restrict the amount of cracking during the reaction. However for comparison, greater conversions of n-heptane were observed over Pt/CoAlPO-5 at 350°C, where > 83% n-heptane was converted with selectivities to isomers > 76% and selectivities to cracking products now a great deal higher at > 23%.

These studies correlate very well to previously reported literature, which states that cobalt substituted Pt/MeAlPOs have greater activity than Pt/SAPO materials. This is due to the type of substitution, for example silicon island formation would reduce the materials acidity[40].

Comparable conversions and selectivities to the Pt/CoAlPO-5 catalyst were observed for the Pt/Zeolite-β catalyst at 250°C.

In all cases, conversion of reactant increased with increasing reaction temperature. Additionally, whatever the acid strength of the catalysts, some cracking of the isomers always transpired. It can therefore be proposed that selectivity is governed by porosity rather than by acidity. The framework geometry plays a vital role in the reaction as it can have an effect on the diffusion of reactants and products into and out

of the catalyst. One-dimensional systems have offered the best results for the n-heptane hydroisomerisation reaction as further re-arrangements of the isomers take place within the channels. This ultimately produces more multi-branched products, which are not trapped within the material, and therefore cannot inhibit the onset of carbonaceous residues. Throughout this study, the one-dimensional AFI and ATS-type catalysts were found to be the most active frameworks studied. However the pore size of the CHA-type catalysts prevented the n-heptane molecule reacting and so no conclusions can be drawn from this study so as to compare three-dimensional systems.

Unfortunately time restrictions meant that no time on stream (TOS) reactions were carried out. However, it is fair to say that the majority of the catalysts would most likely have coked relatively quickly and some were found to have already started to deactivate over the two-hour reaction time. This cannot be entirely avoided since the presence of free hydrogen within the reacting environment would lead to hydride transfer and ultimately the formation of carbonaceous deposits within the pores of the catalyst. Coke can also form on the platinum sites due to the cracking of alkanes to C_1-C_5 hydrocarbons, however this can be beneficial as the coke suppresses the cracking of alkanes in limiting the number of platinum sites [41].

Although one or two of the catalysts were found to be as catalytically active as Pt/zeolite-β, it is very unlikely that they would continue at this level for very long. In addition some of the catalysts were found to be more selective in the short-term for the production of isomers and cracking products. One big disadvantage that should be taken into account is that Pt/AlPOs and Pt/SAPOs perform their best at elevated reaction temperatures, over 50°C higher than Pt/zeolite-β, for example comparable conversions and selectivitys to the Pt/CoAlPO-5 catalyst were observed for the Pt/zeolite-β catalyst at 250°C.

5.6 References

(1) Motor Industry Council website, http://www.mic.org.mt/EUINFO/qeua/q&a40.htm, **2002**.

(2) The United Kingdom Parliament website, http://www.parliament.the-stationery-office.co.uk/pa/cm199798/cmhansrd/vo980731/text/80731w16.htm, **1998**.

(3) Her Majesty's Stationery office website, http://www.legislation.hmso.gov.uk/si/si1994/Uksi_19942295_en_1.htm, **2000**.

(4) The UK Petroleum Industry Association (UKPIA) website, http://www.ukpia.com, **2002**.

(5) Timeline Science website, http://www.timelinescience.org/resource/students/midgley/midgley.htm.

(6) PetrolGauge.com website, http://www.petrolgauge.com/guide/ie.asp?db=WikiAsp&dbname=DefaultDb&a=edit&o=AboutPetrol.

(7) Caprino, L.; Togna, G. I. *Environ. Health Perspect.* **1998**, *106*, 115-125.

(8) Hogue, C. *Chem. Eng. News* **2000**, *78*, 6.

(9) Helmenstine, A. M. http://chemistry.about.com ,**2004**.

(10) Mitchell, L. http://www.greenleft.org.au/back/1994/130/130p28.htm

(11) Bong, D. T., L.; http://www.visionengineer.com, **2000**.

(12) Kouwenhoven, H. W.; van Zijl.-Langhout, W.C. *Chem. Eng. Progress* **1971**, *67*, 65.

(13) Jimenez, C.; Romero, F.J.; Roldan, R.; Marinas, J.M.; Gomez, J.P. *Applied Catalysis A: General* **2003**, 1-11.

(14) Modica, F. S. US Patent No. 5 233 121, **1993**.

(15) Martens, J. A.; Tielen, M.; Jacobs, P.A. *Studies in Surface science and catalysis* **1989**, *49*, 46-50.

(16) Campelo, J. M.; Lafont, F.; Marinas, J.M. *Applied Catalysis A: General* **1997**, *152*, 53-62.

(17) Parlitz, B.; Schreier, E.; Zubowa, H.-L.;Eckelt, R. *Journal of Catalysis* **1995**, *155*, 1-11.

(18) Chaar, M. A.; Butt, J.B. *Applied Catalysis A: General* **1994**, *114*, 287-293.

(19) Sinha, A. K.; Sivasanker, S. *Catalysis Today* **1999**, *49*, 293-302.

(20) IZA Structure Database Website, http://www.iza-structure.org/databases, **2004**.

(21) Gallezot, P.; Alarcon-Diaz, A.; Dalmon, J.A.; Renouprez, A.J.; Imelik. B. *Journal of Catalysis* **1975**, *39*, 334-349.

(22) Reagan, W. J.; Chester, A.W.; Kerr, G.T. *Journal of Catalysis* **1981**, *69*, 89-100.

(23) Feast, S.; Englisch, M.; Jentys, A.; Lercher, A. *Applied Catalysis A: General* **1998**, *174*, 155-162.

(24) van den Broek, A. C. M.; van Grondlle, J.; van Santen, R.A. *Journal of Catalysis* **1997**, *167*, 417-425.

(25) Ostgard, D. J.; Kustov, K.R.; Poeppelmeier; Sachtler, W.M.H. *Journal of Catalysis* **1992**, 342-357.

(26) Csicsery, S. M. *Zeolites* **1984**, *4*, 202-213.

(27) Derouane, E. G. *Studies in Surface science and catalysis* **1980**, *5*, 5-10.

(28) Raybaud, P.; Partrigeon, A.; Toulhoat, H. *Journal of Catalysis* **2001**, *197*, 98-112.

(29) Weisz, P. B.; Swegler, E.W. *Science* **1957**, *126*, 31-32.

(30) Patrigeon, A.; Benazzi, E.; Travers, Ch.; Bernhard, J.Y. *Studies in Surface science and catalysis* **2000**, *130*, 2411-2417.

(31) Jimenez, C.; Romero, F.J.; Gomez, J.P. *Recent Res. Devel. Pure and Applied Chem* **2001**, *5*, 1-21.

(32) Boulet, M.; Bourgeat-Lami, E.; Fajula, F; Des Courieres, T.; Garrone, E. *Proceedings, 9th International Zeolite Conference, Montreal* **1992**, *2*, 389.

(33) Zhang, W.; Smirniotis, P.G. *Journal of Catalysis* **1999**, *182*, 400-416.

(34) Tusar, N. N.; Mali, G.; Arcon, I.; Kaucic, V.; Ghanbari-Siahkali, A.; Dwyer, J. *Microporous and Mesoporous Materials* **2002**, *55*, 203-216.

(35) Zenonos, C.; Sankar, G.; Cora, F.; Lewis, D. W.; Pankhurst, Q. A.; Catlow, C. R. A.; Thomas, J. M. *Phys. Chem. Chem. Phys.* **2002**, *4*, 5421-5429.

(36) Partrigeon, A.; Benazzi, E.; Travers, Ch.; Bernhard, J.Y. *Catalysis Today* **2001**, *65*, 149-155.

(37) Meriaudeau, P.; Tuan, V.A.; Lefebvre, F.; Nghiem, V.T.; Naccache, C. *Microporous and Mesoporous Materials* **1998**, *22*, 435-449.

(38) Chen, N. Y.; Degnan, T.F.; Smith, C.M. *Molecular Transport and Reactions in Zeolites*, VCH Publishers, New York, **1994**.

(39) Hochtl, M.; Jentys, A.; Vinek, H. *Journal of Catalysis* **2000**, *190*, 419-432.

(40) Hochtl, M.; Jentys, A.; Vinek, H. *Microporous and Mesoporous Materials* **1999**, *31*, 271-285.

(41) Noordhoek, N. J.; Schuring, D.; M. de Gauw, F.J.M.; Anderson, B.G.; M der Jong, A.; A. de.Voigt, M.J.; van Santen, R.A. *Ind. Eng. Chem. Res.* **2002**, *41*, 1973-1985.

Chapter 6

Study into the activity of several cobalt substituted polyoxometalates and the influence of intercalation between the sheets of a layered double hydroxide for the oxidation of cyclohexane

6.1 Chapter Overview

This chapter concentrates on the properties of several cobalt-substituted polyoxometalates (POM's) and polyoxometalate pillared layered double hydroxides (POM-LDH's). The results show the preparation of three cobalt substituted tungsten Keggin ions, and the successful intercalation of these materials within the layers of a double hydroxide (LDH) material comprised of zinc and aluminium. The as synthesised materials were characterised for crystallinity, purity and co-ordination by X-ray diffraction (XRD), X-ray absorption fine structure (XAFS) and infrared (IR) techniques. Chemical analysis of the LDH was undertaken to clarify the true composition of the prepared material. Finally, catalytic studies for the oxidation of cyclohexane in the presence of molecular oxygen and *tert*-butyl hydrogen peroxide TBHP were performed and the results obtained proved that the layered double hydroxide substituted polyoxometalate Zn_2Al-$K_7H[Co(II)(Co(II).H_2O)W_{11}O_{39}].14H_2O$ was the more active material.

6.2 Background on the Cyclohexane Oxidation Reaction

Cyclohexane conversion is important in the production of adipic acid (one of the basic feedstock's for the production of nylon 6,6) and ε-caprolactam (a basic feedstock in the production of nylon 6). The initial step for both these materials is the oxidation of cyclohexane to produce cyclohexanol and cyclohexanone (figure 6.1). The ketone/ alcohol mix is then converted to adipic acid by oxidation with nitric acid and to ε-caprolactam by cyclohexanone oximation and Beckmann rearrangement route.

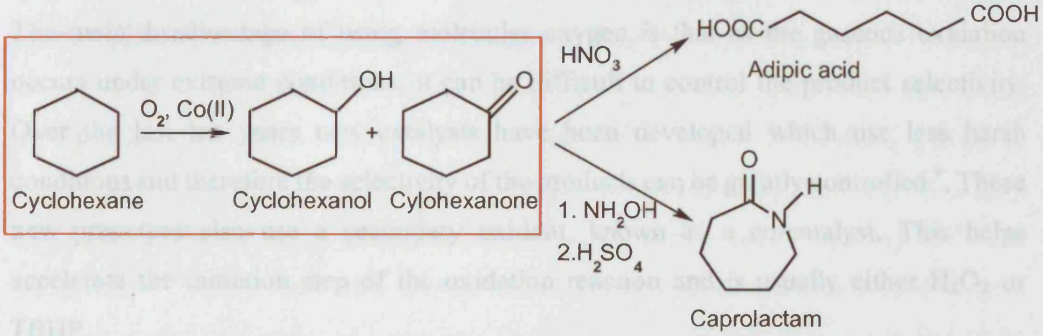

Figure 6.1 *Schematic depicting the conversion of cyclohexane to adipic acid and ε–caprolactam (the oxidation reaction within the red box is the area which has been research into)*

6.2.1 Cobalt substituted catalysts for the cyclohexane oxidation reaction

Cobalt substituted redox catalysts have been investigated for many years into their effective selective oxidation of cyclohexane using molecular oxygen [1-3].

Cobalt substituted AlPO-5 and -36 frameworks have been researched in great depth and are known to be very efficient catalysts for this reaction. Our aim however

was to investigate alternative materials, for example the Keggin ion and the pillaring of this material within a layered double hydroxide, to see how their porous and expandable framework adapted to this reaction.

Metal-substituted polyoxometalates are good oxidation catalysts for this reaction due to their rigid co-ordination sites surrounding the metal centre, their high stability towards oxygen donors and the possibility to incorporate several transition metals within their structure [4,5].

Both hydrogen peroxide (H_2O_2) [6,7], *tert*-butyl hydrogen peroxide (TBHP) [8] and molecular oxygen [9] have all been used as oxidants for the cyclohexane reaction using polyoxometalate catalysts. The advantage of using molecular oxygen is that the rate of the C-H bond cleavage is high, therefore favouring the formation of large quantities of cyclohexyl hydroperoxide, which then decomposes to cyclohexanol and cyclohexanone. The main disadvantage of using molecular oxygen is that as the gaseous oxidation occurs under extreme conditions, it can be difficult to control the product selectivity. Over the last ten years new catalysts have been developed which use less harsh conditions and therefore the selectivity of the products can be greatly controlled [9]. These new processes also use a secondary oxidant, known as a co-catalyst. This helps accelerate the initiation step of the oxidation reaction and is usually either H_2O_2 or TBHP.

6.3 Introduction to Polyoxometalate Layered Double Hydroxides

Since the late 1980's a great amount of work has been carried out into the pillaring and catalytic properties of layered double hydroxides (LDH's) [10-13]. The substitution of large anions, for example polyoxometalates (POM's), can be achieved between the brucite layers of an LDH through direct synthesis, ion exchange or co-precipitation [14]. The interlamellar space between the layers is capable of swelling on introduction of the anions and thereby is able to control the catalytic activity of the material. Numerous POM's having the Keggin structure have been substituted as pillars [15], each of which performs catalytically different due to their varying negative charges and consequently their differently sized pores.

6.3.1 Introduction to polyoxometaltes

Polyoxometalates were first synthesised back in 1826 by Berzelius [16], who described obtaining a yellow precipitate from the mixing of ammonium molybdate and phosphoric acid, now commonly known as 12-molybdophosphate. The material was introduced into analytical chemistry in 1848 by Svanberg and Struve [17], however the true compositions of heteropoly acids (commonly known today as polyoxometalates) were not properly determined until the discovery of the tungstosilicic acids and their salts by Marignac [18]in 1862. By 1910, sixty different types of heteropolyanions had been synthesised. The first attempt at understanding the co-ordination of these materials was undertaking in 1908 by Miolati and Pizzighelli [19], who proposed a hypothesis based on Werner's co-ordination theory, this was later developed by Rosenheim. During the next 25 to 30 years Rosenheim made a huge impact in the field of polyanion chemistry, which included the Miolati-Rosenheim (MR) theory that heteropoly acids were based on six-co-ordinate heteroatoms with MO_4^{2-} or $M_2O_7^{2-}$ anions as bridging groups or ligands, for example, $H_8[Si(W_2O_7)_6]$ (commonly known today as, $H_4[SiW_{12}O_{40}]$). However, in 1929 Pauling noticed that the crystal radii of (molybdenum) Mo^{6+} and (tungsten) W^{6+} were in fact more appropriate for the octahedral co-ordination of oxygen. In doing so he proposed a new structure for the 12:1 complexes, this was based on an arrangement of twelve MoO_6 or WO_6 octahedra, which surrounded a central XO_4 tetrahedron. Although Pauling was wrong in assuming that the MoO_6 or WO_6 octahedra only corner-shared everything else that he proposed were correct and led to further, more direct attention into the structural properties of heteropolyanions.

It was only four years after this discovery by Pauling that Keggin [20,21] used x-ray diffraction (XRD) techniques to solve the structure of $H_3PW_{12}O_{40}.5H_2O$. He proved that whilst Pauling was correct in assuming that the anion was based on octahedral WO_6 units, not only where they corner-shared but in fact they were also edge-shared. Soon afterwards, the structure of the anion was confirmed by Bradley and Illingworth of which their own investigations by powder diffraction on $H_3PW_{12}O_{40}.29H_2O$ [22] proposed the same co-ordination as Keggin.

Polyoxometalates (POM's) are themselves very strong Brönsted acids, as has been established by IR spectroscopic studies of pyridine adsorption [23]. They are stronger than conventional acid catalysts, POM > H_2SO_4 > zeolite, and are highly soluble in

polar solvents, though insoluble but transferable into non-polar solvents such as hydrocarbons. The POM's important features also include its high structural mobility and multifunctionality [23,24]. Their high acidity together with the fact that they are very efficient oxidants exhibiting fast reversible multielectron redox transformations under mild operating conditions, are the main reasons why they are very important catalysts [15]. The Keggin type polyoxometalate and their salts, have incurred the most attention as a potentially viable catalyst, due to their wide availability as a starting material and their relatively high thermal stability.

The Keggin ion structure of the saturated anion can be represented by the formula $[XM_{12}O_{40}]_{x-8}$, where X is the central heteroatom (e.g. Si, Co, P), M is the addenda atom (typically tungsten (W) or molybdenum (Mo)) and x is its co-ordination state. It is possible for the anion to possess both primary (central) and secondary (peripheral) heteroatoms. The primary heteroatom (central) is essential in order to complete the polyanion structure, although it may not be located in the centre of the anion. The addenda atom can also be partially substituted by many other metal ions, e.g. V^{5+}, Co^{2+} [15].

In the case of $Co(II)W_{12}O_{40}^{5-}$, the structure is composed of a central tetrahedral CoO_4 heteroatom, surrounded by twelve edge and corner shared WO_6, as shown in figure 6.2. This structure, referred to as the α-form, was the one originally reported by Keggin in 1933 [15].

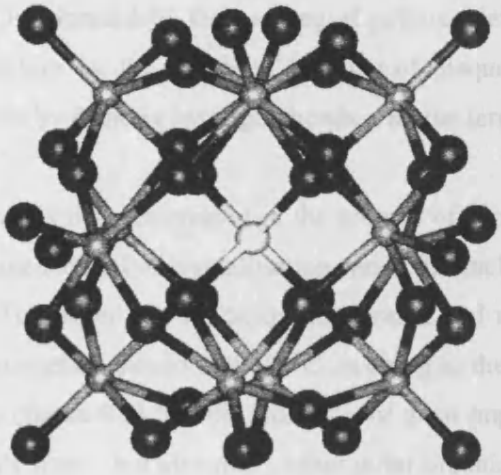

Figure 6.2 *Polyhedral representation of the Keggin ion* $[XM_{12}O_{40}]_{x-8}$ *(the large white sphere represents the cobalt heteroatom, the small light grey spheres represent the tungsten atoms and the dark grey spheres represent the oxygen atoms)*

Although the majority of heteroatoms possess tetrahedrally co-ordinated structures, based on the Keggin ion, there are also a number of 'lacunary' or 'defect' derivatives that are produced by the removal of one or more MO_6 octahedra [15]. The first octahedron removed is a MO^{n+} group, subsequent octahedra are lost as either MO_2 or MO_3 units.

The potential protonation centres in a Keggin anion are located in the three types of outer oxygen atoms. These include the terminal oxygen's, M=O, and both the corner shared and edge shared bridging oxygen's, M-O-M. It is assumed that in the gas phase the edge shared bridging M-O-M oxygen's are most likely to be protonated whereas in the liquid phase it is suggested that all the bridging oxygen atoms are protonated due to them possessing a higher electron density than the terminal oxygen atoms. In the case of solid polyoxometalates, it is thought that the more accessible terminal oxygen's may be

the ones protonated since when forming the crystal structure it is these protons that take part in the linking of the neighbouring polyoxometalates. It has thus been discovered using x-ray and neutron diffraction techniques, that the crystal structure of $H_3[PW_{12}O_{40}].6H_2O$ is formed by the packing of polyoxometalate anions into a body-centred cubic structure by the hydrogen bonding of diaquahydrogen ions. Each ion connects four anions by forming hydrogen bonds with the terminal M=O oxygen's [25].

The large voids that are created in the process of forming the ionic crystal can accommodate a large amount of crystallisation water, as much as 30 molecules of water per anionic unit. The water can be easily dehydrated and rehydrated by heating the material to temperatures of around 100-150°C. In doing so the volume of the crystal cell shrinks or expands (figure 6.3) [26]. This process is of great importance to heterogeneous catalysis as not only water, but also many other polar organic molecules, e.g. alcohols, amines etc. can also enter and leave the structure [23].

Once dehydrated the almost planar diaquahydrogen ions take on a different shape. The structure of the bulk proton site is assumed to form directly upon dehydration and is suggested as playing a major role in pseudoliquid catalysis by solid polyoxometalates [23,27].

Advantages of using POM's as homogeneous catalysts are that they are non-corrosive materials, they create fewer side reactions and posses high protonation rates. Disadvantages on the other hand include high cost, poor availability and the recovery and/ or recyclability of the materials is very difficult if not impossible. For this reason the trend has moved towards the pillaring of these materials, i.e. heterogenising the homogeneous catalyst.

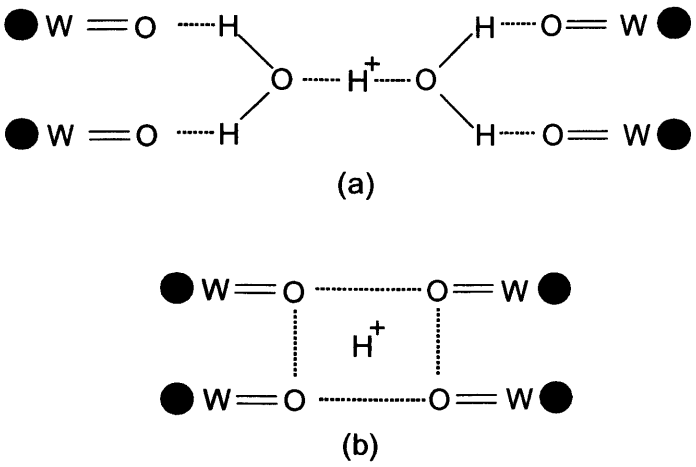

Figure 6.3 *Schematic demonstration of the bulk proton sites in (a) aqueous $H_3[PW_{12}O_{40}].6H_2O$ and (b) dehydrated $H_3[PW_{12}O_{40}]$*

6.3.2 Synthesis of polyoxometalates

Polyoxometalates are nanosized metal-oxygen cluster anions which, when in solution, form by a self assembly process and can be isolated as solids with appropriate counter-cations, e.g. H^+ and alkali metal cations.

Cobalt containing Keggin ions have been studied in great detail by a number of people as to its many features including its magnetic properties [28]. Other Keggin ion analogues have also been investigated, for example iron, manganese, chromium and germanium, although to nowhere near the same extent as the cobalt species [6,7,29-32]. It has also been discovered during synthesis, that tungsten tends to adopt the Keggin structure more easily than molybdenum and that the tungstic acids are more acidic, have a lower oxidation potential and are more thermally stable at elevated temperatures (ca. 450^0C) [24] compared to the molybdic acids.

6.3.3 History of layered double hydroxides

Layered Double Hydroxides (LDH's), also known as 'hydrotalcites' or 'anionic clays', are the only group of materials in which it is possible to exchange anions between an infinite series of charged layers.

Hydrotalcite was first discovered back in 1842 in Sweden although its exact formula wasn't published until 1915 when Manasse described it as, $[Mg_6Al_2(OH)_{16}]CO_3.4H_2O$ [33]. It was not until some twenty-five years later though that interest in this area grew. This was due to a series of papers published by Feitknecht, on what he described as 'doppelschichtstrukturen' (double sheet structures) [34]. His description of the material was a structure, which comprised of layers of one metal hydroxide intercalated with a layer of a second metal hydroxide. This was later severely criticised by Allmann and Taylor, who, using single crystal x-ray diffraction, discovered that actually both the cations were in fact in the same layer [35,36].

There are two possible forms of naturally occurring LDH's, rhombohedral and hexagonal (figure 6.4) [37]. The difference between the two is that whilst for the hexagonal form the lattice parameter, c, is equal to only twice the interlayer separation, for the rhombohedral form, c is three times the interlayer separation.

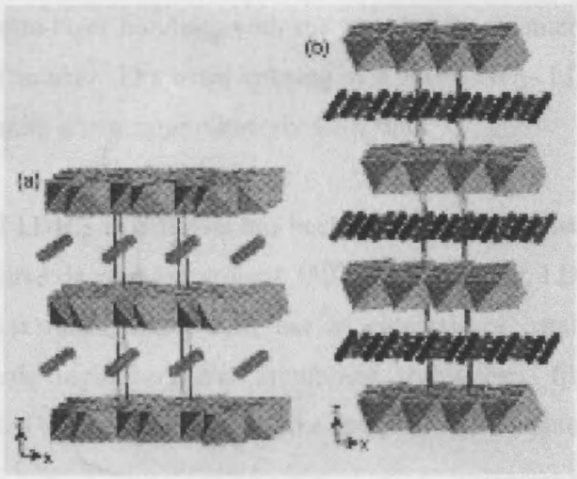

Figure 6.4 *Polymorphic representation of the general structure of an LDH: (a) hexagonal and (b) rhombohedral*

The chemical composition of an LDH is given by the general formula, $[M^{2+}_{(1-x)}M^{3+}_{x}(OH)_2]A_{n-x/n}..mH_2O$, where M^{2+} is a divalent cation (e.g. Ca^{2+}, Mg^{2+}, Zn^{2+} etc.), M^{3+} is a trivalent metal cation (e.g. Al^{3+}, Fe^{3+}, Mn^{3+} etc.) and An^- is a simple or complex organic or inorganic anion (e.g. Cl^-, NO_3^{2-}, CO_3^{2-} etc.). For pure phases, the value of x lies between 0.17 and 0.33 [38]. Several people have also synthesised LDH's with two different M^{2+}/ M^{3+} cations [39-41].

The structure of an LDH consists of layers of metal cations of similar ionic radii, which are joined together by edge-sharing M^{2+}/ M^{3+} $(OH)_6$ octahedra, forming numerous two-dimensional sheets stacked together by hydrogen bonding of the hydroxyl groups of adjacent sheets. Substitution of trivalent metal cations for divalent ions introduces a charge imbalance, thereby creating an overall positively charged framework. This is balanced by the interlayer anions, between adjacent layers maintaining the charge neutrality of the material [42]. Also present in the interlayer region are water molecules. As proved by NMR experiments, the extensive hydrogen bonds between the water molecules and both the metal hydroxide layers and the interlayer anions are said to be continuously breaking and reforming. The overall amount of water in the interlayer regions depends on several factors including, the nature of the interlayer anions, the water vapour and temperature [43,44].

The flexible host lattice of an LDH is characterised by their ability to expand on intercalation in order to accommodate the guest species in a perpendicular direction to the layers, causing disruption to the weak intra-layer forces. The layered lattices occupy strong covalent intra-layer bonding, with the van der Waals interactions between the layers being a lot weaker. The basal spacing of a Zn-Al-NO_3- LDH is approximately 8.9Å, with the brucite sheets approximately 4.8Å thick [45].

The use of LDH's in catalysis has been extensively reviewed by Cavini *et al* [46]. Most LDH structures decompose around 350°C, nevertheless, LDH's still have many uses. Most interest falls around their use as catalysts or catalyst supports. Other applications include separation and membrane technology, filtration, scavenging, controlled release of anions and electroactive and photoactive materials [47].

6.3.4 Synthesis of layered double hydroxides

As described previously in section 6.3.3, layered double hydroxides can be synthesised using numerous cations and anions. In particular, magnesium and zinc are predominantly used as the divalent cations whilst aluminium is used as the trivalent cation. Previous work has found that the Mg_2Al-LDH is structurally unstable even under mild conditions. In comparison, the Zn_2Al-LDH has been reported to be more stable, particularly when pillared with the robust Keggin anion [48].

The four main forms of anions used to occupy the interlayer space and balance out the interlayer net positive charge are Cl^-, NO_3^{2-}, SO_4^{2-} and CO_3^{2-}. The preparation of the nitrate form of a LDH has been found to be difficult as carbon dioxide in the atmosphere can contaminate the synthesis. For this reason most LDH's are prepared under an argon or nitrogen atmosphere [14]. However, the nitrate form of a LDH has also been found to be beneficial for the facile intercalation of polyoxometalates, with the trend for the order of preferred exchange being $NO_3^{2-} > Cl^- > SO_4^{2-} > CO_3^{2}$.

The synthesis of LDH materials can be performed using several different methods, for example co-precipitation and ion exchange methods. Millipore water is used throughout the preparation so as not to introduce unwanted ions into the synthesis. The main problems that occur during synthesis are over concentration if not enough stirring of the mixture is ensured and inaccurate addition speed of each solution as the pH of the reaction mixture has to be carefully monitored throughout the synthesis.

6.3.5 Intercalation of polyoxometalates

Polyoxometalates that are pillared within another material, e.g. layered double hydroxides, possess a greater surface area, hence are more important for catalytic applications. The degree of acidity and catalytic activity of the final material depends on several factors, for example, the type of support used, the amount of polyoxometalate loading and pre-treatment to name but a few. Several supports that have been used in the past include both acid and neutral materials, e.g. silica, active carbon, ion-exchange resins, layered double hydroxides etc. [23,24].

The POM's are pillared between the positively charged layers of the LDH. The orientation of the Keggin anions within the layers is perpendicular to the inorganic layers [49-51]. The gallery height prior to intercalation of a Keggin ion POM is 8.9Å. After intercalation the layers swell to approximately 9.8Å, dependant on the POM pillared (figure 6.5) [45].

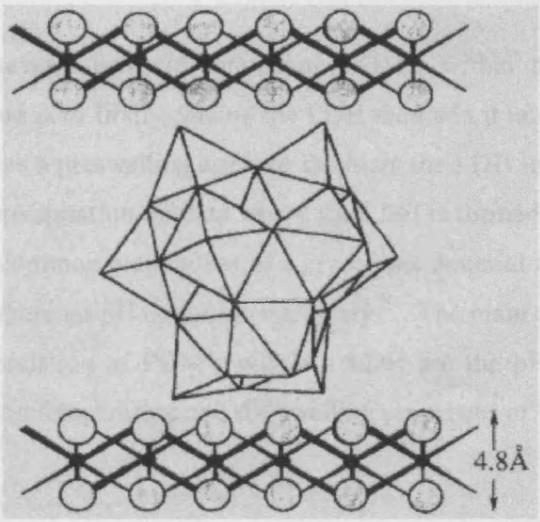

Figure 6.5 *Schematic representation of the pillaring of a polyoxometalate anion with Keggin structure within the layers of a LDH material*

Previous work using XRD, BET and thermal analysis have shown that POM-LDH materials can retain their crystallinity and structure up to about 200°C, suggesting that these materials should be used solely for low temperature catalytic reactions [45].

The POM-LDH materials structural and chemical features have made them useful for several important catalytic applications. Their shape selective nature lends them effective catalysts for the epoxidation of alkenes [52] and the selective oxidation of

ortho-xylene and *ortho*-tolualdehyde [53]. A vast amount of research has been carried out into their photo-catalytic properties and applications, for example the photo-oxidation of isopropyl alcohol to acetone [12,54]. Other applications where POM's may be applied to catalysis include the oxidation of alkanes, phenols and olefins, environmental issues for cleaning polluted areas and in the green technology of converting wood pulp into paper.

6.3.6 Synthesis of polyoxometalate intercalated layered double hydroxides

There are several ways to intercalate POM's within the layers of a LDH material. One method is to firstly calcine the LDH then add it into an aqueous solution of POM, another uses a preswelling agent to facilitate the LDH ion exchange and there is also a direct co-precipitation method where the LDH is formed around the POM salt [10-12,55,56]. The most common preparation of a crystalline material though is a simple ion exchange method where no pH control is necessary [51]. The main considerations to note for successful intercalation of POM's within a LDH are the pH and charge of both materials, the reaction temperature and the swelling properties of the LDH.

6.3.7 Aims and Objectives

For the reasons mentioned so far in this chapter it was decided that cobalt and tungsten substituted polyoxometalate materials would be prepared and intercalated within the channels of a zinc and aluminium layered double hydroxide. The materials were characterised and subsequently analysed for the cyclohexane oxidation reaction. Information was obtained on how the intercalation of the different cobalt substituted POM's species within a LDH increased the catalytic performance of the material.

6.4 Experimental

6.4.1 Preparation of the materials

The polyoxometalates were prepared using solution chemistry techniques and the layered double hydroxide material was prepared using a co-precipitation method and hydrothermal techniques, both of which have been previously reported. The final polyoxometalate layered double hydroxide species were prepared under reflux conditions that were developed in parallel to the preparation of the materials.

6.4.1.1 Preparation of $K_6[SiCo(II).(H_2O)W_{11}O_{39}]$

A solution containing 3.15g of glacial acetic acid (Aldrich) and 11.5g of silicon tungstic acid (Aldrich) in 25g of distilled water was prepared and to it were added 6.12g of potassium hydrogen carbonate (Aldrich) to decrease the pH of the solution to 6. Once this pH had been reached the solution was heated close to its boiling point and a hot solution containing 0.8g of cobalt acetate tetrahydrate (Aldrich) and 2g of water were added. Subsequently, another solution containing 15g of potassium acetate (Aldrich) and 0.5g of acetic acid (Aldrich) dissolved in 8g of water was also added. The resulting solution was stirred for a further 15 minutes then filtered hot using a Buchner funnel and flask. The filtrate was left to crystallise for four hours and the resulting red crystals were recovered by further filtration. The material was recrystallised by dissolving in boiling water, cooling back to room temperature and after two hours further crystallisation, large red crystals were once again collected by filtration prior to analysis.

6.4.1.2 Preparation of $K_7H[Co(II)(Co(II).H_2O)W_{11}O_{39}].14H_2O$

19.8g of sodium tungstate dihydrate (Aldrich) was dissolved in 40g of distilled water and the pH of the solution adjusted to 7 with the addition of 3.5g acetic acid (Aldrich). The resulting colourless solution was heated to 120°C using vigorous stirring then 2.5g of cobalt acetate tetrahydrate (Aldrich) dissolved in 13g of water was added dropwise. The initial colourless solution became immediately dark blue, which after fifteen minutes slowly changed to green as the reaction progressed. The green solution was cooled and the insoluble solid filtered out. Once again the solution was heated up to 120°C and a hot solution containing 13g of potassium chloride (Aldrich) in 25g of water was added. Heating was maintained for 15 minutes, then the solution was cooled to room temperature and kept at 5°C overnight for crystallisation to take place. The green crystals were collected using a Buchner funnel and flask and dried at room temperature, prior to analysis.

6.4.1.3 Preparation of $K_5H_5[Co(III)W_{12}O_{40}].16H_2O$

4g of the polyoxometalate $K_7H[Co(II)(Co(II).H_2O)W_{11}O_{39}].14H_2O$, was dissolved in 20ml of 1M hydrochloric acid (Aldrich). The solution was heated to 110°C under vigorous stirring until a solid started forming. The solid was filtered off using a Buchner funnel and flask and the filtrate left for crystallisation at –3°C for 36 hours. Several large green crystals formed and were recovered once again by filtration and dried at room temperature, prior to analysis.

6.4.1.4 Preparation of Zn_2Al-NO_3

Two solutions were firstly prepared, one acidic and one basic. For the acidic solution, 19.61g of Zinc nitrate (Aldrich) and 71g of millipore water were placed in a 100ml glass beaker and stirred on a hot-plate until fully dissolved, then 9.88g of

Aluminium nitrate (Aldrich) was added and the stirring continued until all had dissolved. For the basic solution, 11.36g of sodium nitrate (Aldrich) and 82.31g of millipore water were placed into a 100ml plastic beaker and stirred on a hot plate until fully dissolved. To this was added 6.38g of sodium hydroxide pellets (Aldrich) and the beaker replace onto the hotplate until all had dissolved.

The two mixtures were then combined via a co-precipitation method. The acidic and basic solution were added dropwise, using 50ml plastic syringes with their connecting plastic tubes taped to a stirred 100ml plastic beaker, with the aid of a double peristaltic pump set at 60ml/min. The final pH of the solution was approximately 5.9, calculated using an automatic pH meter.

The solution was placed into an autoclavable bottle and placed into an oven at 60°C overnight (about 19 hours). Once removed and cooled the material was filtered using a Buchner flask and funnel and washed with distilled water until the filtrate was of a neutral pH. The solid was dried in an oven at 60°C overnight, then analysed.

6.4.1.5 Preparation of Zn_2Al-$K_6[SiCo(II).(H_2O)W_{11}O_{39}]$

A simple ion exchange procedure was used to intercalate the POM within the layers of the LDH. 4.5g of the previously prepared $K_6[SiCo(II).(H_2O)W_{11}O_{39}]$ was dissolved in 15ml of millipore water and added dropwise using a peristaltic pump (60ml/min) to a 50ml beaker containing a vigorously stirred slurry of the previously prepared Zn_2Al-NO_3, 1.5g dissolved in 10ml of millipore water. The mixture was heated at a constant temperature of 90°C in an oil bath. Several aliquots of the sample were analysed over a period of time and it was discovered that after 6 hours the material had been successfully pillared. The material was filtered using a Buchner funnel and flask and analysed.

6.4.1.6 Preparation of Zn_2Al-$K_7H[Co(II)(Co(II).H_2O)W_{11}O_{39}].14H_2O$

Again a simple ion exchange procedure was used to intercalate this POM material within the layers of the LDH. 4.5g of the previously prepared $K_7H[Co(II)(Co(II).H_2O)W_{11}O_{39}].14H_2O$ was dissolved in 15ml of millipore water and added dropwise using a peristaltic pump (60ml/min) to a 50ml beaker containing a vigorously stirred slurry of the previously prepared Zn_2Al-NO_3, 1.5g dissolved in 10ml of millipore water. The mixture was heated at a constant temperature of 90°C in an oil bath. Several aliquots of the sample were analysed over a period of time and it was found that after 25 hours the material had been successfully pillared. The material was filtered using a Buchner funnel and flask and analysed.

6.4.1.7 Preparation of Zn_2Al-$K_5H_5[Co(III)W_{12}O_{40}].16H_2O$

Once more the simple ion exchange procedure was used to intercalate this POM material within the layers of the LDH. 4.5g of the previously prepared $K_5H_5[Co(III)W_{12}O_{40}].16H_2O$ was dissolved in 15ml of millipore water and added dropwise using a peristaltic pump (60ml/min) to a 50ml beaker containing a vigorously stirred slurry of the previously prepared Zn_2Al-NO_3, 1.5g dissolved in 10ml of millipore water. The mixture was heated at a constant temperature of 90°C in an oil bath. Several aliquots of the sample were analysed over a period of time and it was found that after 6 hours the material had been pillared successfully. The material was filtered using a Buchner funnel and flask and analysed.

6.4.2 Characterisation

6.4.2.1 XRD measurements

Phase purity, crystallinity and successful intercalation of the as synthesised materials was accounted for by X-ray diffraction (XRD) measurements analysed using a Siemens D500 employing Cu-$K\alpha_1$ radiation. In a typical experiment, the sample was pressed onto a plate and smoothed prior to the plate being loaded into position. The materials were analysed over a range of 5-60 degrees (2θ) at a rate of 0.02 degrees a second.

6.4.2.2 XAS measurements

X-ray absorption spectroscopy (XAS) analysis was carried out to ascertain the co-ordination and successful intercalation of the as synthesised materials.

Co K-edge XAS measurements were carried out on station 8.1 at the Daresbury Laboratory (DL). The station is equipped with a Si(111) double crystal monochromator, two ion chambers (one for measuring the incident beam intensity, the other for measuring the transmitted beam intensity) and a thirteen element Canberra fluorescence detector for collecting information on dilute samples. In a typical experiment, approximately 100mg of the polyoxometalate sample was pressed into a 20mm disc and placed into an *in situ* cell and positioned in the beam. XAS spectra for each of the as synthesised materials were recorded at room temperature under a flow of nitrogen for approximately one hour. The data was then analysed using a suite of programs available at the Daresbury Laboratory, namely EXCALIB, EXBROOK and EXCURV98.

6.4.2.3 IR measurements

IR measurements were carried out to ascertain the co-ordination and successful intercalation of the as synthesised materials.

IR analysis was achieved using an IFS 66V Bruker FTIR spectrometer fitted with a KBr beam splitter and DLATGS detector. In a typical experiment, approximately 1mg of the polyoxometalate sample was added to approximately 100mg of KBr and the material ground to a fine powder in a pestle and mortar. The material was then pressed into a 15mm OD disc before being placed onto a plate and loaded into position. The resolution used was $4cm^{-1}$ and 32 scans were performed per analysis.

6.4.2.4 Chemical analysis

Chemical analysis was undertaken on the LDH material to check its true composition. In a typical experiment, the sample was diluted in solvent then analysed using an atomic absorption spectrometer (AAS).

6.4.2.4.1 Quantitative information

The data obtained from the chemical analysis of the zinc and aluminium LDH was given in parts per million (ppm). Using equation 6.1 below the molar ratio of the LDH was calculated [57].

$$\text{Molar Ratio X} = \frac{\text{Molar Ratio Al}}{\text{Molar Ratio Zn} + \text{Molar Ratio Al}} \qquad (6.1)$$

6.4.2.5 Catalytic analysis

The gaseous reaction of cyclohexane to predominantly cyclohexanone and cyclohexanol was performed in a batch reactor. For these experiments, approximately 20mg of the catalyst (powder, particle size approximately 5-20μm) were placed into the autoclavable reactor along with the feed, which consisted of 15g cyclohexane, 1g acetonitrile and 1g TBHP. The reactor was then sealed and heated to approximately 83°C on which 4 bar molecular oxygen was introduced to the system and the reaction started. The reactor was constantly stirred throughout the reaction. After 24 hours, the material was cooled to room temperature then the contents analysed using a Varian 3400 gas chromatograph (GC) equipped with a 15m phenylmethylsilicone 5% semi-capillary column and FID detector. Mesitylene was used as the internal standard and the results obtained were calculated by area normalisation techniques.

6.4.2.5.1 Quantitative information

Maximum conversion possible from the experiment was calculated using the ideal gas law as detailed below in equation 6.2.

$$PV = nRT \qquad (6.2)$$

Where P is the pressure of a gas, V the volume it occupies, n is the number of moles of gas present, R is the universal gas constant and T its temperature (in Kelvin).

Turnover number (TON) also known as turnover frequency (TOF) were calculated to compare the catalysts activities. TON is the absolute number of passes through the catalytic cycle (typically one equivalent of reactant is converted to one equivalent of product, per equivalent of catalyst) before the catalysts becomes deactivated. TON is defined as the amount, in moles, of reactant divided by the amount,

in moles, of catalyst, as represented below in equation 6.3. A large TON (for example, $10^6 - 10^{10}$) implies that the catalyst is stable and has a long life span.

$$TON = \frac{\textit{(number of moles of cyclohexane reacted)}}{\textit{(number of moles of catalyst)}} \qquad (6.3)$$

6.5 Results and Discussion

6.5.1 XRD study of the as synthesised catalysts

X-ray diffraction (XRD) patterns of the as synthesised layered double hydroxide (LDH), polyoxometalates (POM's) and subsequent polyoxometalate layered double hydroxide (POM-LDH) materials are shown below in figure 6.9. These patterns have been compared to previously published work and correlate accurately suggesting that the materials are indeed phase pure. The LDH and POM materials were found to be crystalline however the POM-LDH's were not so crystalline.

The nitrate form of the LDH possesses *d*-spacings of the [003] and [006] planes of 8.8 and 4.4Å respectively. If there were any carbonate impurity present within the sample then peaks for the [003] and [006] planes should be visible at 7.8 and 3.9Å respectively [58]. As this was not the case and the only peaks visible are associated with the nitrate form of the material then it can be conceived that the material was phase pure.

In addition, the XRD patterns of the polyoxometalate intercalated layered double hydroxide (POM-LDH) materials demonstrate successful intercalation as it was observed that the interlayer distance of the POM-LDH patterns increased. The patterns for the POM-LDH materials show in total three approximately equally spaced peaks which were assigned as the (d_{001}) reflections of the hydrotalcite phases [51].

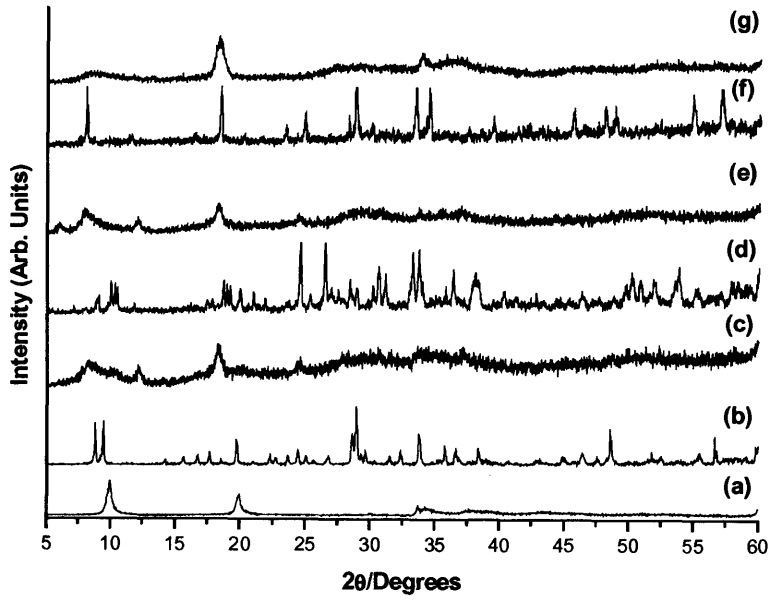

Figure 6.6 *XRD patterns of the as synthesised (a) Zn_2Al-NO_3, (b) $K_6[SiCo(II).(H_2O)W_{11}O_{39}]$, (c) Zn_2Al-$K_6[SiCo(II).(H_2O)W_{11}O_{39}]$, (d) $K_5H_5[Co(III)W_{12}O_{40}].16H_2O$, (e) Zn_2Al-$K_5H_5[Co(III)W_{12}O_{40}].16H_2O$, (f) $K_7H[Co(II)(Co(II).H_2O)W_{11}O_{39}].14H_2O$ and (g) Zn_2Al-$K_7H[Co(II)(Co(II).H_2O)W_{11}O_{39}].14H_2O$ catalysts*

6.5.2 XAS study of the as synthesised catalysts

The XANES (figure 6.7) and EXAFS (figure 6.8 and table 6.1) data, taken from the XAS analysis of the cobalt-substituted materials are shown and discussed below. During analysis, some of the materials were observed to undergo a reduction reaction in the beam. This has led to some of the results exhibiting a mixture of both octahedral and tetrahedral cobalt. (N.b. unfortunately the data for one of the materials, $K_7H[Co(II)(Co(II).H_2O)W_{11}O_{39}].14H_2O$, was very poor and so couldn't be included)

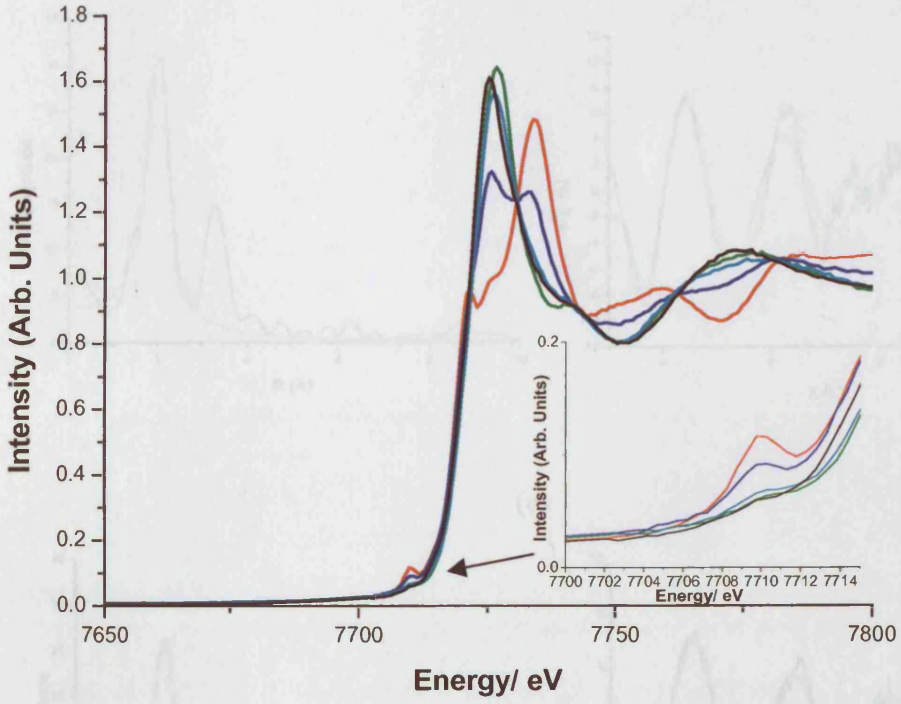

Figure 6.7 *Comparison of the pre-edge peak of the Co K-edge XANES for the as synthesised cobalt substituted Keggin ions, namely (-) $K_6[SiCo(II).(H_2O)W_{11}O_{39}]$, (-) Zn_2Al-$K_6[SiCo(II).(H_2O)W_{11}O_{39}]$, (-) Zn_2Al-$K_7H[Co(II)(Co(II).H_2O)W_{11}O_{39}].14H_2O$, (-) $K_5H_5[Co(III)W_{12}O_{40}].16H_2O$ and (-) Zn_2Al- $K_5H_5[Co(III)W_{12}O_{40}].16H_2O$ (the inset shows a clearer view of the pre-edge peak)*

(a)

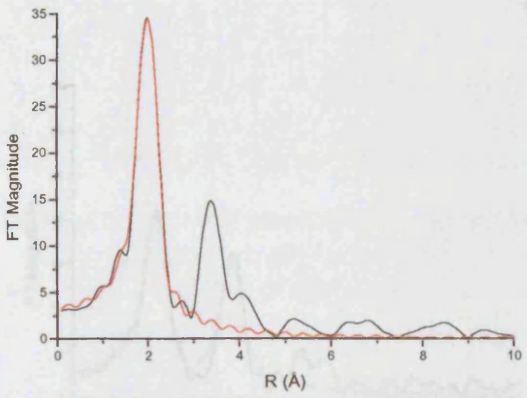
FT Magnitude
R (Å)

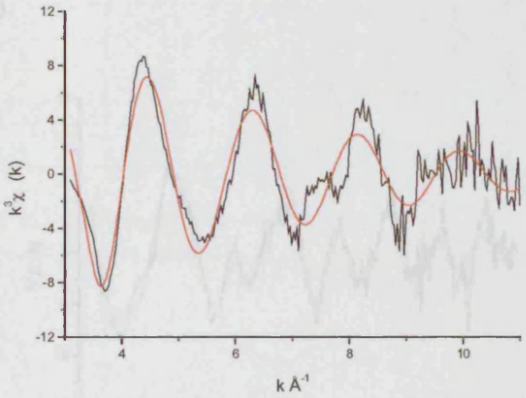
k³χ (k)
k Å⁻¹

(b)

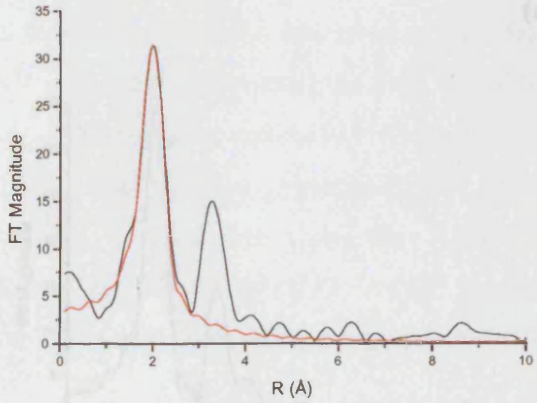
FT Magnitude
R (Å)

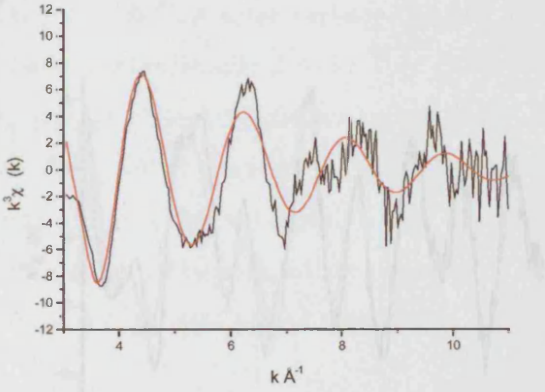
k³χ (k)
k Å⁻¹

(c)

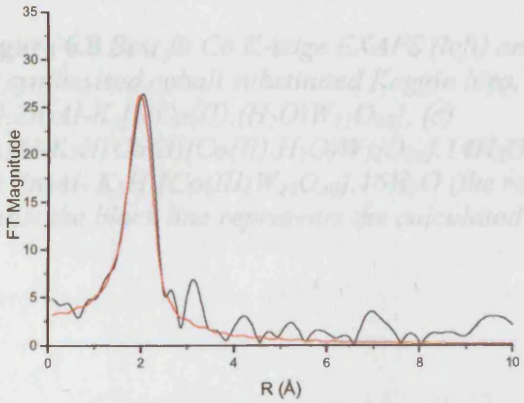
FT Magnitude
R (Å)

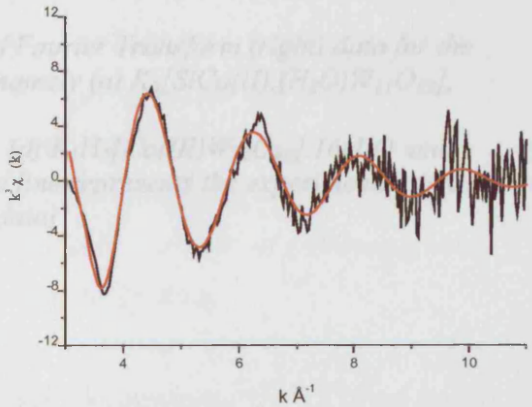
k³χ (k)
k Å⁻¹

(d)

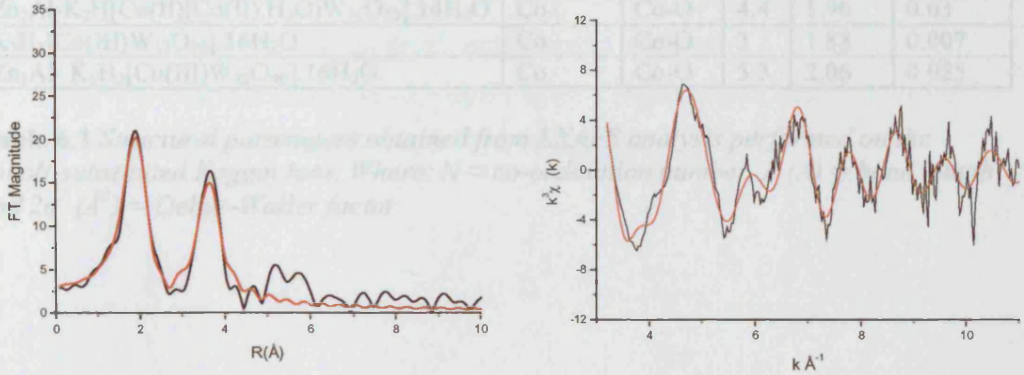

(e)

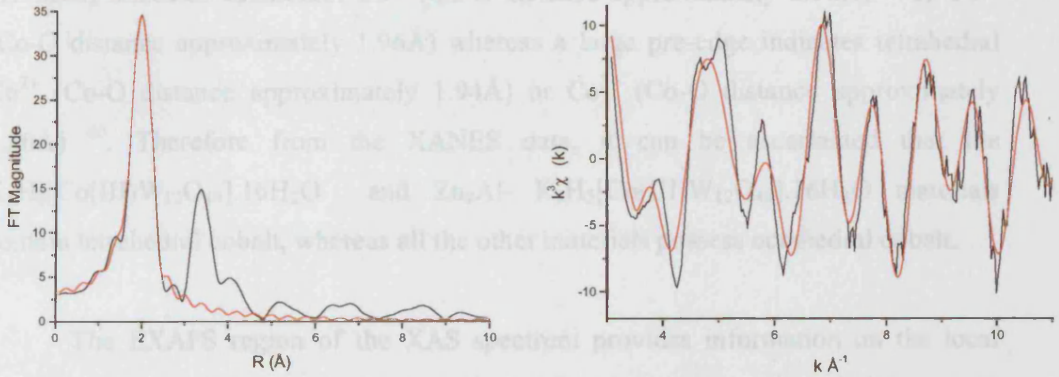

Figure 6.8 *Best fit Co K-edge EXAFS (left) and Fourier Transform (right) data for the as synthesised cobalt substituted Keggin ions, namely (a) $K_6[SiCo(II).(H_2O)W_{11}O_{39}]$, (b) Zn_2Al-$K_6[SiCo(II).(H_2O)W_{11}O_{39}]$, (c) Zn_2Al-$K_7H[Co(II)(Co(II).H_2O)W_{11}O_{39}].14H_2O$, (d) $K_5H_5[Co(III)W_{12}O_{40}].16H_2O$ and (e) Zn_2Al- $K_5H_5[Co(III)W_{12}O_{40}].16H_2O$ (the red line represents the experimental data whilst the black line represents the calculated data)*

Material	K-edge	Atom pair	N	R (Å)	$2\sigma^2$ (Å^2)
$K_6[SiCo(II).(H_2O)W_{11}O_{39}]$	Co	Co-O	5	2.05	0.016
Zn_2Al-$K_6[SiCo(II).(H_2O)W_{11}O_{39}]$	Co	Co-O	5.5	2.07	0.021
Zn_2Al-$K_7H[Co(II)(Co(II).H_2O)W_{11}O_{39}].14H_2O$	Co	Co-O	4.4	1.96	0.03
$K_5H_5[Co(III)W_{12}O_{40}].16H_2O$	Co	Co-O	3	1.88	0.007
Zn_2Al- $K_5H_5[Co(III)W_{12}O_{40}].16H_2O$	Co	Co-O	5.3	2.06	0.025

Table 6.1 *Structural parameters obtained from EXAFS analysis performed on the cobalt-substituted Keggin ions. Where: N = co-ordination number, R (Å) = bond length and $2\sigma^2$ (Å^2) = Debye-Waller factor*

The XANES region of the XAS spectrum provides information on both the oxidation state and co-ordination of the absorbing species [59]. A small pre-edge (figure 6.7 inset) indicates octahedral Co^{2+} (Co-O distance approximately 2.10Å) [60] or Co^{3+} (Co-O distance approximately 1.96Å) whereas a large pre-edge indicates tetrahedral Co^{2+} (Co-O distance approximately 1.94Å) or Co^{3+} (Co-O distance approximately 1.80Å) [60]. Therefore from the XANES data, it can be ascertained that the $K_5H_5[Co(III)W_{12}O_{40}].16H_2O$ and Zn_2Al- $K_5H_5[Co(III)W_{12}O_{40}].16H_2O$ materials contain tetrahedral cobalt, whereas all the other materials possess octahedral cobalt.

The EXAFS region of the XAS spectrum provides information on the local geometry of a specific atom. In this case the local co-ordination of the cobalt ions were studied, using only the first shell of the atom for data interpretation. Here it was observed that the cobalt ions substituted in the tetrahedral 2+ position for Zn_2Al-$K_5H_5[Co(II)W_{12}O_{40}].16H_2O$. For $K_5H_5[Co(III)W_{12}O_{40}].16H_2O$, it was most likely that there was a mixed oxidation state of tetrahedral Co^{3+} and Co^{2+} since the bond distance measured was 1.88Å. This may have been due to the sample having been reduced when in the beam. As for all the other materials, they were analysed as possessing bond lengths indicative of octahedral cobalt substituted in the 2+ state.

The co-ordination number (N) and the Debye-Waller factor ($2\sigma^2$ (Å^2)) are larger than normal due to self-absorption, which is itself due to a large amount of cobalt present within the materials.

6.5.3 IR study of the as synthesised catalysts

In addition to the XAS results, the co-ordination geometry of the cobalt-polyoxometalates were also investigated using infrared analysis.

Evidence for the retention of Keggin POM's within the layers of the LDH is provided by the IR data in figures 6.9, 6.10, 6.11 and 6.12.

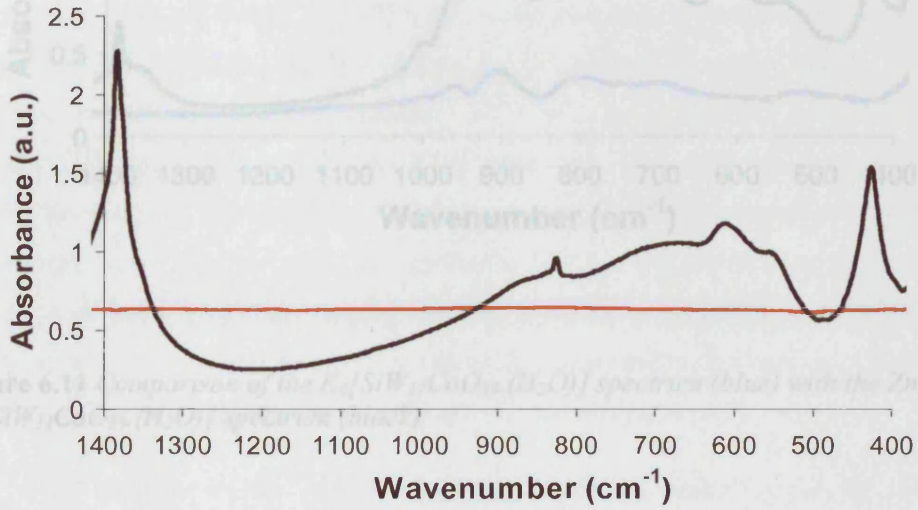

Figure 6.9 *Comparison of a blank KBr spectrum (red) with the Zn_2Al-NO_3 spectrum (black)*

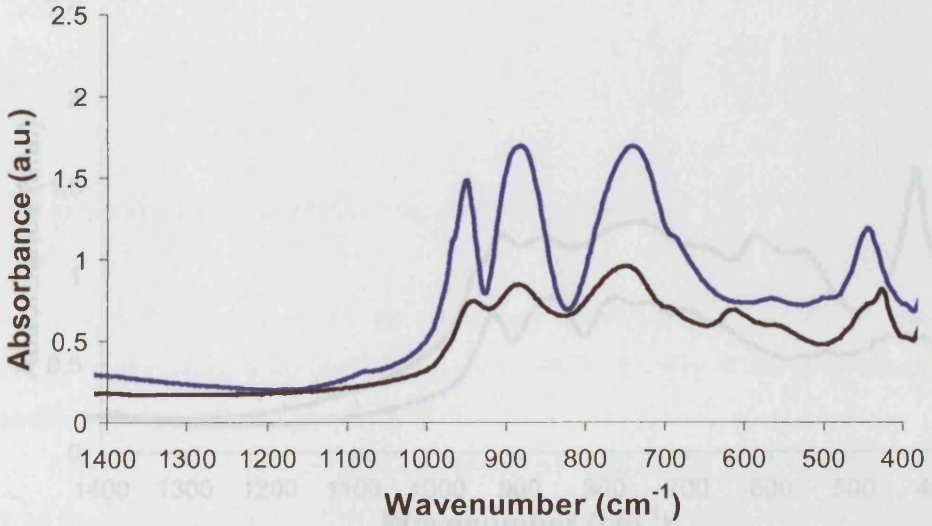

Figure 6.10 *comparison of the $K_5H_5[Co(III)W_{12}O_{40}].16.H_2O$ spectrum (blue) with the Zn2Al- $K_5H_5[Co(III)W_{12}O_{40}].16.H_2O$ spectrum (black)*

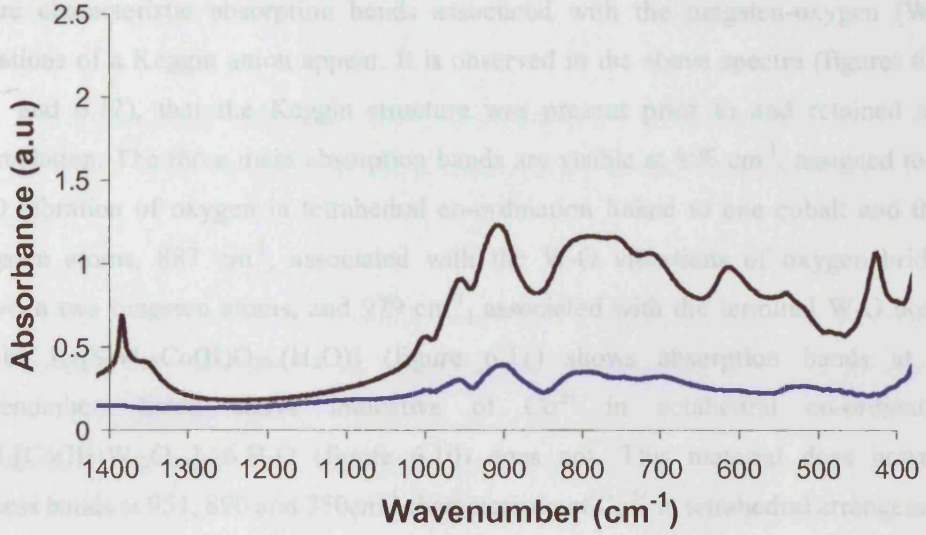

Figure 6.11 *Comparison of the $K_6[SiW_{11}CoO_{39}.(H_2O)]$ spectrum (blue) with the Zn_2Al-$K_6[SiW_{11}CoO_{39}.(H_2O)]$ spectrum (black)*

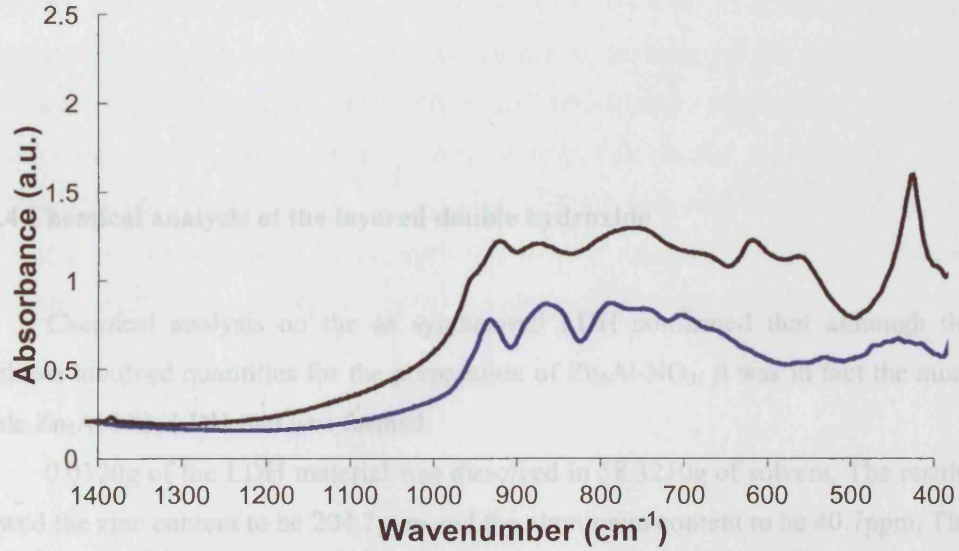

Figure 6.12 *Comparison of the $K_7H[Co(II)(Co(II).H_2O)W_{11}O_{39}].14H_2O$ spectrum (blue) with the Zn_2Al-$K_7H[Co(II)(Co(II).H_2O)W_{11}O_{39}].14H_2O$ spectrum (black)*

The pure $Zn_2Al\text{-}NO_3^{2-}$ material has no absorption in the range 700-1100cm^{-1}, where characteristic absorption bands associated with the tungsten-oxygen (W-O) vibrations of a Keggin anion appear. It is observed in the above spectra (figures 6.10, 6.11 and 6.12), that the Keggin structure was present prior to and retained after intercalation. The three main absorption bands are visible at 808 cm^{-1}, assigned to the W-O vibration of oxygen in tetrahedral co-ordination linked to one cobalt and three tungsten atoms, 887 cm^{-1}, associated with the W-O vibrations of oxygen bridged between two tungsten atoms, and 979 cm^{-1}, associated with the terminal W-O bonds. Whilst $K_6[SiW_{11}Co(II)O_{39}.(H_2O)]$ (figure 6.11) shows absorption bands at the wavenumbers listed above indicative of Co^{2+} in octahedral co-ordination, $K_5H_5[Co(III)W_{12}O_{40}].16.H_2O$ (figure 6.10) does not. This material does however possess bands at 951, 890 and 750cm^{-1} characteristic of Co^{3+} in tetrahedral arrangement. In addition, figure 6.9 once again guarantees the fact that the nitrate form of the LDH has in fact been prepared successfully, as there is a sharp peak at 1380cm^{-1} characteristic of the presence of nitrate anions. For comparison, the spectra of the pure $Zn_2Al\text{-}NO_3^{2-}$ LDH and KBr blank spectra are also shown (figure 6.9).

The decrease in the intensities of the absorption peaks for the IR spectra representing the POM-LDH's is due to the hydrogen bonding interactions between the protonated POM anion and the hydroxyl anion in the brucite sheet.

6.5.4 Chemical analysis of the layered double hydroxide

Chemical analysis on the as synthesised LDH confirmed that although the synthesis involved quantities for the preparation of $Zn_3Al\text{-}NO_3$, it was in fact the more stable $Zn_2Al\text{-}NO_3$ LDH that was formed.

0.0320g of the LDH material was dissolved in 58.3210g of solvent. The results showed the zinc content to be 204.7ppm and the aluminium content to be 40.7ppm. The molar ratio of the material when calculated using equation 6.1 was found to be $Zn_{(0.55)}Al_{(0.27)}\text{-}NO_{3(x)}$.

6.5.5 Catalytic investigation for the Cyclohexane oxidation reaction using the as synthesised catalysts

The maximum conversion of cyclohexane under the parameters used in this analysis was 4.92%. This was calculated using equation 6.2, described earlier in this chapter.

As shown by the results given in table 6.5, It is shown that both the layered and non-layered POM's synthesised via various techniques described earlier in this chapter (6.3.1), are active for the conversion of cyclohexane. The results show that a small amount of cyclohexane was converted over the pure Zn_2Al-NO_3 although the most active catalyst prepared was the di-substituted Zn_2Al-$K_7H[Co(II)(Co(II).H_2O)W_{11}O_{39}].14H_2O$, which converted cyclohexane to predominantly cyclohexanone and cyclohexanol, with a TON of 77. Insertion of the POM between the layers of the LDH produces more active/ selective catalysts than when in their pure form. The majority of materials studied were more selective to the formation of cyclohexanone than cyclohexanol or other by-products. Furthermore, the formation of adipic acid and other by-products tended to be favoured more for the non-layered materials as opposed to the layered materials. The lower formation of by-products by the POM-LDH's is most likely due to their increased shape selective properties and hence reduced access to the POM active sites. It is unlikely that the activities observed for the LDH catalysts are due to leaching of the POM ions into solution as no anions are generated in the oxidation reaction for the displacement of the POM ions from the LDH surfaces. In addition no-colour change was observed in the catalyst after the reaction. However, leaching of the cobalt ions from the POM into solution was not investigated. Once again this was not expected to have occurred and hence should not have had any impact towards the catalyst's activities.

CATALYST IDENTIFICATION	Cyclohexane Conversion (%)	SELECTIVITY (%)						Ratio -one/ -ol	TON
		-one	-ol	-one & -ol	Adipic Acid	X [a]	Others		
Zn_2Al-NO_3	1.1	33.1	39.6	72.7	1.1	22.2	3.8	0.84	2
$K_5H_5[Co(II)W_{12}O_{40}].16H_2O$	1.3	35.9	26.6	62.5	0.8	28.1	8.6	1.35	37
Zn_2Al- $K_5H_5[Co(II)W_{12}O_{40}].16H_2O$	1.5	41.7	32.5	74.2	0.6	25.2	0	1.28	48
$K_6[SiW_{11}CoO_{39}.(H_2O)]$	2.0	40.9	35.6	76.5	2.2	18.6	2.7	1.15	53
Zn_2Al-$K_6[SiW_{11}CoO_{39}.(H_2O)]$	2.3	42.2	42.2	84.4	0.6	12.1	2.9	1.00	65
$K_7H[Co(II)(Co(II).H_2O)W_{11}O_{39}].14H_2O$	1.6	33.6	37.4	71.0	1.2	26.8	1.0	0.90	47
Zn_2Al-$K_7H[Co(II)(Co(II).H_2O)W_{11}O_{39}].14H_2O$	2.5	44.6	40.8	85.4	1.1	12.6	0.9	1.09	77

Table 6.2 *Cyclohexane oxidation results for the layered and non-layered polyoxometalate materials. Reaction conditions: 0.2g of catalyst, $P(O_2)$ = 1 bar, reaction temperature = 83°C, TOS = 24 hrs, Feed: 15g of cyclohexane, 1g of acetonitrile and 1g of TBHP. [a] X is an unknown product with a chromatographic peak at t = 11.4 minutes.*

6.6 Summary and Conclusions

$Zn_2Al\text{-}NO_3^{2-}$ layered double hydroxide, as confirmed by chemical analysis, a series of polyoxometalates and the intercalation of these POM's within the layers of the LDH precursor have been successfully synthesised. The success in the synthesis of the POM-LDH's was due to slightly altering several previously reported conventional pillaring methods based on the size and complexity of the POM anion being investigated. The winning formulation was found to be with the use of wet LDH slurry and the POM in solution. Reaction temperature was kept constant throughout each of the POM intercalation's, although the time-scale for successful pillaring varied depending on the size of the POM. No pH changes where necessary to the solution throughout the reaction.

X-ray diffraction studies found that the synthesised materials were both crystalline and phase pure and corroborated the fact that the pillaring was successful since the patterns showed the first two peaks of the LDH phase to have expanded. Intercalation was further backed up by XAS analysis which found the presence of cobalt ions within the samples. Bond lengths of the cobalt incorporated species were analysed as being mainly octahedral Co^{2+} with the exception of $K_5H_5[Co(II)W_{12}O_{40}].16H_2O$ and $Zn_2Al\text{-}K_5H_5[Co(II)W_{12}O_{40}].16H_2O$ which were found to contain tetrahedral Co^{3+} and Co^{2+} respectively. Additionally, Infrared studies also found intercalation to have been a success and the same cobalt geometries were again found on analysis of the data.

Catalytic investigations into the activity of the pure LDH and POM materials were compared against the intercalated POM-LDH's. Although overall these catalysts weren't excellent for the conversion of cyclohexane, a trend was observed showing that the pillared POM-LDH's were more active for the reaction than the pure materials. Each of the layered materials studied exhibited more selectivity towards the formation of cyclohexanone than cyclohexanol or other by-products however more adipic acid was observed to form on reaction with the non-layered materials. The most active catalyst was found to be the di-substituted $Zn_2Al\text{-}K_7H[Co(II)(Co(II).H_2O)W_{11}O_{39}].14H_2O$, which converted cyclohexane to predominantly cyclohexanone and cyclohexanol, with a TON of 77. This increased activity was most likely due to the presence of Co^{2+} in tetrahedral co-ordination.

6.7 References

(1) Thomas, J. M.; Raja, R.; Sankar, G.; Bell, R. G. *Nature* **1999**, *398*, 227-230.

(2) Sankar, G.; Raja, R.; Thomas, J. M. *Catal. Lett.* **1998**, *55*, 15-23.

(3) Indira, V.; Joy, P. A.; Gopinathan, S.; Gopinathan, C. *Indian J. Chem. Sect A-. Bio-Inorg. Phys. Theor. Anal. Chem.* **1998**, *37*, 473-481.

(4) Nishiyama, Y.; Nakagawa, Y.; Mizuno, N. *Angew. Chem.-Int. Edit.* **2001**, *40*, 3639-3645.

(5) Mizuno, N.; Nozaki, C.; Hirose, T. O.; Tateishi, M.; Iwamoto, M. *J. Mol. Catal. A-Chem.* **1997**, *117*, 159-168.

(6) Mizuno, N.; Kiyoto, I.; Nozaki, C.; Misono, M. *J. Catal.* **1999**, *181*, 171-174.

(7) Mizuno, N.; Nozaki, C.; Kiyoto, I.; Misono, M. *J. Am. Chem. Soc.* **1998**, *120*, 9267-9272.

(8) Neumann, R.; Khenkin, A. M. *Inorg. Chem.* **1995**, *34*, 5753-5760.

(9) Shilov, A. E.; Shul'pin, G. B. *Chem. Rev.* **1997**, *97*, 2879-2932.

(10) Chibwe, K.; Valim, J. B.; Jones, W. *Abstr. Pap. Am. Chem. Soc.* **1989**, *198*, 20.

(11) Drezdzon, M. A. *Inorg. Chem.* **1988**, *27*, 4628-4632.

(12) Kwon, T.; Tsigdinos, G. A.; Pinnavaia, T. J. *J. Am. Chem. Soc.* **1988**, *110*, 3653-3654.

(13) Drezdzon, M. A. *Acs Symposium Series* **1990**, *437*, 140-148.

(14) Wang, J. D.; Serrette, G.; Tian, Y.; Clearfield, A. *Appl. Clay Sci.* **1995**, *10*, 103-115.

(15) Pope, M. T. *Heteropoly and Isopoly Oxometalates*; Springer-Verlag, **1983**.

(16) Berzelius, J. *Pogg. Ann.* **1826**, *6*, 369-380.

(17) Svanberg, L.; Struve, H. *Prakt.Chem.* **1848**, *44*, 257-291.

(18) Marignac, C. *Ann. Chem. Phys.* **1863**, *69*, 41-48.

(19) Miolati, A. *Prakt.Chem.* **1908**, *77*, 439.

(20) Keggin, J. F. *Nature* **1933**, *131*, 908-910.

(21) Keggin, J. F. *Proc.Roy.Soc. A* **1934**, *144*, 75-77.

(22) Bradley, A. J.; Illingworth, J. W. *Proc.Roy.Soc. A* **1936**, *157*, 113-117.

(23) Okuhara, T.; Mizuno, N.; Misono, M. *Advances in Catalysis,* **1996**, *41*, 113-252.

(24) Kozhevnikov, I. V. *Chem. Rev.* **1998**, *98*, 171-198.

(25) Brown, G. M.; Noe-Spirlet, M. R.;Bushing, W. R.;Levy, H. A. *Acta Crystallogr* **1977**, *33*, 1038-1046.

(26) Kozhevnikov, I. V. (conference notes), NATO ASI, *Polyoxometalate Molecular Science,* **2001**.

(27) Mizuno, N.; Misono, M. *Chem. Rev.* **1998**, *98*, 199-217.

(28) Maestre, J. M.; Lopez, X.; Bo, C.; Poblet, J. M.; Casan-Pastor, N. *J. Am. Chem. Soc.* **2001**, *123*, 3749-3758.

(29) Souchay, P.; Teze, A.;Herve, G. *C.R. Acad. Sc. Paris* **1972**, 1013-1016.

(30) Pope, M. T.; Varga, G. M. *Inorg. Chem.* **1966**, *5*, 1249-1254.

(31) Mair, J. A.; Waugh, J. L. T. *Journal of the Chemical Society*, **1950**, 2372-2376.

(32) Brown, D. H. *Journal of the Chemical Society,* **1962**, 4408-4410.

(33) Manasse, E. *Atti Soc. Toscana Sci. Nat.* **1915**, *24*, 92-93.

(34) Feitknecht, W.; Gerber, M. *Helv. Chim. Acta* **1942**, *25*, 131-134.

(35) Taylor, H. F. W. *Miner. Mag* **1969**, *37*, 338-340.

(36) Allmann, R. *Acta Crystallogr* **1968**, *24*, 972-975.

(37) Khan, A. I.; O'Hare, D. *J. Mater. Chem.* **2002**, *12*, 3191-3198.

(38) Narita, E.; Kaviratna, P.; Pinnavaia, T. J. *Chem. Lett.* **1991**, 805-808.

(39) Basile, F.; Fornasari, G.; Gazzano, M.; Vaccari, A. *Appl. Clay Sci.* **2000**, *16*, 185-200.

(40) Fernandez, J. M.; Ulibarri, M. A.; Labajos, F. M.; Rives, V. *J. Mater. Chem.* **1998**, *8*, 2507-2514.

(41) Kooli, F.; Crespo, I.; Barriga, C.; Ulibarri, M. A.; Rives, V. *J. Mater. Chem.* **1996**, *6*, 1199-1206.

(42) Pesic, L.; Salipurovic, S.; Markovic, V.; Vucelic, D.; Kagunya, W.; Jones, W. *J. Mater. Chem.* **1992**, *2*, 1069-1073.

(43) Nickel, E. H.; Clarke, R.M. *Am, Mineral* **1976**, *61*, 366-372.

(44) Brindley, G. W.; Kikkawa, S. *Am, Mineral* **1979**, *64*, 836-843.

(45) Pinnavaia, T. J.; Chibwe, M.; Constantino, V. R. L.; Yun, S. K. *Appl. Clay Sci.* **1995**, *10*, 117-129.

(46) Cavani, F.; Trifiro, F. *Catal. Today* **1997**, *34*, 269-279.

(47) Rives, V.; Ulibarri, M. A. *Coord. Chem. Rev.* **1999**, *181*, 61-120.

(48) Gardner, E.; Pinnavaia, T. J. *Appl. Catal. A-Gen.* **1998**, *167*, 65-74.

(49) Weir, M. R.; Kydd, R. A. *Inorg. Chem.* **1998**, *37*, 5619-5624.

(50) Weir, M. R.; Kydd, R. A. *Microporous Mesoporous Mat.* **1998**, *20*, 339-347.

(51) Hu, C. W.; He, Q. L.; Zhang, Y. H.; Liu, Y. Y.; Zhang, Y. F.; Tang, T. D.; Zhang, J. Y.; Wang, E. B. *Chem. Commun.* **1996**, 121-122.

(52) Tatsumi, T.; Yamamoto, K.; Tajima, H.; Tominaga, H. *Chem. Lett.* **1992**, 815-818.

(53) Twu, J.; Dutta, P. K. *J. Phys. Chem.* **1989**, *93*, 7863-7868.

(54) Kwon, T.; Doeuff, M.; Pinnavaia, T. J. *Abstr. Pap. Am. Chem. Soc.* **1989**, *198*, 253

(55) Narita, E.; Kaviratna, P. D.; Pinnavaia, T. J. *J. Chem. Soc.-Chem. Commun.* **1993**, 60-62.

(56) Dimotakis, E. D.; Pinnavaia, T. J. *Inorg. Chem.* **1990**, *29*, 2393-2394.

(57) Misra, C.; Perrotta, A. J. *Clay Clay Min.* **1992**, *40*, 145-150.

(58) Olanrewaju, J.; Newalkar, B. L.; Mancino, C.; Komarneni, S. *Mater. Lett.* **2000**, *45*, 307-310.

(59) Iwasawa, Y. *X-ray Absorption Fine Structure for Catalysts and Surfaces*; World Scientific Publishing Company Pte. Ltd, **1996**.

(60) Muncaster, G.; Sankar, G.; Catlow, C. R. A.; Thomas, J. M.; Coles, S. J.; Hursthouse, M. *Chem. Mat.* **2000**, *12*, 16-19.

Chapter 7

Final Conclusions

Overall, the research within this thesis was very successful in identifying and understanding the acid and redox catalytic properties of a series of metal substituted aluminophosphates, silicoaluminophosphates and polyoxometalates.

The aim of the work discussed in chapter three, was to investigate the shape selective and redox properties associated firstly with the substitution of different metal ions within individual aluminophosphate frameworks, and secondly the substitution of the same metal ion within different aluminophosphate frameworks.

In summary, several transition metals were successfully substituted into a variety of microporous frameworks. Characterisation was achieved via X-ray diffraction (XRD) patterns of the as synthesised aluminophosphates, which found the materials to be phase pure. Previously reported XAS data obtained within our research group was used to understand how the transition metal ions were incorporated within the framework materials. Studies into the catalytic activity of the as synthesised materials for the methanol to olefin (MTO) reaction found the same trend for each of the frameworks studied. Both the cobalt and manganese substituted materials converted the greatest amount of methanol and were the most active catalysts. Catalytic selectivitys varied dependent on the microporous structure of the catalysts. The activity trend observed was Co> Mn> Fe> Ti. As expected, it was found that the small-pore materials were more selective for the production of light olefins in contrast to the higher hydrocarbons produced on reaction over the large-pore catalysts. In particular MnAlPO-5 was the best catalyst for the selective production of C_3-C_5 olefins at 350°C and TOS = 30 minutes, with methanol conversion > 97%.

A time on stream (TOS) study was carried out to determine the extent to which the Co and Mn substituted AlPO-18 catalysts continued to convert methanol feed. These results showed that there was no significant decline in either activity or selectivity for both catalysts, for up to two hours. The performance of the catalyst was also tested after regeneration. Once again the results suggested that there was no significant decline in the conversion level after a further two-hour reaction. The slight decrease that was

noticed was likely to be due to the formation of coke. Based on the initial conversion after each cycle and under the conditions employed in this study, it was proposed that there was no significant leaching of the active metal centres during reaction.

To determine as to which cobalt-substituted framework was most active, a comparative study of the cobalt substituted catalysts was carried out at 350°C, TOS = 30minutes. The trend observed for the catalytic activity in terms of amount methanol converted was CoAlPO-18> CoAlPO-5> CoAlPO-36> CoAlPO-39.

Comparing this information to previous XAS studies into the co-ordination and geometry of the cobalt substituted ions within these different framework topologies, one explanation that could be drawn as to why the above trend is observed is that whereas the cobalt ion in CoAlPO-18 undergoes complete oxidation upon removal of the SDA (Co(II) to Co(III)) and reduction upon reaction with methanol yielding Brønsted acid sites. Whereas, the cobalt ion in CoAlPO-5 and CoAlPO-36 are only observed to partially oxidise (no data has yet been collected for CoAlPO-39 and therefore it is not possible to discuss how this may affect the catalytic performance of this material) and the remaining Co(II) ions are believed to be associated with Lewis acid sites which may not participate in the methanol dehydration reaction. Therefore although the selectivity to products varies in consideration to the pore size of the material under investigation, if all the cobalt ions were to have oxidised in the CoAlPO-36 framework, then this one-dimensional material may have been more active towards the methanol to olefin reaction.

Chapter four was based around an investigation into the state of iron, cobalt and titanium ions within the zeolite-β and AlPO-5 materials. Catalytic studies were performed for the hydroxylation of phenol to ascertain what effect this and temperature had on the catalyst activities.

In brief, several iron and cobalt exchanged zeolite-β and AlPO-5 materials were synthesised via ion-exchange techniques in relation to a paper published by Wang *et al.* X-ray diffraction studies found the materials to be both crystalline and phase-pure, on comparison to previously reported patterns outlined in the IZA structure database. The EDAX results did not completely agree with those found in the work reported by Wang et al [1] since here surface analysis was employed whereas they had used bulk analysis. For this reason the information in table 3.4 cannot be used quantitatively however it can be used as a suggestion of approximate levels of each element within the materials. The

results also show that there was preferential exchange of the metal ions within the zeolite. Investigations into the local geometry of the ion-exchanged zeolites by EXAFS analysis revealed that for each of the materials, cobalt ions were present in the octahedral 2+ state, whilst the iron ions were in tetrahedral sites with a mixture of 2+ and 3+ oxidation states. Unfortunately poor data quality for the AlPO-5 exchanged materials due to high background noise and therefore no reasonable information was obtainable.

Overall, the catalytic results demonstrate that the exchange of metal ions into the extra framework sites significantly improved the conversion of phenol. Catalytic investigations observed no reaction over pure AlPO-5, whereas >5% phenol was converted over pure NH_4-β at both 40°C and 60°C indicating that the non-metal exchanged materials were not active for the reaction. The studies revealed that of all the exchanged materials, $CoFeNH_4$-β were observed to be the most active catalyst for the hydroxylation of phenol with H_2O_2 at 40°C and selective towards the production of dihydroxybenzenes at 40°C. In addition, although no reaction was observed for any of the exchanged AlPO-5 catalysts at 40°C, at 60°C FeAlPO-5 was observed as being the most active of all the catalysts investigated. The most preferable catalyst however must be the one which is most active at temperatures as close to ambient as possible. Unfortunately time restrictions prevented further studies into the leaching of the metal ions, however this would be an interesting study to see as to whether these remained stable if successive reactions were performed.

Chapter five centred on investigating the use of alternative materials for the isomerisation of paraffins. Due to more intense European laws regarding the limitation of aromatic compounds in gasoline coming into effect over the last decade many investigations have been and are still being carried out into the use of alternative compounds as a solution to the problem. One idea that has been suggested is the isomerisation of n-heptane, to mono and multi-branched products. Our research was based around the investigation of a series of bifunctional platinum impregnated silicoaluminophosphate (Pt/SAPO) and metal substituted aluminophosphate (Pt/MeAlPO) catalysts.

In summary, twelve materials of AFI, ATS and CHA-type frameworks were successfully synthesised and characterised by XRD. Results found them to be crystalline and phase-pure upon comparison with previously reported literature. On

impregnation of the platinum species within the framework, apart from the exception of the zinc substituted topologies, all the materials retained their crystalline structures. Zinc substituted materials were observed to collapse upon calcination, prior to impregnation. An *in situ* study into the local co-ordination of three calcined and reduced platinum impregnated aluminophosphates revealed that in each case the results confirmed that the reduction procedure resulted in the production of platinum metal particles with typical bond lengths of approximately 2.74Å and 2.02Å respectively. The most important result was the presence of a low coordination number for Pt-Pt, which indicated that small metal particles were present in the catalyst. Analysis into the physical properties of the materials revealed important information leading to further understanding of the catalytic reactions. The majority of the materials exhibited a high TPD pyridine chemisorption capacity, consistent for materials that are highly acidic. Two high intensity peaks were observed, indicating that there are at least two different types of adsorbing sites of differing acidic strengths present within their frameworks. Specific surface area and thermogravimetric measurements of the materials produced results predictable for these types of materials. The only exception being in the case of the zinc substituted framework materials whose surface areas were found to be very low. This is due to the collapse of the structures during calcination as discovered by XRD.

The catalytic behaviour of the Pt/SAPOs and Pt/MeAlPOs were found to be influenced not only by the strength of the acid sites but also by the size of the pores and location of the catalytically active hydroxyl groups. For example, in the case of Pt/MgAlPO-36, the catalyst was found to be the most acidic out of all the materials studied and indeed was the most active in converting n-heptane. However the catalytic study found the Pt/CoAlPO-5 material was the most active for the selective conversion of n-heptane to isomers. The trend observed for the overall activity and hence conversion of n-heptane for the hydroisomerisation reaction at 330°C was found to be: Pt/MgAlPO-36 > Pt/CoAlPO-36 > Pt/CoAlPO-5 > Pt/ZnSAPO-36 > Pt/MgAlPO-5 > Pt/SAPO-5 > Pt/ZnAlPO-36 > Pt/ZnAlPO-5. The first three catalysts only differed by around 10% in their activity, converting 59.05%, 53.66% and 48.16% of n-heptane respectively. However, the important factor here is not in the conversion of n-heptane, but in the selectivity to isomers produced during the reaction. Here the trend observed is very different: Pt/SAPO-5 > Pt/CoAlPO-5 > Pt/MgAlPO-5 > Pt/ZnAlPO-36 > Pt/ZnSAPO-36 > Pt/ZnAlPO-5 > Pt/CoAlPO-36 > Pt/MgAlPO-36. The difference in

the selectivity to isomers for the first three catalysts was < 5%. Overall, the most effective catalyst for this reaction was Pt/CoAlPO-5. Lower temperatures are favoured as they restrict the amount of cracking during the reaction. However for comparison, greater conversions of n-heptane were observed over Pt/CoAlPO-5 at 350°C, where > 83% n-heptane was converted with selectivities to isomers > 76% and selectivities to cracking products now a great deal higher at > 23%. These studies correlate very well to previously reported literature, which states that cobalt substituted Pt/MeAlPOs have greater activity than Pt/SAPO materials. This is due to the type of substitution, for example island formation would reduce the materials acidity.

Comparable conversions and selectivities to the Pt/CoAlPO-5 catalyst were observed for the Pt/Zeolite-β catalyst at 250°C. In all cases, conversion of reactant increased with increasing reaction temperature. Additionally, whatever the acid strength of the catalysts, some cracking of the isomers always transpired. It can therefore be proposed that selectivity is governed by porosity rather than by acidity. The framework geometry plays a vital role in the reaction as it can have an effect on the diffusion of reactants and products into and out of the catalyst. One-dimensional systems have offered the best results for the n-heptane hydroisomerisation reaction as not only can further re-arrangements of the isomers take place within the channels. This ultimately produces more multi-branched products, which are not trapped within the material, and therefore cannot inhibit the onset of carbonaceous residues. Throughout this study, the one-dimensional AFI and ATS-type catalysts were found to be the most active frameworks studied. However the restricted pore size of the CHA-type catalysts prevented the n-heptane molecule reacting and so no conclusions can be drawn from this study so as to compare three-dimensional systems.

Unfortunately time restrictions meant that no time on stream (TOS) reactions were carried out. However, it is fair to say that the majority of the catalysts would most likely have coked relatively quickly and some were found to have already started to deactivate over the two-hour reaction time. This cannot be entirely avoided since the presence of free hydrogen within the reacting environment would lead to hydride transfer and ultimately the formation of carbonaceous deposits within the pores of the catalyst. Coke can also form on the platinum sites due to the cracking of alkanes to C_1-C_5 hydrocarbons, however this can be beneficial as the coke suppresses the cracking of alkanes in limiting the number of platinum sites.

Although one or two of the catalysts were found to be as catalytically active as Pt/zeolite-β, it is very unlikely that they would continue at this level for very long. In addition some of the catalysts were found to be more selective in the short-term for the production of isomers and cracking products. One big disadvantage that should be taken into account is that Pt/AlPOs and Pt/SAPOs perform their best at elevated reaction temperatures, over 50°C higher than Pt/zeolite-β, for example comparable conversions and selectivitys to the Pt/CoAlPO-5 catalyst were observed for the Pt/zeolite-β catalyst at 250°C.

The aim of the work discussed in chapter six was to investigate the properties of several cobalt-substituted polyoxometalates (POM's) and polyoxometalate pillared layered double hydroxides (POM-LDH's) and to study their activity for the oxidation of cyclohexane in the presence of TBHP.

Several materials were successfully synthesised, including a $Zn_2Al\text{-}NO_3^{2-}$ layered double hydroxide, a series of polyoxometalates and the intercalation of these POM's within the layers of the LDH precursor. X-ray diffraction studies found that the synthesised materials were both crystalline and phase pure and corroborated the fact that the pillaring was successful since the patterns showed the first two peaks of the LDH phase to have expanded. Intercalation was further backed up by XAS analysis which found the presence of cobalt ions within the samples. Bond lengths of the cobalt incorporated species were analysed as being mainly octahedral Co^{2+} with the exception of $K_5H_5[Co(II)W_{12}O_{40}].16H_2O$ and $Zn_2Al\text{-}$ $K_5H_5[Co(II)W_{12}O_{40}].16H_2O$ which were found to contain tetrahedral Co^{3+} and Co^{2+} respectively. Additionally, Infrared studies also found intercalation to have been a success and the same cobalt geometries were again found on analysis of the data.

Catalytic investigations into the activity of the pure LDH and POM materials were compared against the intercalated POM-LDH's. Although overall these catalysts were not very active for the conversion of cyclohexane, a trend was observed showing that the pillared POM-LDH's were more active for the reaction than the pure materials. Each of the layered materials studied exhibited more selectivity towards the formation of cyclohexanone than cyclohexanol or other by-products however more adipic acid was observed to form on reaction with the non-layered materials. The most active catalyst was found to be the di-substituted $Zn_2Al\text{-}$ $K_7H[Co(II)(Co(II).H_2O)W_{11}O_{39}].14H_2O$, which converted cyclohexane to

predominantly cyclohexanone and cyclohexanol, with a TON of 77. This increased activity was most likely due to the presence of Co^{2+} in tetrahedral co-ordination.

In summary, several catalytic materials described within this thesis showed promising potential applications for both acid catalysed and oxidation reactions. Further detailed studies and improvements are necessary to attract commercial interest in some of these systems.

Appendix

Peak	Result (%)	Retention Time (minutes)	Area Counts
1	0.2892	0.956	7127
2	6.2538	2.887	154104
3	0.0238	3.327	587
4	36.1400	7.219	890543
5	2.2491	9.213	55421
6	9.9888	11.393	246139
7	11.8856	11.807	292879
8	12.2895	12.254	302832
9	4.9870	12.821	122888
10	3.2847	13.310	80941
11	4.2492	18.892	104707
12	1.7681	19.821	43569
13	2.7357	20.575	69413
14	3.8554	28.666	95003
Total:	99.9999		2464153

Figure A *Chromatogram obtained from analysis into the MTO reaction over CoAlPO-5, TOS = 10 minutes, Temperature = 350°C*

Peak	Result (%)	Retention Time (minutes)	Area Counts
1	0.2393	0.972	10930
2	3.2238	2.910	147236
3	0.0138	3.346	629
4	30.4049	7.209	1388641
5	4.5244	9.201	206637
6	9.1283	11.380	416904
7	19.7598	11.773	902460
8	11.8841	12.237	542768
9	4.7446	12.809	216692
10	3.1789	13.298	145184
11	0.1135	18.112	5185
12	4.2887	18.885	195872
13	1.9910	19.804	909132
14	2.9648	20.566	135408
15	2.3706	28.112	108269
16	1.1695	28.634	53414
Total:	100.0000		4567161

Figure B *Chromatogram obtained from analysis into the MTO reaction over CoAlPO-5, TOS = 45 minutes, Temperature = 350°C*

	RUN 1					RUN 2					RUN 3			
Mixed Std.	**RT**	**RRT**	**Area**	**RRF**	**Mixed Std.**	**RT**	**RRT**	**Area**	**RRF**	**Mixed Std.**	**RT**	**RRT**	**Area**	**RRF**
CH4	0.94	1.00	858	1	**CH4**	0.95	1.00	559	1	**CH4**	0.85	1.00	450	1
C2H4	2.88	3.07	1496	0.573529	**C2H4**	2.89	3.04	837	0.667861	**C2H4**	2.79	3.28	765	0.588235
C2H6	3.32	3.53	1752	0.489726	**C2H6**	3.13	3.29	853	0.655334	**C2H6**	3.23	3.80	868	0.518433
C2H2	4.15	4.41	1314	0.652968	**C2H2**	4.16	4.38	798	0.700501	**C2H2**	4.09	4.81	757	0.594452
C3H6	7.23	7.69	4671	0.183687	**C3H6**	7.24	7.62	2657	0.210388	**C3H6**	7.17	8.44	2357	0.190921
C3H4	8.92	9.49	1959	0.437979	**C3H4**	8.94	9.41	1335	0.418727	**C3H4**	8.88	10.45	1162	0.387263
C4H10	12.46	13.26	3893	0.220396	**C4H10**	12.46	13.12	2301	0.242938	**C4H10**	12.41	14.60	1701	0.264550

Table A *External Standardisation data for the mixed standardised gas canister*

	RUN 1					RUN 2					RUN 3			
Alkane Std.	**RT**	**RRT**	**Area**	**RRF**	**Alkane Std.**	**RT**	**RRT**	**Area**	**RRF**	**Alkane Std.**	**RT**	**RRT**	**Area**	**RRF**
CH4	0.91	1.00	29099	1	**CH4**	0.93	1.00	23091	1	**CH4**	0.94	1.00	3143	1
C2H6	3.32	3.65	49750	0.584905	**C2H6**	3.31	3.56	43425	0.531744	**C2H6**	3.31	3.52	5812	0.540778
C3H8	7.32	8.05	62980	0.462036	**C3H8**	7.29	7.84	62130	0.371656	**C3H8**	7.29	7.76	8572	0.366659
C4H10	12.55	13.79	73458	0.396131	**C4H10**	12.49	13.43	84753	0.272451	**C4H10**	12.49	13.29	12567	0.250099
C5H12	19.98	21.96	80041	0.363551	**C5H12**	19.89	21.39	105233	0.219427	**C5H12**	19.91	21.18	16580	0.189566

Table B *External Standardisation data for the alkane standardised gas canister*

	RUN 1				RUN 2				RUN 3		
Alkene Std.	**RT**	**Area**	**RRF**	**Alkene Std.**	**RT**	**Area**	**RRF**	**Alkene Std.**	**RT**	**Area**	**RRF**
C2H4	2.84	5898	1	C2H4	2.90	6139	1	C2H4	2.86	6289	1
C3H6	7.17	8591	0.686532	C3H6	7.25	9014	0.681052	C3H6	7.20	9210	0.683792
C4H8	12.19	9360	0.630128	C4H8	12.30	11437	0.536767	C4H8	10.25	12450	0.583447
C5H10	19.50	13617	0.433135	C5H10	19.63	15740	0.390025	C5H10	19.58	16950	0.41158
C6H12	27.85	21086	0.279712	C6H12	27.94	22871	0.268419	C6H12	27.89	23045	0.274065

Table C *External Standardisation data for the alkene standardised gas canister*

	RRF	RT
CH4	1.00	0.91
C2H4	0.56	2.90
C2H6	0.58	3.30
C3H6	0.38	7.20
C3H8	0.40	7.30
C4H8	0.33	12.19
C4H10	0.31	12.55
C5H10	0.23	19.50
C5H12	0.26	19.98
DME	0.58	9.14
C6H12	0.15	27.9

Table D *Averaged values for the data of all the standardised gas canisters*

Workstation:
Instrument : Varian Star #1
Channel : 1 = INTGR 1

Bus Address : 25
Sample Rate : 20.00 Hz
Run Time : 74.962 min

** Star Chromatography Workstation Version 5.51 ** 01159-6320-243-0705 **

Chart Speed = 0.17 cm/min Attenuation = 68 Zero Offset = -16%
Start Time = 0.000 min End Time = 74.962 min Min / Tick = 1.00

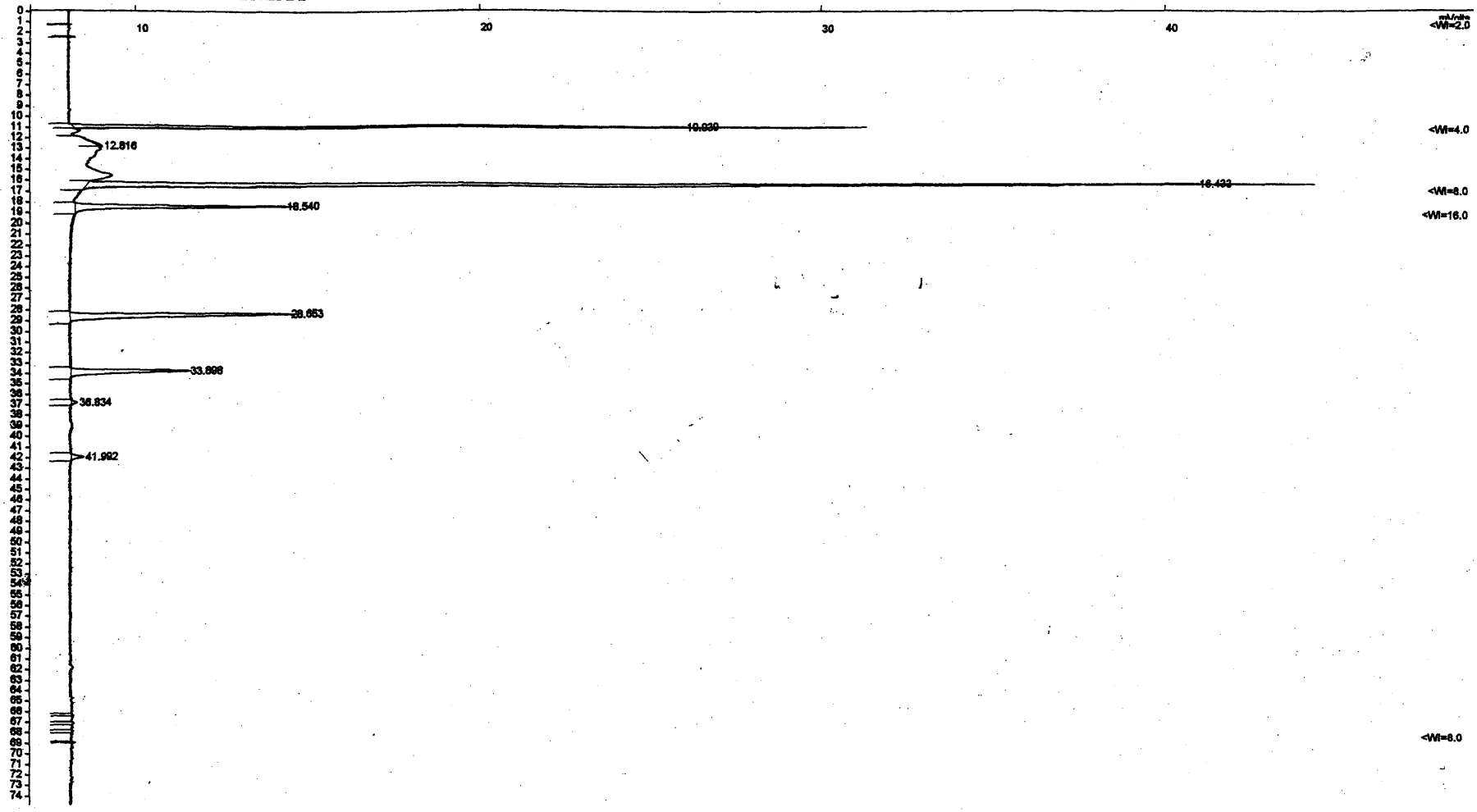

Figure C *Chromatogram obtained from the calibration of the reactants and products for the catalytic hydroxylation of phenol*

	RT	Area Counts	RRF
Hydroquinone	10.939	205445	0.3280
Benzoquinone	16.433	470205	0.1423
Catechol	18.540	97824	0.6889
Phenol	28.653	124176	0.5427
4-Fluorophenol	33.898	67395	1

Table E *RRF values for the calibrated phenol hydroxylation standards*

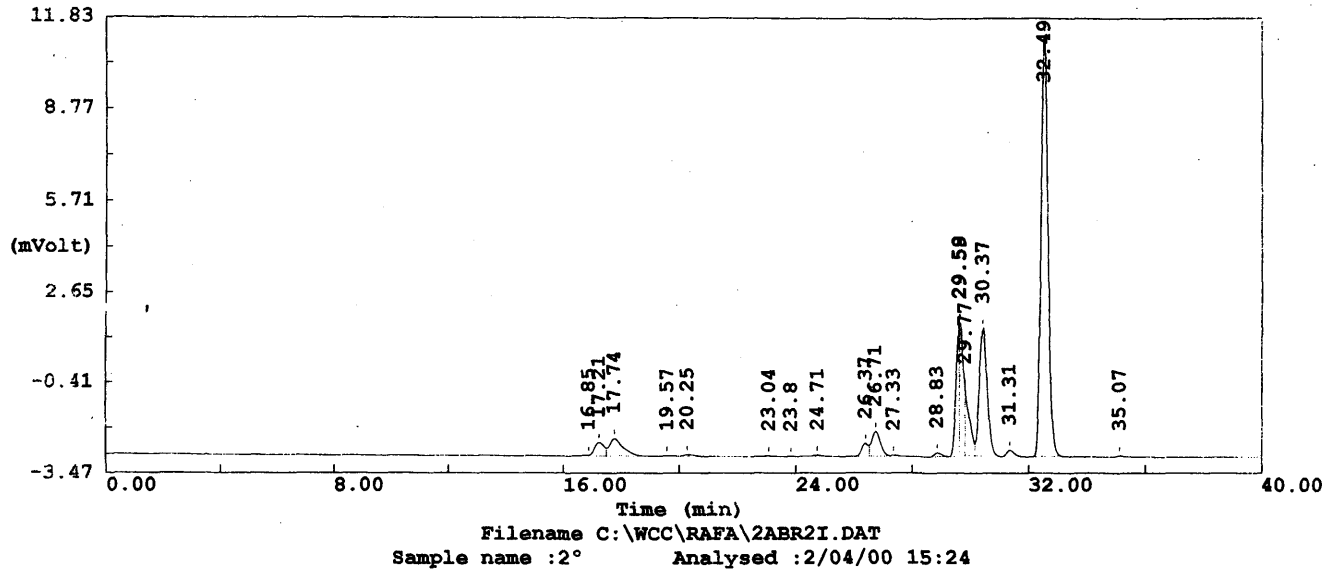

Filename C:\WCC\RAFA\2ABR2I.DAT
Sample name :2° Analysed :2/04/00 15:24

RAFA ROLDÁN

Operator ID : Rafa Company Name : César
Method Name : prueba Method File : RAFA.MTH
Analysed : 2/04/00 15:24 Printed : 29/04/2003 18:08

Sample ID : 2° Channel : Channel D
Analysis Type : UnkNown (Area) Calc. Method : Area %
Chromatogram : C:\WCC\RAFA\2ABR2I.DAT

Warning Chromatogram has been subjected to manual integration.

Retention Time (Min)	Area (mV/Sec*10)	Area %	Responce Fact.	Concentration
16.85	3743	0.077	0.00000	0.0773
17.21	106139	2.192	0.00000	2.1918
17.74	193143	3.988	0.00000	3.9884
19.57	4485	0.093	0.00000	0.0926
20.25	13945	0.288	0.00000	0.2880
23.04	5082	0.105	0.00000	0.1049
23.80	2117	0.044	0.00000	0.0437
24.71	9340	0.193	0.00000	0.1929
26.37	68728	1.419	0.00000	1.4192
26.71	174466	3.603	0.00000	3.6027
27.33	5296	0.109	0.00000	0.1094
28.83	22834	0.472	0.00000	0.4715
29.58	364423	7.525	0.00000	7.5253
29.59	382493	7.898	0.00000	7.8984
29.77	244608	5.051	0.00000	5.0511
30.37	800992	16.540	0.00000	16.5404
31.31	41573	0.858	0.00000	0.8585
32.49	2392687	49.409	0.00000	49.4087
35.07	6551	0.135	0.00000	0.1353
	4842643			100.0000

Figure D *Chromatogram obtained from analysis into the hydroisomerisation of n-heptane over Pt/Zeolite-β, TOS = 30 minutes, Temperature = 250°C*

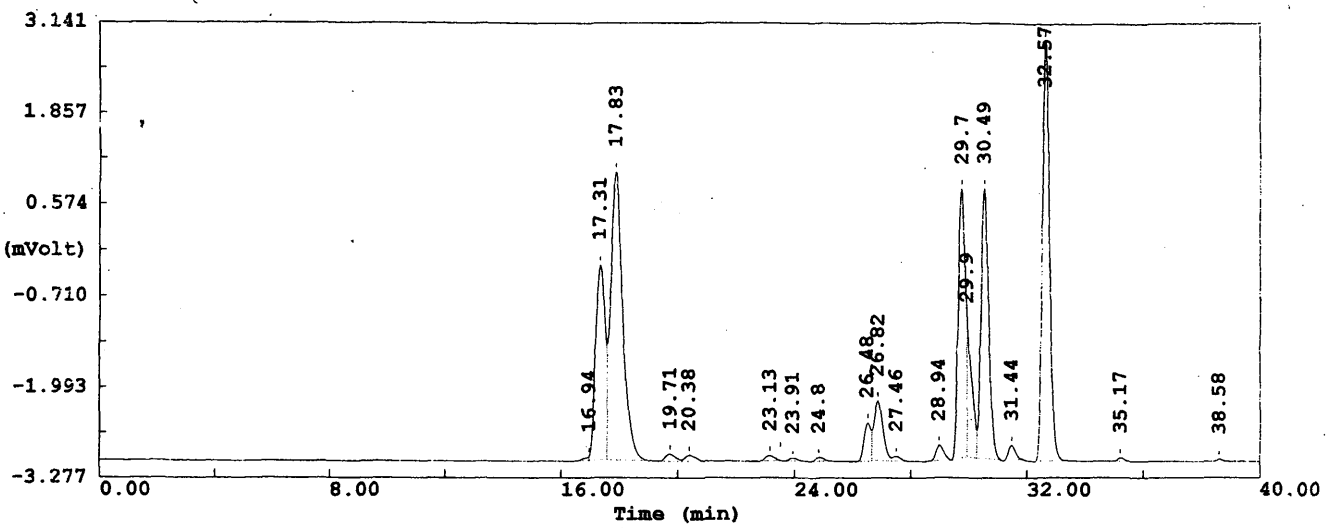

Filename C:\WCC\RAFA\2ABR5I.DAT
Sample name :5° Analysed :2/04/00 17:34

RAFA ROLDÁN

Operator ID	: Rafa	Company Name	: César
Method Name	: prueba	Method File	: RAFA.MTH
Analysed	: 2/04/00 17:34	Printed	: 29/04/2003 18:10
Sample ID	: 5°	Channel	: Channel D
Analysis Type	: UnkNown (Area)	Calc. Method	: Area %
Chromatogram	: C:\WCC\RAFA\2ABR5I.DAT		

Warning Chromatogram has been subjected to manual integration.

Retention Time (Min)	Area (mV/Sec*10)	Area %	Responce Fact.	Concentration
16.94	5970	0.124	0.00000	0.1238
17.31	633658	13.138	0.00000	13.1379
17.83	1177320	24.410	0.00000	24.4098
19.71	23967	0.497	0.00000	0.4969
20.38	21075	0.437	0.00000	0.4370
23.13	15895	0.330	0.00000	0.3295
23.91	7670	0.159	0.00000	0.1590
24.80	11733	0.243	0.00000	0.2433
26.48	87632	1.817	0.00000	1.8169
26.82	178320	3.697	0.00000	3.6972
27.46	12467	0.258	0.00000	0.2585
28.94	41353	0.857	0.00000	0.8574
29.70	640211	13.274	0.00000	13.2738
29.90	212582	4.408	0.00000	4.4075
30.49	698591	14.484	0.00000	14.4842
31.44	35556	0.737	0.00000	0.7372
32.57	1007039	20.879	0.00000	20.8793
35.17	7688	0.159	0.00000	0.1594
38.58	4412	0.091	0.00000	0.0915
	4823137			100.0000

Figure E *Chromatogram obtained from analysis into the hydroisomerisation of n-heptane over Pt/Zeolite-β, TOS = 30 minutes, Temperature = 275°C*